

**Development and validation of a new
musculoskeletal hand and elbow model and its
application in the medical field**



Universität Regensburg

Dissertation
in order to obtain
the degree in Human Sciences
(Dr. sc. hum.)

of the
Faculty of Medicine
University of Regensburg

submitted by
Maximilian Melzner

2022

Supervisor: Prof. Dr.-Ing. Sebastian Dendorfer

1st Mentor: Prof. Dr.-med. Christian Pfeifer

2nd Mentor: Prof. Dr-rer. nat. Elmar Lang

Day of Defence: 19.01.2023

List of acronyms

Acronyms used in this thesis are listed subsequently.

Acronyms

AMCL	Anterior medial collateral ligament
AMMR	AnyBody managed model repository
AMS	AnyBody Modeling System™
CMC	Carpometacarpal
CV	Coefficient of variation
DIP	Distal interphalangeal
DOF	Degree of freedom
ECR	Extensor carpi radialis
ECU	Extensor carpi ulnaris
ED	Extensor digitorum
EMG	Electromyography
FCR	Flexor carpi radialis
FCU	Flexor carpi ulnaris
FDK	Force-dependent kinematics
FDI	First dorsal interosseous
FDS	Flexor digitorum superficialis
FPB	Flexor pollicis brevis
KT	Kneeling technique
LHS	Latin hypercube sampling
MCP	Metacarpophalangeal

MEPS	Mayo Elbow Performance Score
MPP	Manual perineal protection
MVC	Maximum voluntary contraction
PCSA	Physiological cross-sectional area
PIP	Proximal interphalangeal
PMCL	Posterior medial collateral ligament
RCL	Radial collateral ligament
ROM	Range of motion
SD	Standard deviation
ST	Standing technique
UCL	Ulnar collateral ligaments

Zusammenfassung

Die vorliegende Dissertation befasst sich mit der muskuloskelettalen Modellierung und Simulation der menschlichen Hand und des Ellenbogens. Dabei besteht die Auseinandersetzung mit der Hand und dem Ellenbogen jeweils aus drei wesentlichen Aspekten: Der Modellentwicklung, der Modellvalidierung und der klinischen Anwendung des jeweiligen Modells. Grundlage hierfür ist jeweils die muskuloskelettale Mehrkörpersimulations-Software AnyBody™ (Anybody, Aalborg, Dänemark), die auf dem Prinzip der inversen Dynamik beruht.

Das Handmodell, das in Kooperation mit Lucas Engelhardt vom Ulmer Zentrum für Wissenschaftliches Rechnen entwickelt wurde, beruht dabei auf einer eigens dafür an der Westböhmische Universität in Pilsen durchgeführten anatomischen Studie von insgesamt 16 seziierten oberen Extremitäten. Das daraus entwickelte Modell weißt grundlegende Neuerungen bei der muskuloskelettalen Modellierung der Hand auf; unter anderem die Einbettung der Hand in ein holistisches Ganzkörpermodell, die Möglichkeit einer patienten-spezifischen Skalierung, sowie die Realisierung mehrere weitere Besonderheiten der menschlichen Hand (wie z.B. der Ansatz der lumbrikalen Muskeln an der Sehne des Flexor Digitorum Profundus) - siehe Kapitel 4

In mehreren Validierungsschritten (siehe Kapitel 5 - 7) wurde das entwickelte Handmodell anschließend mit Literaturwerten bzw. experimentell erhobenen Daten verglichen. Die erste Validierungsstufe bestand dabei aus einem Vergleich von numerisch bestimmten Muskelmomentenarmen mit experimentellen Literaturwerten (siehe Kapitel 5). Anschließend wurden von insgesamt fünf Freiwilligen das elektromyographische Potential von zehn verschiedenen ex- und intrinsischen Muskeln sowie Bewegungsaufnahmen während der Ausübung von sieben unterschiedlichen Handbewegungen erhoben. Somit konnte ein Vergleich von numerisch

und experimentell bestimmten Muskelaktivitätsmustern gezogen werden (siehe Kapitel 6). Der finalen Validierungsschritt befasst sich mit der Fragestellung in wie weit sich die Streuungen der dem Modell zugrundeliegenden Daten auf die Vorhersagen des Modells auswirkt. Hierfür wurden die Muskelansatzpunkte sowie die Muskelstärken gemäß der in der Kadaverstudie der Universität Pilsen erfassten Standardabweichungen variiert (siehe Kapitel 7). Keiner der oben erwähnten Validierungsprozesse wies größere Unstimmigkeiten zwischen Modell und entsprechenden Vergleichswerten auf. In der ersten klinischen Fragestellung der dargelegten Arbeit steht die Anwendung des Handmodells auf die Unterstützung des Geburtvorgangs durch einen Geburtshelfer und die Untersuchung zweier verschiedener Techniken bezüglich biomechanischer Aspekte im Vordergrund (siehe Kapitel 8).

Das im Rahmen dieser Arbeit entwickelte Modell des Ellenbogengelenks beruht neben der Studie aus Pilsen auf zahlreichen weiteren Literaturdaten, um die biomechanischen Eigenschaften des Bandapparates abdecken zu können. Die Implementierung der Bandstruktur in Kombination mit dem integrierten force-dependent-kinematic Ansatz weicht das starre Scharniergelenk des Ellenbogens auf, sodass eine Verkippung der Flexionsrotationsachse ermöglicht wird (siehe Kapitel 9). Unter Verwendung von Literaturdaten wird das Ellenbogenmodell in Kapitel 10 validiert. Dabei dienen neben einem Abgleich von Muskelmomentenarmen (analog zur Validierung des Handmodells) unter anderem die Längenänderung und Steifigkeiten der Bänder. Eine klinische Anwendung des Ellenbogenmodells erfolgt in Kapitel 11. Diesbezüglich wird die Stabilität des Ellenbogengelenks gegenüber Varus/Valgus-Momenten für verschiedene Verletzungsszenarien numerisch untersucht und anschließend mit den Erfahrungswerten von praktizierenden Ärzten verglichen.

Nach Abschluss dieser Arbeit stehen somit ein validiertes Ellenbogen- und Handmodell zur Verfügung (wobei Letzteres in naher Zukunft bereits in die Simulationsoftware AnyBody integriert wird), die neben der in dieser zugrundeliegenden Dissertation dargestellten klinischen Anwendungen für zahlreiche weitere Forschungszwecke genutzt werden können.

Abstract

This thesis addresses the musculoskeletal modeling and simulation of the human hand and elbow. The examination of the hand and elbow consists of the following three essential aspects, each: Model development, model validation, and clinical application of the model. The simulation software AnyBody™ (Anybody, Aalborg, Denmark), which is based on the principle of inverse dynamics, is the platform for the modeling.

The hand model, which has been developed in cooperation with Lucas Engelhardt from the Ulm Center for Scientific Computing, is based on an anatomical study of a total of 16 dissected upper extremities conducted at the University of West Bohemia in Pilsen. Due to the embedding in a holistic whole-body model, the possibility of patient-specific scaling, and the realization of several additional features of the human hand (such as the attachment of the lumbrical muscles to the tendon of the flexor digitorum profundus), the model developed in this thesis provides fundamental innovations in musculoskeletal modeling of the hand (see Chapter 4). In several validation steps (see Chapter 5 - 7), the developed hand model was compared to results from prior literature or experimentally collected data. The first validation step involved a comparison of numerically determined muscle moment arms with experimental literature values (see Chapter 5). Subsequently, the electromyographic potential of ten different extrinsic and intrinsic muscles as well as motion recordings during exercise of seven different hand movements were collected from a total of five volunteers. Thus, a comparison of numerically and experimentally determined muscle activity patterns could be drawn (see Chapter 6). The final validation step addresses the question of how far the scatter of the data, on which the model is based, affects predictions made by the model. Hence, the muscle attachment points and the muscle strengths were varied accord-

ing to the standard deviations recorded in the cadaver study of the University of Pilsen (see Chapter 7). None of the above-mentioned validation processes showed major discrepancies between model and corresponding comparative values. The first clinical application of the presented work focuses on the transfer of the hand model to the support of the birth process by an obstetrician and the investigation of two different techniques from a biomechanical perspective (see Chapter 8).

The model of the elbow joint developed within this thesis is based on numerous data gathered from prior literature in addition to the study from Pilsen in order to be able to cover the biomechanical properties of the ligamentous apparatus. Beside the implementation of the ligament structures, the developed elbow model resolves the rigid elbow joint previously represented as a simplified hinge joint in the simulation software AnyBody. The integrated force-dependent-kinematic approach allows for a more anatomically accurate description of the elbow flexion-rotation axis (see Chapter 9). Using literature data, the elbow model is validated in Chapter 10. To this end, the change in length and stiffnesses of the ligaments, among other features, are included in addition to a comparison of muscle moment arms (analogous to the validation of the hand model). A clinical application of the elbow model is given in Chapter 11. In this context, the stability of the elbow joint against varus/valgus moments is numerically investigated for different injury scenarios and subsequently compared with the experience values of practicing physicians.

Upon completion of this work, a validated elbow and hand model will thus be available (whereby the latter is already in the process of being integrated into the AnyBody simulation software), which can be helpful in answering numerous other research questions in addition to the clinical applications presented in this underlying work.

Contents

1	Introduction	1
2	Anatomy and functionality of the human hand and elbow	5
2.1	The human hand	5
2.1.1	Bones and joints	5
2.1.2	Muscles	9
2.2	The human elbow	15
3	The AnyBody modeling system	17
4	Hand model: model development	20
4.1	Introduction	20
4.2	Hand model	22
4.2.1	Anatomical data set	23
4.2.2	Patient-specific scaling and muscle alignment	23
4.2.3	Moments of inertia	26
4.2.4	Finger rhythm	27
4.2.5	Muscle on a muscle	28
4.2.6	Purlicue skin	30
4.2.7	Choice of model accuracy	31
5	Hand model: moment arm validation	32
5.1	Validation	32
5.2	Results	35
5.3	Discussion	39

5.4	Conclusion	44
6	Hand model: experimental validation	45
6.1	Introduction	45
6.2	Materials & Methods	47
6.2.1	Experimental set-up	47
6.2.2	Simulation	52
6.2.3	Data processing	53
6.2.4	Statistical analysis	54
6.3	Results	54
6.4	Discussion	57
6.4.1	The hand model	57
6.4.2	Validation	58
6.5	Conclusion	61
7	Hand model: sensitivity analysis	62
7.1	Introduction	62
7.2	Materials & Methods	64
7.2.1	Experiment set-up	64
7.2.2	Simulation	65
7.2.3	Data processing	66
7.3	Results	67
7.4	Discussion	73
7.5	Conclusion	76
8	Hand model: clinical application - simulation of the manual per-	
	ineal protection	77
8.1	Introduction	77
8.2	Materials & Methods	80
8.3	Results	84
8.4	Discussion	88
8.5	Conclusion	91

9	Elbow model: model development	92
9.1	Introduction	92
9.2	Elbow model	94
9.2.1	Muscles	95
9.2.2	Ligamentous apparatus	96
9.2.3	Varus-Valgus motion	97
10	Elbow model: validation	99
10.1	Validation	100
10.1.1	Muscle moment arms	100
10.1.2	Ligament elongation	100
10.1.3	Ligament tautness	101
10.1.4	Elbow moment	101
10.1.5	Change of cubital angle/rotation axis during flexion	102
10.2	Results	102
10.2.1	Muscle moment arms	102
10.2.2	Ligament elongation	104
10.2.3	Ligament tautness	104
10.2.4	Elbow moment	107
10.2.5	Change of cubital angle/rotation axis during flexion	108
10.3	Discussion	110
10.3.1	Muscle moment arms	110
10.3.2	Ligament elongation	110
10.3.3	Ligament tautness	111
10.3.4	Elbow moment	111
10.3.5	Change of cubital angle/rotation axis during flexion	112
10.3.6	The model	112
11	Elbow model: clinical application - stability analysis	114
11.1	Introduction	114
11.2	Materials & Methods	116
11.3	Results	119
11.4	Discussion	122

11.5 Conclusion	125
12 Conclusion	126
A Supplementary material: Chapter 5	
B Supplementary material: Chapter 6	
C Supplementary material: Chapter 7	
D Supplementary material: Chapter 8	
E Supplementary material: Chapter 11	

List of Figures

2.1	Anatomical overview of the human hand	6
2.2	ROM of the wrist joint	7
2.3	ROM of the CMC thumb joint	7
2.4	ROM of the finger joints	8
2.5	Extrinsic hand muscles - anterior view	10
2.6	Extrinsic hand muscles - posterior view	11
2.7	Intrinsic hand muscles	14
2.8	Anatomical overview of the human elbow	15
2.9	Muscles crossing the elbow joint	16
2.10	Ligamentous apparatus of the elbow	16
4.1	Visualization of wrapping obstacles of the hand model	25
4.2	Moment of inertia of a phalanx	25
4.3	Dependency of the flexion angle for the PIP-DIP joint	27
4.4	Model of the "muscle on a muscle" concept	29
4.5	"Muscle on a muscle": illustration of the mechanism of action	29
4.6	Visualization of the pulcruc skin resistance	30
4.7	Different levels of detail of the hand model regarding the number of muscle representatives	31
5.1	Moment arm comparison between model and literature regarding the wrist joint	36
5.2	Moment arm comparison between model and literature regarding the MCP joint of the index finger	36

5.3	Moment arm comparison between model and literature regarding the CMC joint of the thumb	37
5.4	Effect of different model detail levels on moment arms and calculation time	43
6.1	Maximal voluntary contraction measurement device	49
6.2	EMG sensor and marker placement of the forearm and hand of a test subject.	49
6.3	Simulation interface of the AMS regarding the movements of th hand	53
6.4	Comparison of measured and predicted muscle activities regarding hand movements	55
7.1	Exemplary scattering of muscle activity and joint reaction force due to variation of origin/insertion points and PCSA	68
7.2	Scattering of joint reaction forces and muscle activities on-set time points for the abduction of all fingers	72
7.3	Scattering of joint reaction forces and muscle activities on-set time points for the flexion of the thumb	72
7.4	Scattering of joint reaction forces and muscle activities on-set time points for the abduction of the thumb	73
8.1	AMS interface of the simulation regarding the posture of the obstetrician during delivery	80
8.2	Measuring equipment for recording the movements during the birth process	82
8.3	Comparison of the joint reaction forces of the upper extremity when using different postures for delivery	85
8.4	Comparison of the joint reaction forces of the lower back when using different postures for delivery	86
8.5	Effects of pivoting the elbow on the distal thigh on the acting joint reaction forces	87
9.1	Implementation of the cubital angle within the new musculoskeletal elbow model	95

9.2	Force-strain relationship for the ligament complexes of the elbow . . .	96
10.1	Moment arm comparison between model and literature regarding the flexion of the elbow joint	103
10.2	Moment arm comparison between model and literature regarding the pronation of the elbow joint	103
10.3	Comparison of ligament elongation between model and experimental data according to Morrey and An (1985)	105
10.4	Comparison of the range of tautness during elbow flexion between the model and data from literature	106
10.5	Compared of load-displacement curve between model and literature regarding for full extension	107
10.6	Compared of load-displacement curve between model and literature regarding for 90° flexion	108
10.7	Comparison of the change in the cubital angle during elbow flexion between model and literature data	109
10.8	Symbolic visualization of the change in the rotation axis during elbow flexion of the new elbow model	109
11.1	Graphical interface of the simulation regarding the elbow stability testing	117
11.2	Elbow stability contribution regarding low (2 Nm) valgus and varus moments	120
11.3	Elbow stability contribution regarding high (4 Nm) valgus and varus moments	120
A.1	Moment arm comparison between model and literature regarding the flexion/extension around the wrist joint	
A.2	Moment arm comparison between model and literature regarding the ab-/adduction around the wrist joint	
A.3	Moment arm comparison between model and literature regarding the flexion/extension around the MCP joint of the index finger	
A.4	Moment arm comparison between model and literature regarding the ab-/adduction around the MCP joint of the index finger	

A.5	Moment arm comparison between model and literature regarding the flexion/extension around the CMC joint of the thumb
A.6	Moment arm comparison between model and literature regarding the ab-/adduction around the CMC joint of the thumb
A.7	Moment arm comparison between model and literature regarding the flexion/extension around the MCP joint of the thumb
A.8	Moment arm comparison between model and literature regarding the ab-/adduction around the MCP joint of the thumb
A.9	Moment arm comparison between model and literature regarding the flexion/extension around the DIP joint of the thum
B.1	Marker placement EMG study
B.2	Exemplary muscle activities for task 1 of one test subject

List of Tables

4.1	Relative segment to hand length for each phalanx	24
5.1	Enumeration of the muscles regarding the examination of the moment arms	34
5.2	Moment arm comparison between model and literature regarding all joints and all muscles	38
6.1	EMG sensor placement protocol	48
6.2	Activation of the individual joints or muscles during the respective hand movements	50
6.3	Visualization of the individual hand movements	51
6.4	Comparison of measured and calculated muscle on- and off-set time points for the individual hand movements	56
7.1	Variations in muscle on- and off-set time points due to change in origin/insertion points and PCSA	70
7.2	Variations in joint reaction forces in the hand due to changes in origin/insertion points and PCSA	71
11.1	Overview of the scenarios for the stability testing of elbow joint . . .	118
11.2	Survey results regarding the scenarios' MEPS score and Average contribution of every scenario according to the musculoskeletal simulations	121
B.1	EMG sensor and envelope of corresponding muscles within the AMS.	

C.1 The dimensions of insertion, origin area as well as the physiological cross sectional area for the extrinsic muscles according to Havelková et al. (2020)

C.2 The dimensions of insertion, origin area as well as the physiological cross sectional area for the intrinsic muscles according to Havelková et al. (2020)

C.3 Variation of muscle activities and joint reaction forces during the abduction of all fingers.

C.4 Variation of muscle activities and joint reaction forces during the flexion of the thumb

C.5 Variation of muscle activities and joint reaction forces during the abduction of the thumb

D.1 Effect of pivoting the elbow on the distal thigh on the acting joint reaction forces.

D.2 Joint reaction forces in the upper extremity and lower back during delivery using the standing and kneeling technique

Chapter 1

Introduction

In vivo experiments required to answer musculoskeletal research questions concerning prevention or rehabilitation can usually only be performed at great expense and often only under ethically questionable conditions. To overcome this issue, the last decades showed a surge in the development of simulation models of the human musculoskeletal system. These simulation models are already used in a variety of domains, such as orthopaedic research (Dendorfer et al. 2014, Weber et al. 2014, Putzer et al. 2016) or sports (Kwan et al. 2011, Nakashima et al. 2013) to mention only a few. Additionally, these models can serve as a basis for further analyses, such as finite element models (Schöneegg et al. 2022, Jian-Qiao Peng et al. 2021). Depending on the body part a research question is concerned with, a corresponding simulation model must be available that provides a sufficient level of detail with respect to the respective musculoskeletal components. Since recently the human gait and the resulting boundary conditions for possible prostheses of the lower extremity have received a lot of attention in research, the simulation models of the lower limb provide a relatively high level of detail (Carbone et al. 2015, Carbone 2016).

In contrast, only a few mostly stand-alone models of individual areas of the upper extremity exist. Additionally, these models are neither embedded in a whole-body model (Wu et al. 2014) – and thus can only be used for the biomechanical analysis of very specific tasks – nor do they provide a sufficient level of detail required for many research questions. Recent studies conducted at the Laboratory for Biome-

chanics in Regensburg have focused on advancing a musculoskeletal shoulder model (Aurbach et al. 2020a) within the widely used simulation platform AnyBody™, which has already provided valuable new insights into this area (Aurbach et al. 2020b).

As logical progression of this research, this thesis is dedicated to the development, validation, and clinical application of a hand and elbow model within AnyBody™ in order to complete a musculoskeletal model of the upper extremity embedded in a whole body model. Both models are based on an anatomical study of the University of Pilsen (Havelková et al. 2020). The model of the human hand was developed in close collaboration with Lucas Engelhardt from the Scientific Computing Centre Ulm (see Chapters 4 - 6), such that the Scientific Computing Centre Ulm and the Laboratory of Biomechanics Regensburg contributed equally to the development of the model. To elaborate, the study on the correlation of hand and single phalanx lengths (see Chapter 4) was conducted at the Scientific Computing Centre Ulm and the accompanying experimental validation study in Chapter 6 at the Laboratory for Biomechanics Regensburg. All other minor work packages were always carried out in close collaboration, rendering a precise assignment of to a single institute infeasible. In order to have sufficient confidence in the predictions of such developed musculoskeletal models when answering various research questions, they must be validated accordingly; which means, one must assess to what extent the simulation is able to determine certain target variables. This is usually done by comparing numerically determined and experimentally measured values (Lund et al. 2012). Thus, it is possible to determine indeterminates and limits of the numerical simulation more precisely. Accordingly, the models developed in this thesis are compared with empirical literature data or the results of experimental studies carried out particularly for the purpose of validating the developed models. Since the developed hand model with its large number of degrees of freedom and parameters is very complex, a sensitivity analysis against uncertainties in the determination of the input parameters is performed.

Following validation, the musculoskeletal model of the hand and elbow are used to answer two exemplary, clinically relevant research questions. For the hand model, this is achieved within the framework of manual perineal protection - this is a special hand grip to relieve the perineum of an expectant mother during birth and

thus reduce possible damage (Laine et al. 2008). Since the correct execution of this grip is crucial not only in averting injury to an expectant mother, but also for the physical integrity of the performing obstetrician, musculoskeletal stress in the obstetrician is examined in Chapter 8. In this context, the hand model can ensure a correct introduction of the external forces into the human body, which is crucial for the determination of all further calculated muscle forces and thus joint reaction forces in the further kinematic chain of the human body.

For the elbow model, the clinical application, as shown in Chapter 11, is performed in the context of assessing the stability of the elbow after injuries of its stabilizers. The stability of the joint is an important decision criterion for the subsequent treatment (e.g. non-operative vs. operative) (van Riet 2017). While some cases clearly fall in the non-operative or operative treatment categories, treatment selection for many cases is less clear due to the complex interaction of the stabilizers and the diverse injury patterns. In these cases, the decision regarding non-operative/operative care depends mostly on the subjective assessment of the medical expert. Musculoskeletal simulations provide the ability to analyze a variety of different injury patterns and thus can be used as decision aid for medical specialists by providing a more objective means of assessment through a numerical analysis of elbow stability.

In summary, the objective of the present thesis consists of the following:

1. development of a new hand and elbow model in the AnyBody™ development environment; each with an unprecedented level of detail and the possibility of patient-specific scaling (see Chapter 4 and 9).
2. validation of the two models by comparison with literature data and own experimental studies. This includes the following:
 - regarding the hand model:
 - comparison of numerically calculated muscle moment arms by the model and experimentally measured muscle moment arms from literature (see Chapter 5)

- evaluation of the different timings of on- and off-sets of muscle activities between the numerical model and experimental measurements (see Chapter 6)
 - investigation of the sensitivity and stability of the model regarding anatomical uncertainties the model is based on (see Chapter 7)
 - regarding the elbow model:
 - comparison of numerically calculated muscle moment arms by the model and experimentally measured muscle moment arms from literature (see Chapter 10.1.1)
 - alignment of ligament elongation and tautness between the model and literature data (see Chapter 10.1.2 and 10.1.3)
 - resistance of the elbow regarding an acting moment and the corresponding change in the cubital angle (see Chapter 10.1.4)
 - comparison of the change in the flexion axis of the elbow joint between model and literature data (see Chapter 10.1.5)
3. application of the two new musculoskeletal models to answer initial research questions:
- determination of the forces occurring in obstetricians using different obstetric techniques (see Chapter 8)
 - assessment of elbow stability after the occurrence of common injury patterns (see Chapter 11)

With the completion of this thesis, a new, detailed simulation model of the elbow and the hand is available to the musculoskeletal user community (the latter is currently already being incorporated into the AnyBody Managed Model Repository). Thus, the research presented in this thesis can be useful in addressing numerous other research questions concerning the upper extremity, besides those addressed herein.

Chapters 2 and 3 provide an overview over the anatomy of the hand and elbow and the utilized musculoskeletal simulation software AnyBody™ which constitutes the basis for this presented work.

Chapter 2

Anatomy and functionality of the human hand and elbow

At the beginning of this thesis, the anatomy of the hand, the forearm and the elbow will be discussed, since the existing bones, muscles, ligaments, and the resulting degrees of freedom (DOF) represent important boundary conditions for the corresponding musculoskeletal model. Consequently, basic knowledge of anatomy is an essential component for understanding the functionality of the developed models. If not stated otherwise, this chapter is based on Hirt (2016).

2.1 The human hand

The hand is a highly sensitive gripping mechanism consisting of a total of 27 bones connected to each other by joints that allow a different number of DOFs. These DOFs are controlled by a total of 39 extrinsic and intrinsic muscles via the central nervous system.

2.1.1 Bones and joints

The 27 bones of the human hand can be divided into three subgroups: the carpal bones, the metacarpal bones, and the phalanxes - see Figure 2.1. The individual bones are connected to each other via different joints and therefore have different numbers of DOFs.

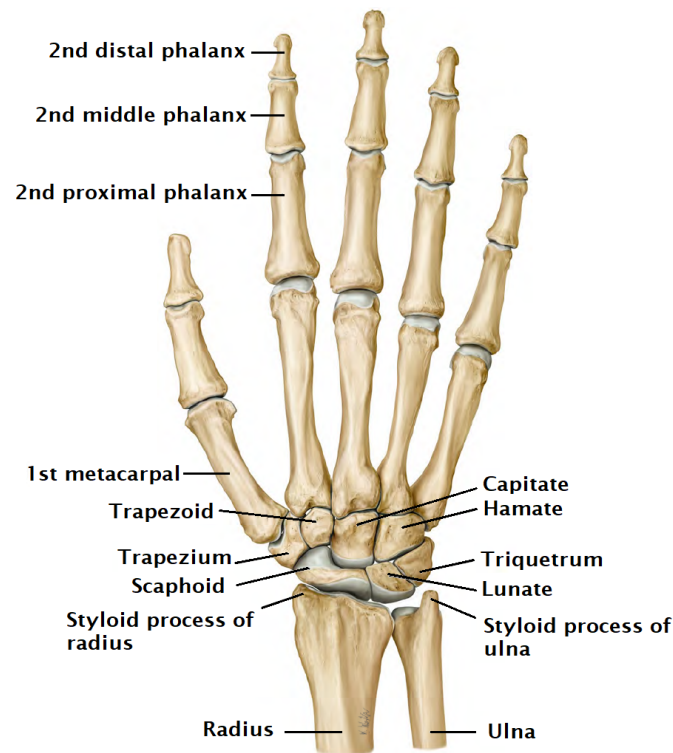


Figure 2.1: Overview of the bones of the human hand and notations - adapted from Schünke et al. (2014) - Figure 27.1

Wrist joint: The ulna and radius are in junction with the proximal row of carpal bones (Scaphoid, Lunate, Triquetrum, Pisiform) via the radiocarpal joint, which in turn is connected to the distal carpal row (Trapezium, Trapezoid, Capitate, Hamate) via the midcarpal joint. The movement of the individual carpal bones among each other is very much restricted by their shape, ligaments and capsules, which results in the midcarpal joint being severely limited in its range of motion (ROM). Overall, the wrist can be considered a universal joint allowing rotation along two axes - palmar flexion and dorsal extension, as well as ulnar and radial abduction (see Figure 2.2). This results in possible extension of about 80° , flexion of around 80° , radial deviation of around 15° to 25° , and ulnar deviation of around 40° to 50° (Schmidt and Lanz 2011).



Figure 2.2: ROM of the wrist joint. Dorsal extension/ palmar flexion (left side) and ulnar and radial abduction (right side) - adapted from Hirt (2016)

CMC joint: The carpometacarpal (CMC) joint is located between the distal row of carpal bones and the metacarpal bones. The CMC joints of the fingers are severely restricted in their mobility-range by ligaments and therefore represent amphiarthrosis. In contrast, the CMC joint of the thumb forms a saddle joint with two DOFs, which allows abduction of 45° , a flexion of 20° , and extension of 45° (Hochschild 2015) - see Figure 2.3. Using this ROM, humans are able to oppose the thumb to the fingers and thus utilize the hand as a sensitive gripping tool.

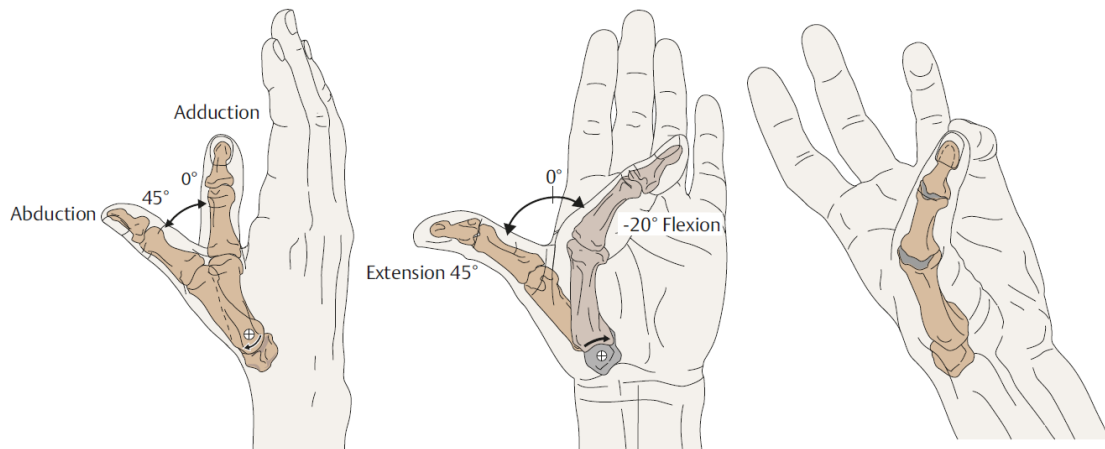


Figure 2.3: ROM of the CMC thumb joint. Abduction/ adduction (left side), flexion/extension (middle). This range of motion allows an opposition of the thumb (right side) making the hand a sensitive grappling tool - adapted from Hochschild (2015)

MCP joint: The metacarpophalangeal joints (MCP) are located between the metacarpal bones and the proximal phalanges. This joint forms a universal joint with two DOFs, allowing ulnar/radial abduction of 15° as well flexion of 90° (see Figure 2.4) for the fingers.

PIP and DIP joint: The interphalangeal joints - the proximal interphalangeal joint (PIP) and distal interphalangeal joint (DIP) - are located between the proximal and middle phalanges and between the middle and distal phalanges, respectively. As the middle phalanx is missing for the thumb, there is no PIP joint for the thumb and the DIP joint is defined between the proximal and distal phalanges. For the thumb as well as for the fingers, the interphalangeal joints are typical hinge joints allowing only flexion and extension (see Figure 2.4).

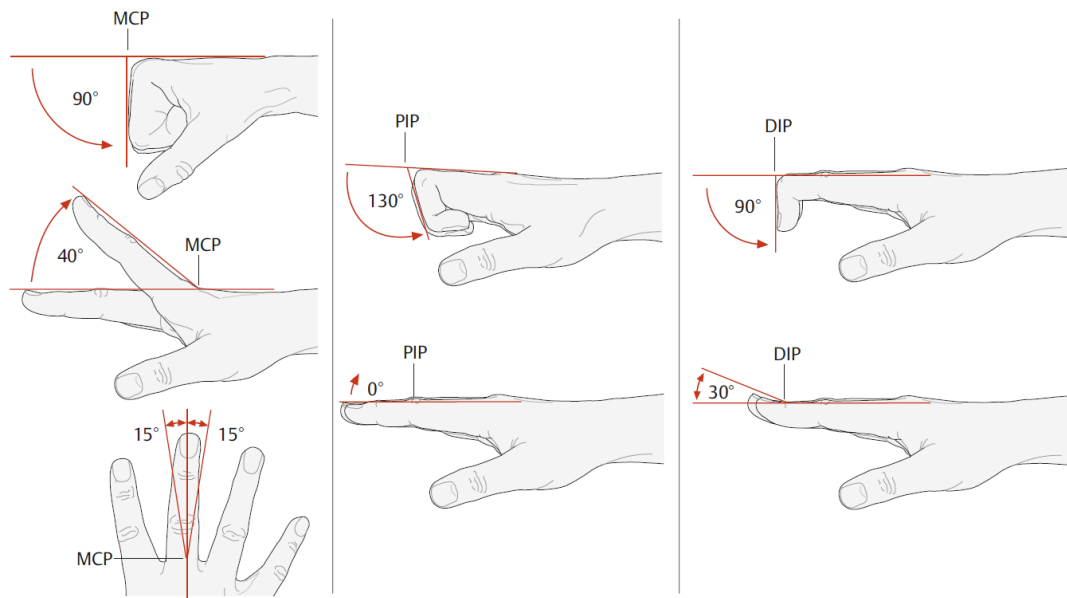


Figure 2.4: ROM of the MCP, PIP and DIP joint of a finger - adapted from Schünke et al. (2014)

2.1.2 Muscles

The hand consists of 39 muscles, which are used to move the individual bones and thus ensure the functionality of the hand. These 39 muscles can be divided into two groups: the extrinsic and intrinsic muscles.

Extrinsic muscles: The origin and the contractile element of the extrinsic muscles are located in the forearm and transmit the generated force to the individual bones via long tendons up to the finger tips to ensure the ROM. According to their main task - bending and stretching the wrist and individual phalanges - these muscles are differentiated in flexors (see Figure 2.5) and extensors (see Figure 2.6), which overlap in several layers.

Intrinsic muscles: In contrast to extrinsic muscles, the origin and insertion point of intrinsic muscles is within the hand. The main function of the intrinsic muscles is abduction/adduction around the MCP joint of the fingers and for the skilled movements of the thumb. An overview of the different layers of the intrinsic muscles is given in Figure 2.7.

In general, muscles are connected to the bones through the tendon origin and insertion points. A unique feature of the human hand, however, is the origin points of the lumbrical muscles. In contrast to regular muscles, the lumbricals do not originate from a bone, but rather from the tendon of the flexor digitorum profundus muscle. Therefore, the force of the lumbrical is transmitted onto the flexor digitorum profundus tendon.

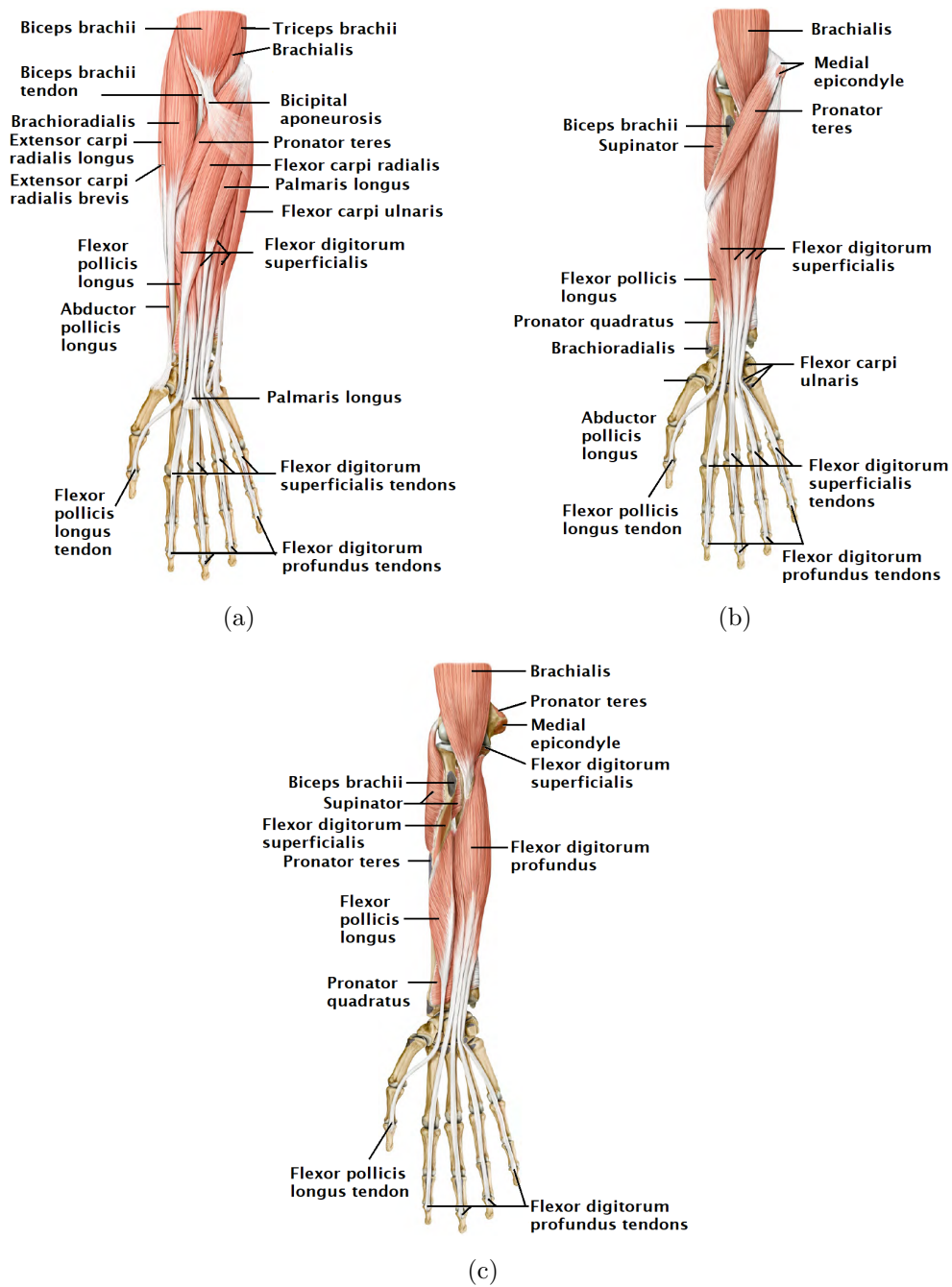


Figure 2.5: Extrinsic hand muscles (anterior view) from superficial (a) to deep layers (c) - adapted from Schünke et al. (2014) - Figure 26.10

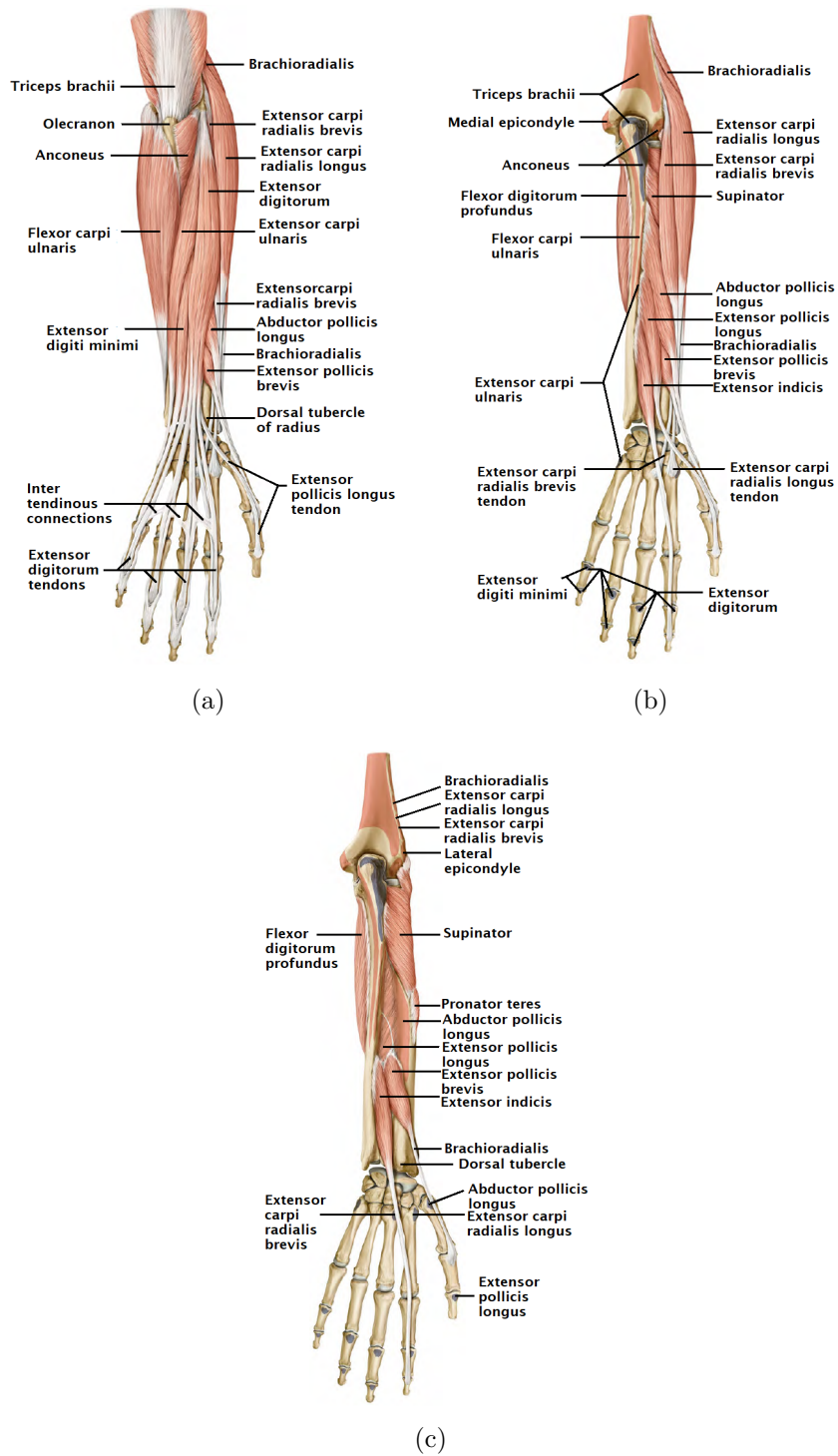
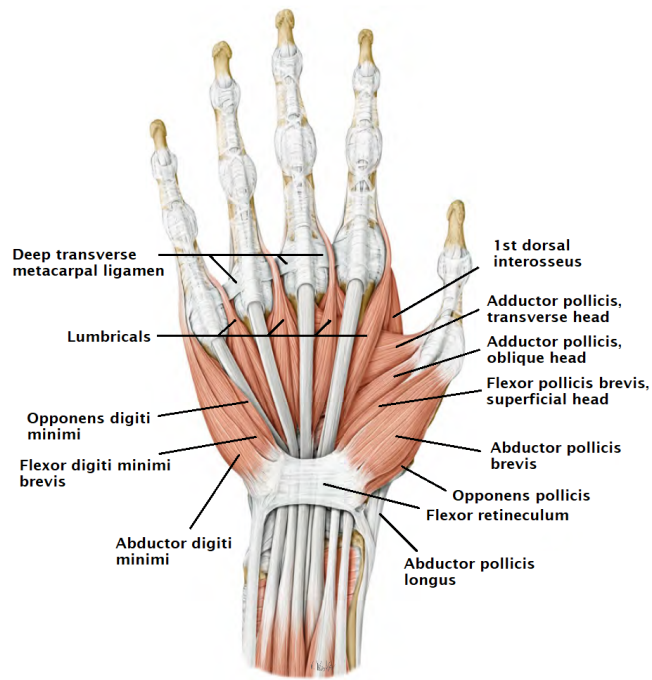
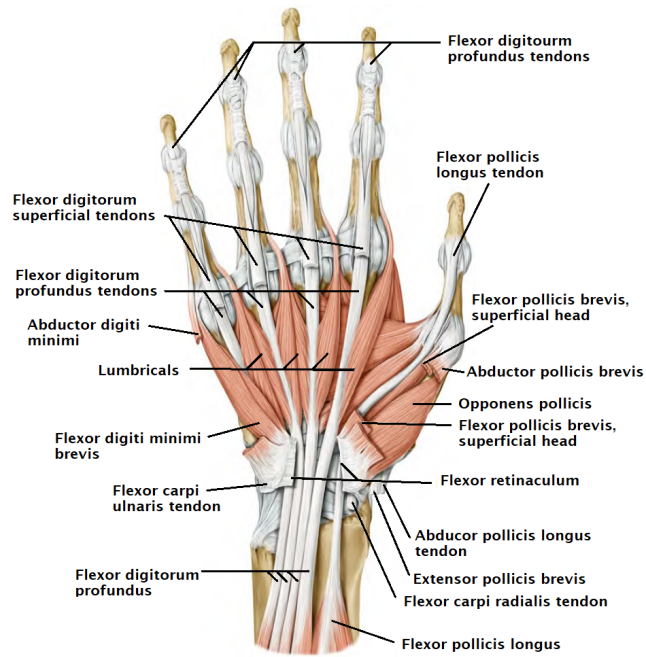


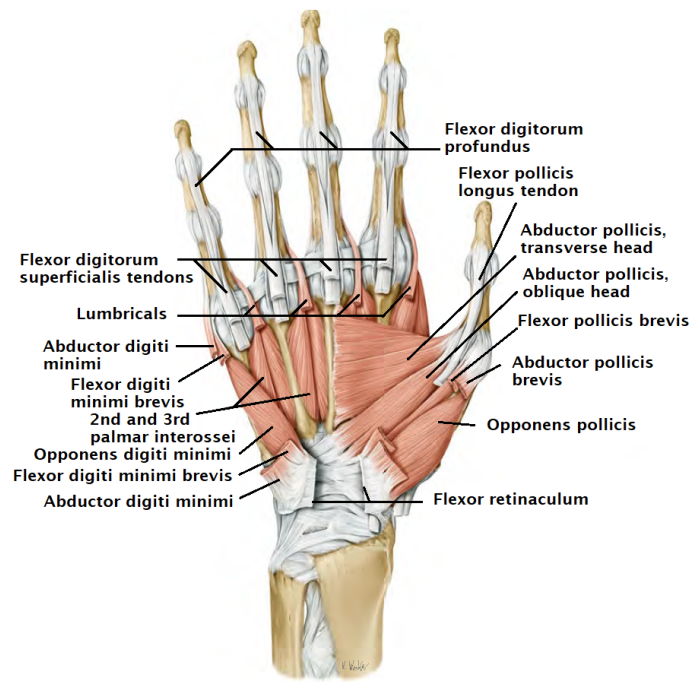
Figure 2.6: Extrinsic hand muscles (posterior view) from superficial (a) to deep layers (c) - adapted from Schünke et al. (2014) Figure 26.11



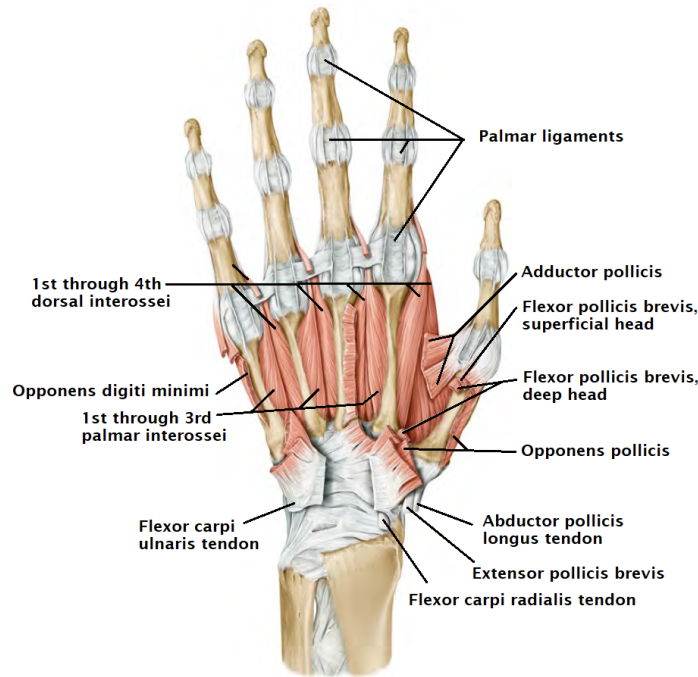
(a)



(b)



(c)



(d)

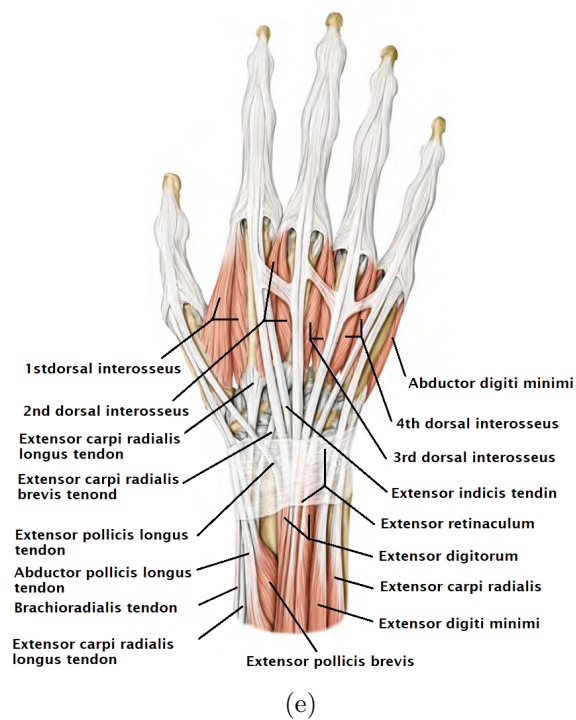


Figure 2.7: Intrinsic hand muscles (palmar view (a)-(d) and dorsal view (e)) from superficial (a) and (e) to deep layers (d) - adapted from Schünke et al. (2014) Figure 27.18-21

2.2 The human elbow

The elbow joint serves as a link between the upperarm and forearm and incorporates all three long bones of the human arm: humerus, radius and ulna (see Figure 2.8).

The elbow joint allows the complex motion of flexion/extension ($150^\circ/10^\circ$) as well as the rotation of the forearm ($\pm 80^\circ - 90^\circ$) (Hochschild 2015). According to the elbow's ROM, the muscles spanning the elbow can be divided into flexors (biceps brachii, brachialis, brachioradialis), extensors (triceps), pronators (pronator teres, pronator quadratus), and supinators (supinator, biceps brachii) - see Figure 2.9.

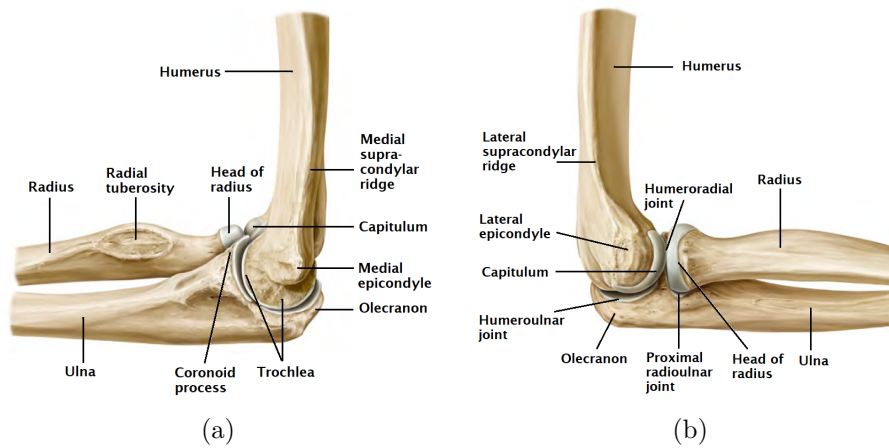


Figure 2.8: Overview of the bones of the human elbow and notations from (a) the medial side and (b) the lateral side - adapted from Schünke et al. (2014) - Figure 26.2

The bone structure of the elbow joints is stabilized by ligaments that provide additional passive forces. On the medial side (see Figure 2.10(a)), the medial collateral ligament, which consists of an anterior, posterior, and transverse part, is the most important. On the lateral side, the radial collateral ligament and the annular ligament are the most important for the stability of the elbow (see Figure 2.10(b)).

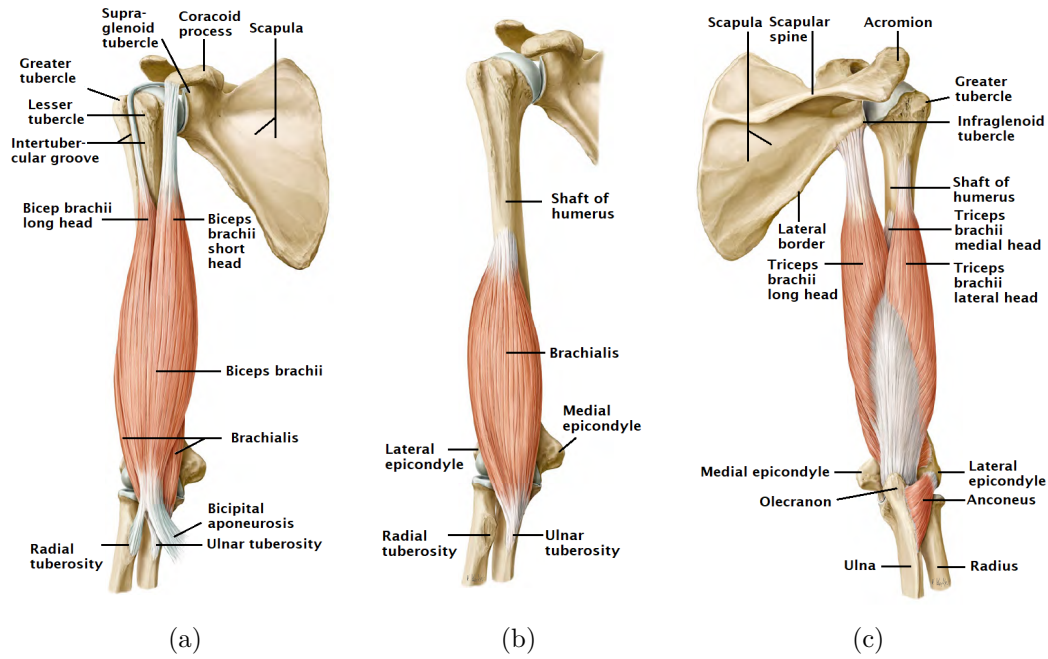


Figure 2.9: Muscles crossing the elbow joint that are responsible for his full ROM - adapted from Schünke et al. (2014) - Figure 25.31-32

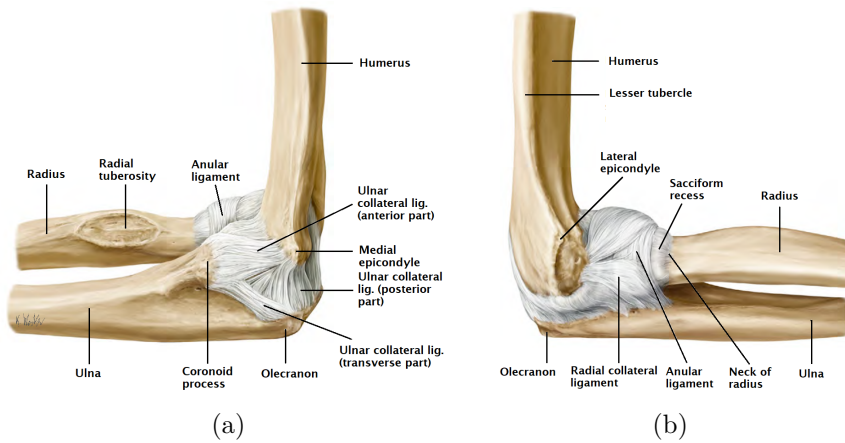


Figure 2.10: Ligamentous apparatus of the elbow - from (a) the medial side (b) the lateral side - adapted from Schünke et al. (2014) - Figure 26.4

Chapter 3

The AnyBody modeling system

Underlying principle

For all musculoskeletal simulation performed in this thesis the AnyBody™ Modeling System (AMS) was used. The AMS uses a holistic human body model and is based on the inverse dynamics principle. Using recorded kinematics (gained by motion capture measurements) and the gained external forces as boundary conditions the AMS is able to calculate the corresponding muscle forces and hence joint reaction forces by solving the following equilibrium equation.

$$Cf = r$$

where $f = [f^{(M)}, f^{(R)}]$ is a vector of muscle and joint forces (whereby $f^{(M)} \geq 0$ and $f^{(M)} \leq f_{i,max}^{(M)}$ as muscles can only pull and not push, and can not exceed their maximal force), r is a vector representing the external and inertia forces, and C is a matrix of equation coefficients.

Since the human body is a redundant system, there is no one unique solution for the equation above for a given combination of motion and external forces. Mathematically, this would result in an infinite number of solutions. However, this problem can be solved in the AMS with the help of an optimization problem of the following form:

$$\begin{aligned}
& \underset{f}{\text{minimize}} \quad G(f^{(M)}) \\
& \text{subject to} \quad Cf = r \\
& \text{with } f_i^{(M)} \geq 0, \quad i = 1 \dots n^{(M)} \quad \text{and} \quad f_i^{(M)} \leq f_{max}^{(M)}, \quad i = 1 \dots n^{(M)}
\end{aligned}$$

where G is the objective function, which defines the criterion for the muscle recruitment and is minimized with respect to all unknown forces in $f = [f^{(M)}, f^{(R)}]$. There are different variants for the objective function. A variant most commonly used to describe muscle recruitment by the nervous system is the following polynomial criterion:

$$G(f^{(M)}) = \sum_{i=1}^{n^{(M)}} \left(\frac{f_i^{(M)}}{N_i} \right)^p$$

where p is the power of the polynomial representing the muscle synergy - the larger p gets, the greater is the muscle synergy and hence the forces are more distributed to all muscles. N_i is the normalization factor of a muscle - the maximal strength f_{max} is usually used for this purpose.

Upper extremity within AnyBody

Depending on the research question to be investigated, a different level of detail of the musculoskeletal model is required. If a model does not show an appropriate level of refinement, the research question may not be answered with sufficient accuracy. While the development of an accurate model of the lower extremity has received considerable attention in recent years (Carbone et al. 2015), less attention has been devoted to the upper extremity.

Looking at the current AMS elbow model, it is apparent that the entire ligamentous apparatus, which is of great importance for the stability of the elbow, is omitted. In addition, the cubital angle (the angle which is formed by the humeral, elbow and wrist), which according to the literature is between 5° and 15° in humans (Oppenheim et al. 1984), is not taken into account at all, so that this angle is set to 0° by default in the AMS.

As far as the hand is concerned, the current AMS includes a distinction between a detailed and an undetailed hand model. In the undetailed model, the hand consists of only one rigid body and thus the ROM is limited to flexion/extension and ulnar/radial abduction of the wrist. While the detailed hand model represents the individual bones by respective rigid bodies, some limitations have to be noted: There are no intrinsic hand muscles in the detailed hand model, and even the extrinsic hand muscles extend only to the distal end of the metacarpal bones. Furthermore, the MCP joint lacks the degree of freedom (DOF) for abduction of the fingers and patient-specific scaling of the individual phalanges.

In order to answer clinically relevant research questions, these limitations of the existing hand and elbow model need to be addressed. Consequently, it is necessary to develop and validate a new corresponding model.

Chapter 4

Hand model: model development

A part of the following chapter has been published in a similar form in the Journal for Computer Methods in Biomechanics and Biomedical Engineering under Engelhardt and Melzner et al. (2020).

4.1 Introduction

The human hand is a highly developed and sophisticated grasping organ containing 27 bones with 36 articulations and 39 active muscles (Kehr and Graftiaux 2017). This contributes to a wide ROM (31 DOFs) while possessing sensitive haptic properties. For controlling this complex system, a high level of interaction between the human brain and the musculoskeletal structure is required. To address various malfunctions because of disorders of the musculoskeletal system, the inverse dynamics modeling approach is an increasingly applied method. With this method, the complex dynamic force distribution in all hand structures can be analyzed in numerous kinds of tasks for physiological as well as for pathological simulations. Research questions regarding the prevention or rehabilitation of the biomechanics of the hand can be explained without the requirement for in vivo or in vitro experiments. Mechanical loads within the hand do not only affect muscle activities and forces in the surrounding joints but also lead to balancing forces in the entire body.

Therefore, a diversified field of problems does not rely on the biomechanics of an isolated hand model alone, but an embedment into a holistic human body model. Numerous research groups conducted musculoskeletal simulations of the human hand over recent decades.

Holzbaur et al. (2005) implemented an entire upper limb model, including the human hand within the OpenSim (Seth et al. 2018) framework. This model is based on the experimental and anatomical data of An et al. (1979), Lieber et al. (1990), Jacobson et al. (1992), Lieber et al. (1992), and Murray et al. (2000). The model copes with 26 muscles crossing the wrist and finger joints, but lacks the intrinsic muscles.

Lee et al. (2015*b*) solved this limitation by implementing intrinsic muscles for the fingers. On the basis of the experimental data of An et al. (1979), the muscle pathing was optimized to achieve an improved alignment with the moment arm behavior of each joint (Lee et al. 2015*a*). Further enhancements regarding the length-dependent passive properties of the extrinsic index finger muscles was done by Binder-Markey and Murray (2017).

The model from Ma'touq et al. (2019) also included the biomechanics of the thumb and its intrinsic muscles based on the same literature data as Lee et al. (2015*a*) and Lippert (2006). In contrast to the previous ones, this model implements the human forearm and hand as a standalone framework in Simulink® (The MathWorks, Inc., USA). As proposed by Mirakhorlo et al. (2018) and Kerkhof et al. (2018), the usage of one single source for anatomic data is fundamental.

De Monsabert et al. (2018) showed that using multiple sources instead of a single one can lead to errors of up to 180% in the calculated muscle forces. Therefore, Mirakhorlo et al. (2018) implemented an OpenSim hand/wrist model, based on an anatomical study of one single cadaver specimen (Mirakhorlo et al. 2016). Nevertheless, it is a standalone model of the upper extremity based on one cadaver and can thus not be used in a broader scope.

The AnyBody Modeling System (AMS) is a musculoskeletal modeling platform containing body scaling functions that incorporate body mass and percentage of fat and influence the muscle and bone dimensions accordingly, which features a patient-specific scaling of the hand model. The AMS is a widely applied simulation platform for musculoskeletal modeling using an inverse dynamics approach. Fur-

thermore, it contains sophisticated algorithms to optimize complex motion capture data, like the movement of thumb and fingers. The AMS also provides the Any-Body Managed Model Repository (AMMR) (Lund et al. 2019), which includes a generic human body model and a collection of human body parts. The AMMR contained only single fingers in detail by Wu et al. (2008, 2009), which are not implemented in the full-body model. A complete comprehensive model of the hand was still lacking.

Therefore, the aim of this thesis was the development and validation of a detailed human hand model within an existing, commonly used framework for inverse dynamics simulation, including:

- Anatomical data from a consistent source containing sixteen cadaveric specimens
- All intrinsic and extrinsic muscles of the entire hand (fingers and thumb)
- The possibility of patient-specific scaling

4.2 Hand model

The detailed hand model was embedded in the AMS Version 7.2 and AMMR 2.2.2 (Lund et al. 2019). The AMMR full-body model was used as a basis. Only the forearm and hand were modified. For the proposed detailed hand model, 22 hand segments (including ulna and radius) modeled as rigid bodies linked by physiological idealized joints were used, allowing 31 DOFs. The joints of the DIP and PIP were modeled as revolute joints for flexion/extension movements and the MCP joint as a universal joint. Hereby flexion/extension and ab/adduction were achieved. Joint positioning and orientation was achieved in accordance to literature studies (An et al. 1979, Buchholz et al. 1992) and an anatomical study by the University of West Bohemia (UWB) (Havelková et al. 2020), following the International Society of Biomechanics recommendations for joint coordinate systems (Wu et al. 2005). Further, the axes of rotation of the thumb's joints were modeled in separated revolute joints as depicted by Hollister et al. (1995). To reduce the complexity, the carpal bones were treated as one rigid body as in other

models described in the literature (Lee et al. 2015b, Mirakhorlo et al. 2018, Ma'touq et al. 2019). The wrist joint has two rotational axes according to Kobayashi et al. (1997), which implies flexion/extension and ab/adduction.

4.2.1 Anatomical data set

Anatomical data were obtained by a study at the UWB by Havelková et al. (2020), which included dissecting sixteen cadaveric forearms and magnetic resonance imaging scans. Through this study, the patient-specific bone surfaces and muscle properties like physiological cross-sectional area (PCSA), muscle length, and origin, via-, and insertion points, as well as the alignment of the muscles were obtained. The whole data set, including a short description of the data obtaining procedure, is freely available (Havelková et al. 2020). The means of all values were calculated and implemented into the model. Because the use of multiple anatomical data can lead to large deviations in the result according to De Monsabert et al. (2018), the mean values of the sixteen measured samples were calculated and implemented into the model. Further, the muscle alignment was obtained according to the magnetic resonance imaging scans of one exemplary cadaver specimen of the anatomical study.

4.2.2 Patient-specific scaling and muscle alignment

Regarding patient-specific scaling, it is not always feasible to measure all dimensions of each finger segment. However, Buchholz et al. (1992) proposed a linear correlation r_s between the hand length l_H and that of each finger bone l_s .

$$r_s = \frac{l_s}{l_H}$$

Because the study of Buchholz et al. only included the dimensions of six hands, a study with the X-ray data of 71 patients (anonymous anterior posterior X-Ray scans of entire human hands - 49 women and 22 men) was performed to determine a more accurate relationship. To determine the relative lengths of the individual finger bones, all bone lengths were measured and related to the respective hand.

This results in the following data for all fingers as shown in Table 4.1. The average hand length was 190.5 mm (± 12.7 mm) and the average hand width was 84.7 mm (± 6.4 mm).

Thus, the length of the metacarpal (MC) and the proximal-, middle-, and distal phalanges (PP, MP, DP) can be scaled according to the hand length. The scaling of the model affects not only the length of the segments but also the dimension of the wrapping surfaces, assuring an appropriate alignment of the muscle paths. Therefore, various obstacles like tori, cylinders, and ellipsoids were implemented to guarantee a correct and physiological alignment of the muscle tendons – also in extreme positions of the fingers.

Table 4.1: Relative segment lengths (to hand length) of each phalanx (distal phalanx (DP), middle phalanx (MP), proximal phalanx (PP), and metacarpal (MC)) in percent and corresponding standard deviation.

Finger	DP	MP	PP	MCP
Thumb	11.52 (0.99)	-	15.76 (1.32)	23.38 (1.72)
Index	8.82 (1.10)	11.75 (1.00)	20.27 (1.44)	34.82 (2.44)
Middle	9.30 (0.77)	14.31 (1.11)	22.54 (1.54)	33.41 (2.36)
Ring	9.54 (0.84)	13.62 (1.04)	21.05 (1.40)	29.48 (2.07)
Small	8.43 (0.92)	9.56 (1.04)	16.72 (1.20)	27.811 (1.88)

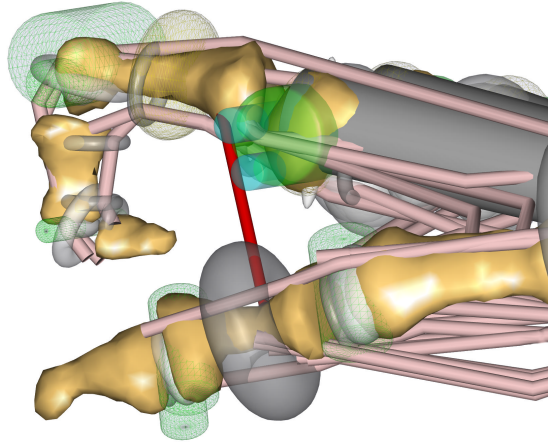


Figure 4.1: Visualization of all wrapping obstacles of the hand model.

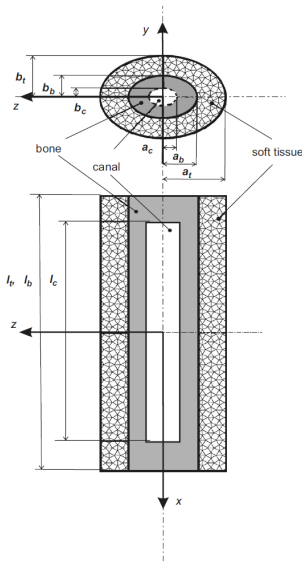


Figure 4.2: According to Wu et al. (2008) the phalanx is approximated by a superposition of ellipsoidal cylinder of a cavity, bone and soft tissue

4.2.3 Moments of inertia

The single phalanx of the finger can be regarded as a hollow bone surrounded by soft tissue. As an approximation, an ellipsoidal cylinder can be assumed for both bone and soft tissue (Robertson et al. 2013) - see Figure 4.2.

Based on this assumption, the individual mass moments of inertia can be calculated as the sum of the one of soft tissue and bone respectively (Wu et al. 2008) according to:

$$\begin{aligned} I_{xx} &= I_{xx}(\text{tissue}) + I_{xx}(\text{bone}) \\ &= \frac{\pi\rho_t}{4}[(a_t b_t l_t)(a_t^2 + b_t^2) - (a_b b_b l_b)(a_b^2 + b_b^2)] + \frac{\pi\rho_b}{4}[(a_b b_b l_b)(a_b^2 + b_b^2) - (a_c b_c l_c)(a_c^2 + b_c^2)] \end{aligned}$$

$$\begin{aligned} I_{yy} &= I_{yy}(\text{tissue}) + I_{yy}(\text{bone}) \\ &= \frac{\pi\rho_t}{12}[(a_t b_t l_t)(3a_t^2 + l_t^2) - (a_b b_b l_b)(3a_b^2 + l_b^2)] + \frac{\pi\rho_b}{12}[(a_b b_b l_b)(3a_b^2 + l_b^2) - (a_c b_c l_c)(3a_c^2 + l_c^2)] \end{aligned}$$

$$\begin{aligned} I_{zz} &= I_{zz}(\text{tissue}) + I_{zz}(\text{bone}) \\ &= \frac{\pi\rho_t}{12}[(a_t b_t l_t)(3b_t^2 + l_t^2) - (a_b b_b l_b)(3b_b^2 + l_b^2)] + \frac{\pi\rho_b}{12}[(a_b b_b l_b)(3b_b^2 + l_b^2) - (a_c b_c l_c)(3b_c^2 + l_c^2)] \end{aligned}$$

where a is the half width, b the half depth, l the length of the cylinder, and ρ the mass density ($\rho_t = 1.0 \text{ g/cm}^3$ and $\rho_b = 1.9 \text{ g/cm}^3$ according to Abé et al. (1996)). For the calculation of the moments of inertia within the model, half width and depth (a and b) are taken from the study by Wu et al. (2008) and the length of the individual fingers is determined using the scaling function (see section 4.2.2). For the bone cavity, 75% of the total length of the finger bone was assumed.

4.2.4 Finger rhythm

In the AMS, it is possible to implement kinematic dependencies between individual joints by defining so-called rhythms, such as the shoulder rhythm (dependency between scapula and clavicle) and the lumbar rhythm (dependency between the lumbar vertebral bodies). Due to the fact that there is also a kinematic dependency between the PIP and DIP joints (Van Zwieten et al. 2015), a finger rhythm was implemented in the hand model based on data from Van Zwieten et al. (2015) (see Figure 4.3) allowing to control the joint angle of the DIP joint via the angle of the PIP joint.

This is important for two reasons. On the one hand, it allows for the realization of a natural hand movement in a hand-driven model. On the other hand, it makes marker tracking based motion capture recordings possible in situations, in which no markers can be applied to the fingertips or the markers are concealed, for instance.

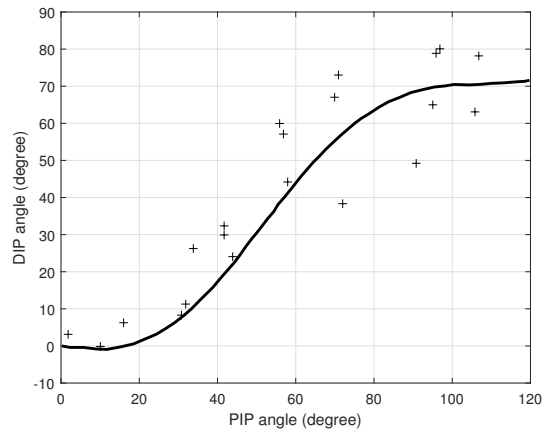


Figure 4.3: Experimental data (crosses) and analytical fit (line) of DIP–PIP flexion angles for a finger according to Van Zwieten et al. (2015)

4.2.5 Muscle on a muscle

Another unique feature of the human hand is the origin points of the lumbricals. In contrast to regular muscles, the lumbricals do not originate from a bone, but the tendon of the flexor digitorum profundus. Therefore, the force of the lumbrical is transmitted onto the flexor digitorum profundus tendon. The following example illustrates how this was realized from the modeling side - introducing the concept "*muscle on a muscle*".

Therefore, let's consider a model consisting of three muscles and two segments connected by a universal joint (which only locks the rotation around the longitudinal axis) (see Figure 4.4(a) and 4.4(b)). For one of the three muscles (muscle C), the insertion point should be on the muscle line of action of another muscle (muscle B).

For this purpose, a mass-less dummy segment is created. In order to determine this segment in space, the rotational DOFs are closed via a corresponding driver, which accesses the rotational measure between the global coordinate system and the dummy segment. The translational degrees of freedom are closed via a linear combinatorial measure between the dummy segments and the origin, as well as between origin and insertion point. An offset can be used to specify the relative distance between the origin and the insertion point at which the dummy segment is placed. With this method, the dummy segment is also able to transmit forces, as the following example demonstrates.

If a flexion of the joint is performed, muscle B is mainly responsible for flexion, whereas muscles A and C are also involved in medial/lateral stabilization of the joint. Figure 4.5(a) shows the activity of the three muscles during flexion. If an activity bound is set to ensure a muscle activity of at least 20% of muscle C, the results shown in Figure 4.5(b) were obtained. As can be seen, artificially increasing the activity of muscle C also results in an increase in the activity of muscle A - the additional transmitted force of muscle C creates a moment along the medial/lateral axis of the joint, which in turn can only be counterbalanced by muscle A.

Through this minimal example, the functioning and functionality of the "*muscle on a muscle*" concept could be illustrated.

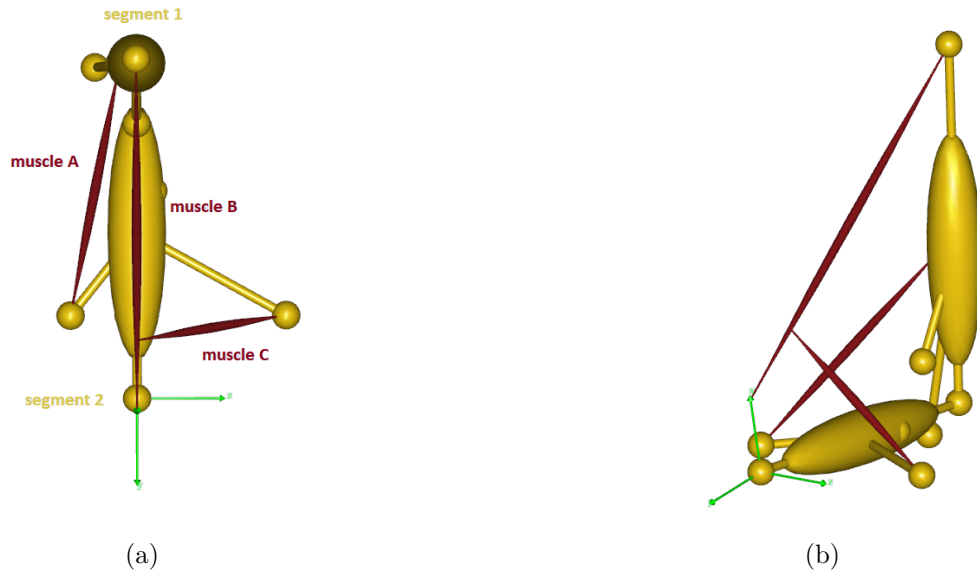


Figure 4.4: Model to evaluate the concept "muscle on a muscle" - consisting of two segments and three muscles. (a) top-view (b) side-view

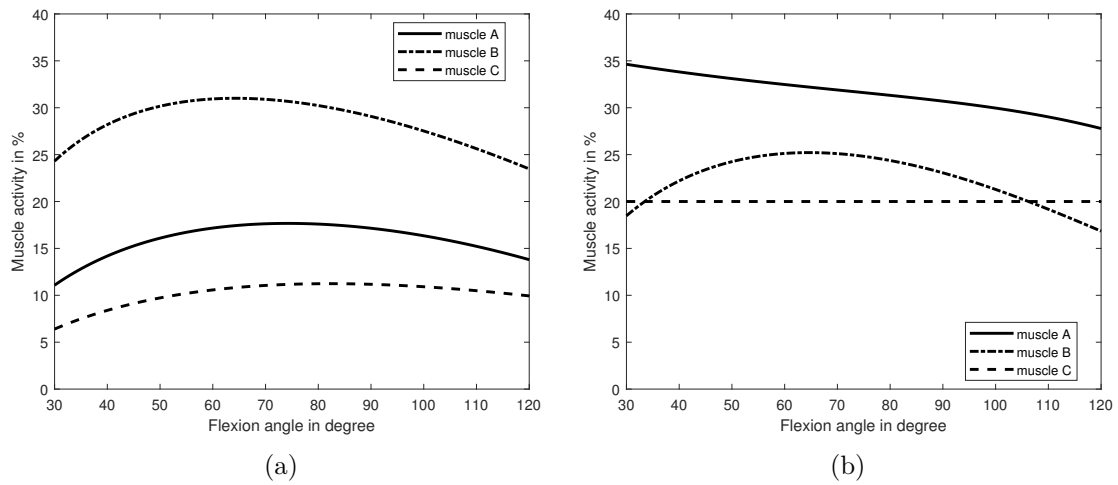


Figure 4.5: Activity of muscles A - C during flexion of the joint from 30° to 120° . (a) "normal" muscle activity (b) muscle activity with generated muscle bound of 20% for muscle C.

4.2.6 Purlicue skin

To model the strengthening of the skin between the fingers during ab/adduction, ligaments simulate the skin resistance. Properties are according to the material investigations by Gallagher et al. (2012). The zero position was assumed according to the positioning of the fingers shown in Figure 4.6. The red line depicts the ligament representing the purlicue skin resistance.

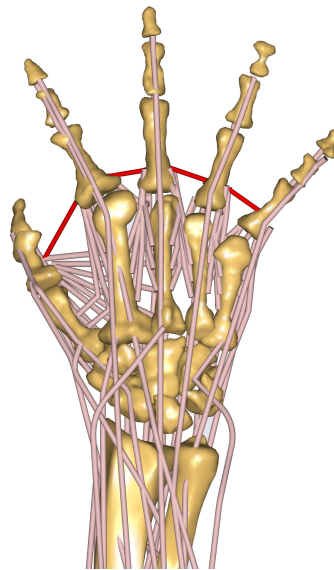


Figure 4.6: The proposed detailed musculoskeletal hand model in the AMS (configuration WRAP-SINGLE). The position of the fingers corresponds to the calibration position of ligaments to simulate the purlicue skin resistance (red).

4.2.7 Choice of model accuracy

Because this detailed representation and guidance of each muscle increased the computational time during the calculation of kinematics and kinetics, the model contains four different stages of accuracy:

- switch between fully detailed muscle alignment in the fingers through wrapping obstacles (WRAP) or via-points (VIA) (see Figure 4.1).
- selection between a splitting of the extrinsic hand muscles in various representatives according to their anatomical origins (MULTIPLE) or one representative for each extrinsic hand muscle (SINGLE) (see Figure 4.7).

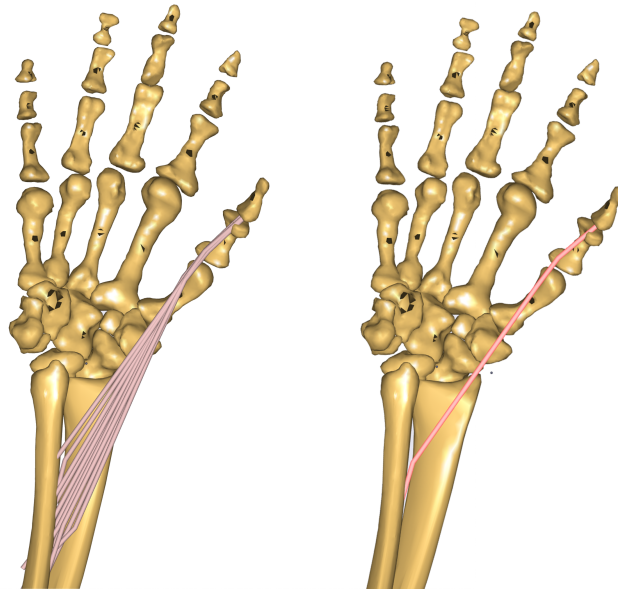


Figure 4.7: Detailed hand model with several representatives of one muscle (FPL) – left side. Hand model with only one representative for the same muscle – right side.

Chapter 5

Hand model: moment arm validation

A part of the following chapter has been published in a similar form in the Journal for Computer Methods in Biomechanics and Biomedical Engineering under Engelhardt and Melzner et al. (2020).

5.1 Validation

For validation purposes, moment arms numerically calculated by the model and experimentally measured moment arms from the literature were compared. This approach was chosen because studies of Maury et al. (1995) and Raikova and Prilutsky (2001) indicated that the line of action and moment arms are critical parameters for muscles to predict muscle and joint reaction forces. Previous validation studies of the AMS by De Zee et al. (2007) and Marra et al. (2015) showed that simulated muscle activities and joint reaction forces fit quite accurately to experimental data. Therefore, when the moment arms of the proposed model fit experimental data, the resulting muscle activities and joint reaction forces of the hand should also correspond to reality.

Even though the model is able to calculate inverse dynamics, this study placed particular emphasis on the importance of the muscle moment arms, and thus on the correct kinematics.

Loren et al. (1996) obtained the muscle moment arm in five upper extremities for the extension/flexion as well as for the ulnar/radial abduction of the wrist. Smutz et al. (1998) used seven cadaveric specimens to obtain the moment arm considering the thumb. The ROM contained the flexion/extension of the DIP joint, the flexion/extension and ab/adduction of the MCP joint, and the flexion/extension and ab/adduction of the CMC joint. In case of the index finger, An et al. (1983) conducted movements of the flexion/extension of the MCP, PIP, and DIP as well as ab/adduction of the MCP joint. Thereby seven cadaveric hands were evaluated. The results of Franko et al. (2011) stated that the moment arms are nearly identical across all digits for each joint (MCP, PIP, DIP). Therefore, for validation purposes, only one finger (the index finger) needed to be addressed. The muscles examined in all three studies are summarized in Table 5.1.

The tendon excursion method introduced by Landsmeer (1961) was used to compute moment arms in experiments (An et al. 1983, Loren et al. 1996, Smutz et al. 1998, Franko et al. 2011) and simulation models. The tendon excursion method uses the length variation of the tendon (dx) because only one axis of a joint is moved and the angular change of the joint (ϕ) to calculate the moment arm (M) of the specific muscle in respect to the chosen joint (An et al. 1983).

$$\frac{dx}{\phi} = M$$

The model was scaled to an average 50 percentile male person (hand length: 182 mm, hand breadth: 85 mm) unless the literature data provided anthropometrics of single specimens (An et al. 1983). To compare the numerical and experimental results, the same kinematic motion was performed in the simulations as in the experiments. Thereby, only the investigated joints were moved through the ROM provided by the literature, all others were locked in neutral position.

Table 5.1: Examined muscles according to the studies of Loren et al. (1996), Smutz et al. (1998), and An et al. (1983).

Wrist joint	
extensor carpi radialis brevis	(ECRB)
extensor carpi radialis longus	(ECRL)
extensor carpi ulnaris	(ECU)
flexor carpi radialis	(FCR)
flexor carpi ulnaris	(FCU)
Thumb	
flexor pollicis longus	(FPL)
extensor pollicis longus	(EPL)
extensor pollicis brevis	(EPB)
abductor pollicis longus	(APL)
flexor pollicis brevis	(FPB)
abductor pollicis brevis	(APB)
adductor pollicis oblique head	(APo)
adductor pollicis transverse head	(APt)
opponents pollicis	(OP)
Index finger	
flexor digitorum superficialis	(FDS)
flexor digitorum profundus	(FDP)
extensor digitorum communis	(EC)
extensor indicis	(EI)
first dorsal interosseous	(FDI)
lumbrical	(LU)
first palmar interosseous	(FPI)

5.2 Results

Figure 5.1 - 5.3 show exemplary the comparison of the experimentally gained literature data and the numerically calculated muscle moment arms of selected muscles. The main flexors and extensors of the wrist follow the trend of the experimental data (Loren et al. 1996) for the flexion/extension of the wrist and remains mostly within the standard deviation (SD); only the FCR muscle displays a small offset (Figure 5.1). Regarding the flexion/extension of the MCP finger joint (5.2) the model prediction shows a comparable progression as the literature data (An et al. 1983), whereby it should be noted that the experimental data is based only on a single finger. Additionally, for the MCP joint of the thumb, the numerically calculated moment arms of the selected flexor/extensor thumb muscles remain within the SD of the literature experiments (Smutz et al. 1998) (Figure 5.3). The progression of all muscles over the flexion/extension and ab/adduction ranges can be found in the Appendix A.

However, An et al. (1983) only provided the exact progression of an exemplary finger for the flexion/extension and ab/adduction along the MCP joint. For the measurements of all examined patients' fingers and all joints (including the PIP and DIP joints), only the mean values along the ROM are given. For this reason, the mean moment arms along the ROM for all muscles and joints are summarized in Table 5.2 for a better comparability. For all simulations, a detailed muscle alignment through wrapping obstacles and one representative for each extrinsic hand muscle were chosen (configuration: WRAP-SINGLE). The hand model was scaled in size according to the literature data.

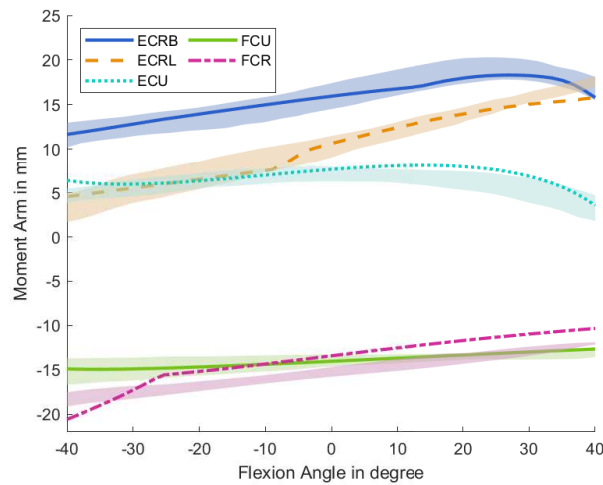


Figure 5.1: Progression of the moment arms for the wrist regarding the extensor and flexor muscles during the extension/flexion phase. Negative angles represent the extension of the wrist, and positives the flexion. Lines represent the simulated results, whereas the shaded areas are the experimental results with SD from Loren et al. (1996).

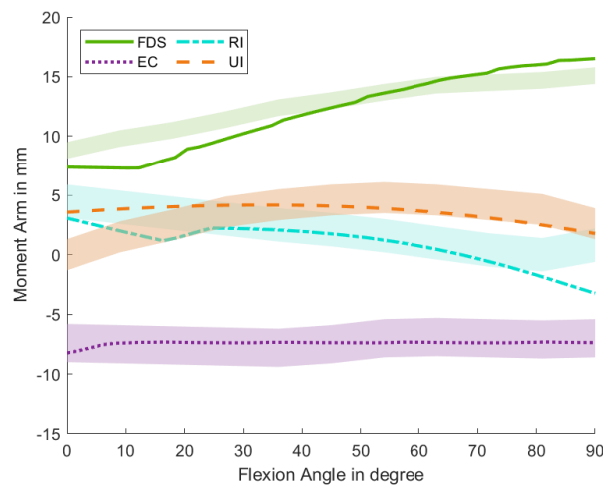


Figure 5.2: Progression of the moment arms for the index finger regarding extrinsic and intrinsic hand muscles during the flexion of the MCP joint. Lines represent the simulated results, whereas the shaded areas highlight the experimental data of one subject with SD from An et al. (1983).

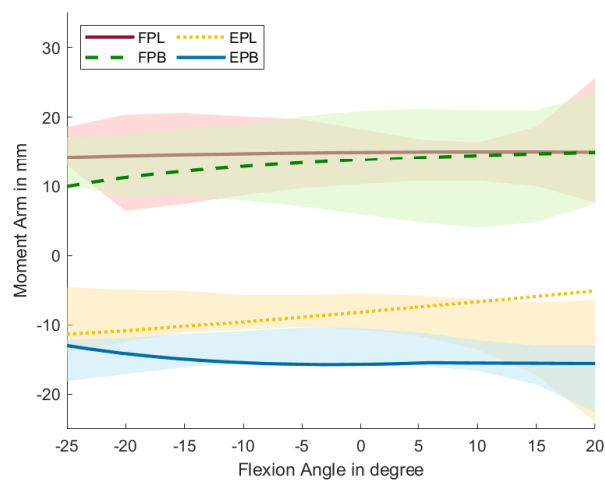


Figure 5.3: Progression of the moment arms for the thumb regarding extensor and flexor muscles during flexion around the CMC joint. Negative angles represent the extension of the CMC joint, and positives the flexion. Lines represent the simulated results, whereas the shaded areas highlight the experimental data with SD from Smutz et al. (1998).

Table 5.2: Mean muscle moment arms (and SD) in mm of the index finger, thumb and wrist during the ROM (extension/flexion, abduction/adduction).

Index Finger		FDS	FDP	EC	EI	RI	LU	UI		
MCP	Model	12.18	8.79	-7.37	-7.37	1.38	10.39	3.81		
Flex/Ext	Exp.	11.9 (0.7)	11.1 (1.1)	-8.6 (1.6)	-9 (1.3)	3.7 (1.4)	9.3 (2.1)	6.6 (2.1)		
MCP	Model	0.13	0.82	0.80	0.29	-7.81	-7.66	12.79		
Abd/Add	Exp.	1.7 (2.0)	1.1 (1.7)	-0.2 (2.5)	1.3 (1.6)	-6.1 (2.1)	-4.8 (1.6)	5.8 (1.7)		
PIP	Model	5.75	7.77	-4.09	-4.02	-	0	0		
Flex/Ext	Exp.	6.2 (1.0)	7.9 (1.1)	-2.8 (1.1)	-2.6 (1.1)	-	-1.8 (1.3)	-2.6 (0.8)		
DIP	Model	-	4.29	-3.67	-3.68	-	0	0		
Flex/Ext	Exp.	-	4.2 (1.4)	-2.2 (0.4)	-1.9 (0.5)	-	-0.7 (0.6)	-1.6 (0.5)		

Thumb		FPL	FPB	EPL	EPB	APL	APB	APt	APo	OP
CMC	Model	14.81	13.24	-8.44	-15.18	-13.07	-0.07	32.15	13.91	0.79
Flex/Ext	Exp.	14.49 (5.02)	13.43 (6.52)	-9.62 (3.93)	-14.39 (2.75)	-7.69 (3.57)	3.36 (3.70)	31.32 (7.68)	22.91 (10.80)	12.56 (5.08)
CMC	Model	-4.45	-9.72	1.12	-0.35	-0.09	-17.95	17.47	-0.24	-8.52
Abd/Add	Exp.	-1.18 (3.84)	-9.41 (5.83)	7.42 (5.28)	-3.58 (4.59)	-9.71 (2.99)	-15.13 (7.08)	16.46 (11.38)	13.62 (12.04)	-4.72 (5.00)
MCP	Model	8.86	6.83	-6.58	-8.49	0	5.04	9.6	-	-
Flex/Ext	Exp.	9.91 (2.16)	6.64 (1.65)	-9.69 (1.44)	-9.04 (1.16)	1.36 (2.21)	6.78 (4.56)	5.26 (3.06)	-	-
MCP	Model	-0.57	-5.17	3.64	1.64	-7.58	8.4	3.27	-	-
Abd/Add	Exp.	-0.06 (2.41)	-8.83 (3.27)	4.37 (1.86)	-1.04 (1.43)	-10.77 (4.39)	4.93 (4.23)	2.96 (4.36)	-	-
DIP	Model	5.86	-	-4.97	-	-	-	-	-	-
Flex/Ext	Exp.	7.82 (1.31)	-	-4.18 (0.77)	-	-	-	-	-	-

Wrist		ECRB	ECRL	ECU	FCR	FCU
Wrist	Model	15.58	10.24	6.86	13.84	13.96
Flex/Ext	Exp.	13.47 - 16.42	8.49 - 10.87	4.21 - 6.35	15.00 - 16.22	13.27- 15.05
Wrist	Model	16.32	21.73	20.03	5.04	16.28
Abd/Add	Exp.	13.99 - 15.79	21.08 - 23.09	25.83 - 29.51	4.01 - 7.13	19.82- 23.59

5.3 Discussion

The aim of this work was the implementation and validation of a developed, detailed hand model in the simulation environment of the AMS. In addition to the successful implementation of a scalable, anatomically representative hand model, the validation by moment arm patterns displays matching results.

Wrist joint

Moment arm patterns inside the wrist display a good alignment with data from the literature, according to Loren et al. (1996). Furthermore, the decay in the ECU muscle during high flexion is predicted accurately, whereas the FCR follows the trend of the data from Loren et al. but showing a small offset.

Regarding the mean moment arm through the ROM, only small deviations from the literature data for the ECU and FCR in extension/flexion and during ab/adduction for the ECRB are notable. All other muscle moment arm averages are within the SD of the compared data. Exceptions are the ECU and FCU muscle during the ab/adduction phase, which show differences up to 5.8 mm. This deviation could result in the patient specification or measure inaccuracies of the experimental data set, because a moment arm of approximately 20 mm/16 mm for the ECU/FCU appears reasonable.

Index finger

The comparison with the data from An et al. (1983) shows that the majority of the respective muscles are within the average moment arms SD or display divergences of less than 1 mm apart. In particular, the intrinsic muscles (LU, RI, UI) show a greater discrepancy in the experimental data than the extrinsic ones. One reason could be that the moment arms of intrinsic muscles are more patient-specific than the extrinsic muscles, which was previously noted by Mirakhorlo et al. (2018). Regarding the progression of the muscle moment arms during the MCP flexion phase, the simulated muscle paths agree well with the experimental observations.

Thumb

The large SD of the experimental dataset from Smutz et al. (1998) shows that the anatomical structure of the thumb can vary considerably among subjects, particularly for the intrinsic muscles. Alternatively, the high SD of the experimental data by Smutz et al. could originate from measurement errors.

Regarding the mean moment arm along the ROM, the majority of the thumb muscles are within the SD. Greater differences occur at the CMC joint for the OP, APo, and APL. The divergence for the APL might originate from the insertion point of the underlying anatomical data set from Havelková et al. (2020), because the insertion point is located closer to the joint than in the experimental data, which restricts the moment arm of the APL. Nevertheless, the simulated moment arm progressions of the extrinsic muscles align well with the data from Smutz et al. (1998). The depicted results show similar moment arm patterns as previously published models by Ma'touq et al. (2019), Mirakhorlo et al. (2018) or Lee et al. (2015b).

Together with the generalized anatomical data set, this leads to the conclusion, that the proposed model represents the musculoskeletal mechanics of the human hand in an accurate manner. Therefore, the muscle forces and joint reaction forces calculated with this model should reflect reality as closely as possible.

Anatomical variability needs to be emphasized in any type of musculoskeletal model, it therefore needs to be kept in mind, that patient specific variations of muscle alignments and unique musculatures can not be considered by such a generalized model. The patient specific scaling in size might cope the most significant anatomical changes in muscle alignment and joint placement, but is limited to this scaling.

To ensure the most accurate possible answers to any research questions, the model is scalable to subject-specific anthropometric data. The necessary degree of detail (WRAP, VIA, MULTIPLE, SINGLE) can be adapted. Additionally, the use of the consistent anatomical dataset (Havelková et al. 2020) from multiple specimens provides generalizability of the model, as claimed by De Monsabert et al. (2018). In addition to many features that contribute to the preciseness of the model, the first implementation of the LU muscles with origins on the FDP tendon leads to

a more accurate prediction of the intrinsic muscle activities. Thereby, the force equilibrium between, for example, the two LU of the index finger, is achieved more physiologically, because each crosses the MCP joint on each side.

Nevertheless, the model is limited, because the origins of the LU muscles are fixed on the neutral position of the FDP tendons, but do not change position when the FDP muscles are contracted. By contrast, simulations show that a manual shifting of the LU origin point according to the calculated shortening of the FDP tendon would only lead to a change in the LU moment arm of 1 mm. Considering the way the moment arm is calculated using the tendon excursion method, this limitation of the LU being fixed explains that the intrinsic muscles have no moment arm in the PIP and DIP joint compared to the experimental data (see Table 5.2).

Regarding the different configurations, computational costs, and the accuracy of the results, the following could be stated: the most detailed model includes more wrapping obstacles within the fingers and more muscle representatives. This increased level of detail leads to the most precise outcome but also more computational expenses and, thus, to an approximately five times longer computational time compared to the simplest detailed model (see Figure 5.4).

As seen in Figure 5.4, the progression of the moment arm is quite similar for the MULTIPLE and SINGLE configurations. This can be explained by the fact that these two configurations differ in the size of the muscles' origin and insertion zone, as indicated in Chapter 4 Figure 4.7. The respective muscle representatives have different muscle paths and correspondingly different moment arms along the wrist and the CMC joint. However, from the MCP on wards, these are all very similar, which leads to only a slight difference in the moment arm for the MCP joint.

The axis of rotation of each joint is not adjusted according to the mean cadaveric specimen data, and therefore, small deviations or offsets of the moment arms can be explained.

The skin resistance between the fingers during ab/adduction is only assumptions according to the data of Gallagher et al. (2012). The material properties of the skin in the forearm by Gallagher et al. are directly transferred to the skin properties because no specific material tests were conducted in the presented anatomic study by Havelková et al. (2020).

Although Eschweiler et al. (2016) had already developed a detailed model of the human wrist within the AMS, this model is not implemented in the proposed detailed hand model, mainly because of the reduction of complexity of the model. The eight carpal bones in the presented model are defined as one rigid segment, allowing no movement between the carpal bones. When the research questions do not address the force distribution inside the wrist joint, Schuind et al. (1995) showed that this lack does not have a great influence on the outcome of the muscle activities. This limitation can be addressed in a future version of the model, where splitting of the wrist joint into an ulnar and radial side might be convenient. Further enhancements might be the implementation of helical joint axes in the thumb joints, as proposed by Kerkhof et al. (2016).

Another point for improvement is the implementation of the extensor mechanism in the fingers. Although the kinematics of the extensor mechanism is partially represented by the finger rhythm, the passive tension whenever it is elongated is currently still omitted when calculating forces in an inverse dynamics simulation. Consequently, slightly altered joint reaction forces on the finger joints could be found, as well as a possible co-contraction in the finger muscles, as stated by MacIntosh and Keir (2017) could be lacking.

In general, the anatomical complexity of the fingers is quite high and the extensor hood is just one example of the inter connectivity within the human hand. Although the model is capable of correctly mapping tendon pulling forces using the obstacle, which transfers forces to segments, passive joint stiffness or damping moments are not yet implemented in the model. How the implementation of these parameters can affect a forward dynamic finger model is shown by Lee and Kamper (2009).

A further step to enhance confidence in the model could be an experimental validation, like a comparison with electromyographical data, as well as testing the outcome of predicted joint reaction forces against measured ones, using instrumented prostheses similar implants of the shoulder of Bergmann (2008).

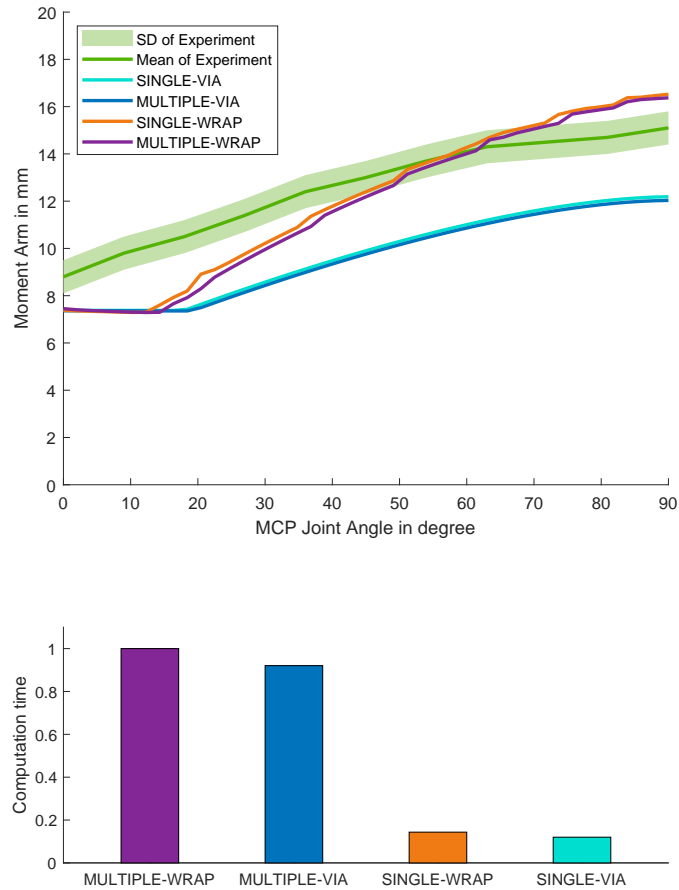


Figure 5.4: Progression of the FDS moment arms during flexion of the MCP index joint with different detailed stages of the model. Clearly notable is, that the model with obstacle methods predicts a better moment arm behaviour. The simple model drastically decreases the computational effort from 100 % (MULTIPLE-WRAP) to 14 % (MULTIPLE-VIA) and from 92 % (SINGLE-WRAP) to 12 % (SINGLE-VIA).

5.4 Conclusion

Chapter 4 presented the development of a musculoskeletal hand model using the AMS framework, that is capable of kinematics as well as inverse dynamics predictions, based on a consistent anatomical dataset. Comparison with experimental moment arm studies showed good correlation and emphasizes the motivation to use the model in an inverse dynamics validation and later in a broad field of applications.

Chapter 6

Hand model: experimental validation

A part of the following chapter has been published in a similar form in the Journal of Biomechanical Engineering under Melzner and Engelhardt et al. (2021).

6.1 Introduction

Musculoskeletal simulations offer enormous potential to provide insights into areas of biomechanics that are difficult to access; especially in areas where numerous mutually influencing structures come together - like in the hand. Over recent decades, numerous research groups have conducted simulations intending to depict this complexity of the human hand (Holzbaur et al. 2005). To address various functions and malfunctions because of disorders of the musculoskeletal system, the inverse dynamics modelling approach is an increasingly applied method.

With this approach, the complex dynamic force distribution in all structures of the hand can be analyzed during activities of daily life for both physiological and pathological evaluations. The major benefit of these models is the enablement of research questions regarding injury prevention and rehabilitation of the biomechanics of the hand without the need for in-vivo or in-vitro experiments. The AMS is a widely utilized simulation software for musculoskeletal modelling using this inverse dynamics approach. The AMS contains body-scaling functions featuring a

patient-specific scaling and algorithms to optimize complex motion capture data, like thumb and finger movements. In future releases of the AMMR, a new comprehensive model of the hand developed in Chapter 4 will be available and for open access. To increase the validation depth of this model, the approach of comparing numerically calculated and experimentally gained moment arms (Franko et al. 2011, Loren et al. 1996, Smutz et al. 1998, An et al. 1983) was used.

This comparison was adopted because studies of Maury et al. (1995) and Raikova and Prilutsky (2001) have indicated that the line of action and moment arms are critical parameters in predicting muscle and joint reaction forces. Therefore, when the moment arms of the proposed model fit experimental data, the resulting muscle activities and joint reaction forces of the hand should also correspond to reality. Furthermore, the above-mentioned models of Holzbaur et al. (2005), Lee et al. (2015b), Mirakhorlo et al. (2018), and Ma'touq et al. (2019) were validated comparing muscle moment arms. However, as stated in the literature (Lund et al. 2012, Hicks et al. 2015), there are many more ways to confirm the validity of a musculoskeletal model. A common type is an indirect validation using the comparison of measured electromyographic (EMG) signals of the muscles with predicted muscle activities of the simulation. Using the EMG signal, the evaluation of the different timings of on- and off-sets of muscle activities between the model and the experiment can result in the validation of a model (De Pieri et al. 2018, Anderson and Pandy 2001).

This experimental validation approach is a decisive step that is necessary in determining whether the model predictions fit the measurements. This consistency between model and reality is crucial when the data obtained from the model (e.g. joint reaction forces) is to be used for answering musculoskeletal research questions. However, to my knowledge, no experimental set-up has to date been conducted in which experimentally captured motion data and simultaneously recorded muscle activities of hand motions are recorded, and the calculated muscle forces of an inverse dynamic approach are compared to the experimental outcomes. Because the moment arm studies of the hand model (see Chapter 5) revealed promising results and a good comparison of the experimental with simulated data, a further trend validation of the model could be realized using measured EMG signals of the muscles.

Therefore, the aim of this study is a further affirmation of the human hand model, based on insights through the EMG results and a more informative trend validation of the new detailed hand model by EMG experiments. This procedure is intended to answer the research question of whether the hand model produces reliable results and, therefore, could be used to address clinical and ergonomic questions in the future – like how the avoidance of certain malfunctions can be used to prevent long-term injuries.

6.2 Materials and Methods

6.2.1 Experimental set-up

To provide a reference dataset for the validation of the musculoskeletal hand model, an experimental study was conducted including five subjects (three males, two females; age = 23.0 ± 2.4 years; weight = 69.2 ± 9.7 kg; height = 1.73 ± 0.11 m; hand length = 18.8 ± 1.4 cm). All persons were right-handed, performing the exercises with their dominant hand, which was not harmed or affected by any illness. Each test person was informed in advance about the procedure of the measurement, and a corresponding written consent was obtained concerning voluntary participation. All procedures performed involving human participation were in accordance with ethical standards and with the 1964 Helsinki Declaration and its later amendments or comparable ethical standards. The anthropometrics of the test persons were obtained to scale the musculoskeletal model afterwards.

For the measurement of the muscle activities, four intrinsic and six extrinsic muscles were considered (see Table 6.1). The EMG activities of these muscles were captured via surface EMG (Delsys Trigno IM and Delsys Trigno Mini, Delsys® Inc., Natick, MA, US.) using the recommended sensor placements according to Criswell (2011) and Barbero et al. (2012). Prior to sensor placement, the skin was cleaned with an alcoholic solution to minimize the influences on the acquired signal resulting from dead skin cells, salt, or grease. For the intrinsic muscles, ECU and FDS, the Trigno Mini sensors were applied, whereas the Trigno IM sensors were used for all others; but all sensor types had the same sampling frequency of 1.1 kHz and recorded only the raw signal without any filters.

Table 6.1: Measured EMG signal of intrinsic and extrinsic muscles. The placement of the sensors was performed according to Criswell (2011)* and Barbero et al. (2012)**. For the measurement, Trigno IM (T-IM) and Trigno Mini (T-Min) sensors from Delsys were applied.

Extrinsic muscles	Sensor	Protocol
Flexor carpi radialis (FCR)	T-IM	**
Flexor carpi ulnaris (FCU)	T-IM	*
Extensor carpi radialis (ECR)	T-IM	*
Extensor carpi ulnaris (ECU)	T-Min	*
Flexor digitorum superficialis (FDS)	T-Min	*
Extensor digitorum (ED)	T-IM	*
Intrinsic muscles	Sensor	Protocol
Abductor pollicis brevis (APB)	T-Min	**
Flexor pollicis brevis (FPB)	T-Min	**
First dorsal interosseous (FDI)	T-Min	*
Abductor digiti minimi (ADM)	T-Min	**

For normalization of the EMG data, maximum voluntary contraction (MVC) measurements following Kendall et al. (1993) were performed. For this purpose, a measuring device was specially constructed - see Figure 6.1. Each subject repeated the MVC measurement three times for each muscle group, and the maximum value was taken as the normalization factor.

The kinematics of each hand movement were recorded with a camera-based motion capture system (Vicon©, Vicon Motion Systems Ltd., Oxford, UK) consisting of 12 cameras. A custom marker set-up of 38 markers (22 on the hand) was designed, capturing the movement of the pelvis, thorax, humerus, forearm, and all segments of the hand. An overview of the marker and EMG sensor placement of the hand is given in Figure 6.2 and in the Appendix - Figure B.1.

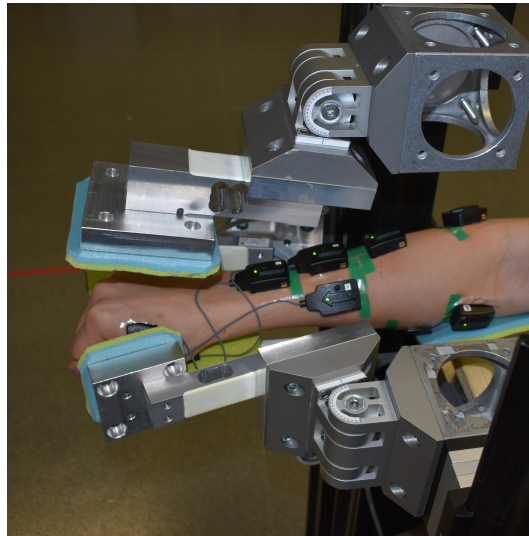
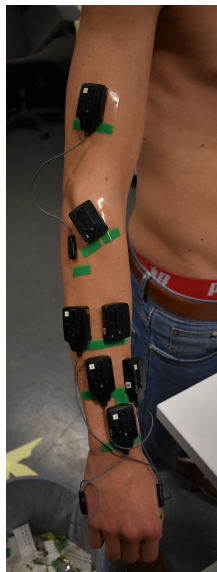
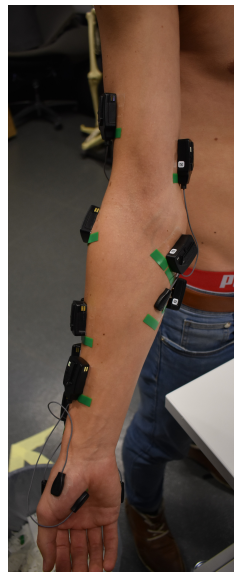


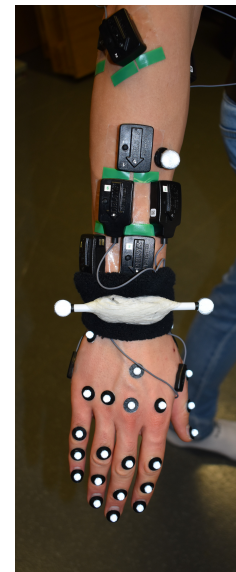
Figure 6.1: Measurement device for the maximal voluntary contraction measurements



(a)



(b)



(c)

Figure 6.2: EMG sensor placement in (a) pronation and (b) supination as well as (c) marker placement of the forearm and hand of a test subject.

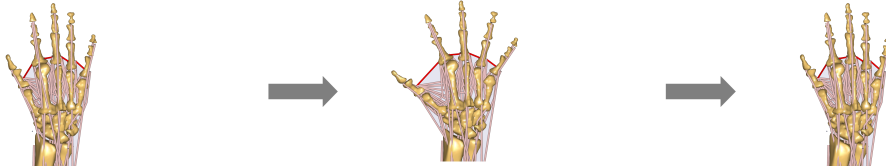
The test subjects performed seven different muscle-specific activation movements for the fingers, thumb, and wrist (see Table 6.3). Additionally, the involved joints and expected active muscles according to Tillmann (2016) are depicted in Table 6.2. Each task was repeated five times within one trial, and each subject repeated every trial three times. Every subject was instructed to use the full ROM in each task and the EMG signals of all sensors were recorded. To guarantee the same initial time of the EMG signals and motion capture recordings, both measuring systems were synchronized.

Table 6.2: Indication the joints moving in each task and the muscles involved in each motion according to Tillmann (2016)

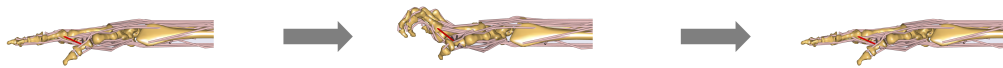
Movement	Involved joint	Involved muscles
Finger ab-/adduction	Metacarpophalangeal joint (finger), carpometacarpal (thumb)	FDI, ADM, FPB, APB
Metacarpophalangeal joint extension	Metacarpophalangeal joint (finger), carpometacarpal (thumb)	ED
Finger flexion	Metacarpophalangeal joint (finger), carpometacarpal (thumb)	FDS
Thumb ab-/adduction	Carpometacarpal (thumb)	FPB, APB
Thumb flexion	Metacarpophalangeal, carpometacarpal (thumb)	FPB, APB
Wrist ab-/adduction	Wrist	FCU, FCR, ECU, ECR, ED
Wrist extension/flexion	Wrist	FCU, FCR, ECU, ECR, ED, FDS

Table 6.3: Sequence of muscle-specific activation movements for the experimental reference dataset. Except for the abduction and flexion of the thumb, the starting position was the pronation of the hand parallel to the floor. For the abduction and flexion of the thumb, the trials were started in a neutral position of the hand. In each movement, the maximal ROM of every subject should be run through.

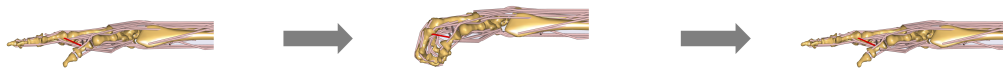
Task 1: Ab-/Adduction of all fingers



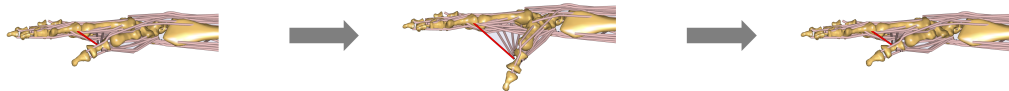
Task 2: Extension of the metacarpophalangeal joint



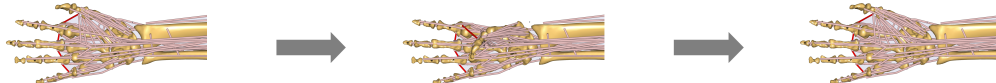
Task 3: Flexion of the fingers



Task 4: Ab-/Adduction of the thumb



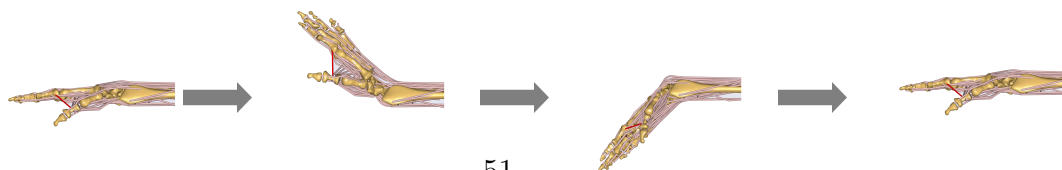
Task 5: Flexion of the thumb



Task 6: Ab-/Adduction of the wrist



Task 7: Ex-/Flexion of the wrist



6.2.2 Simulation

The gained kinematic data were used for the musculoskeletal simulation with AnyBody (AnyBody Technology A/S, Aalborg, Denmark, V. 7. 3 Beta) - see Figure 6.3. For the hand model, the configuration with only one muscle line of action for each muscle but with detailed wrapping pathing was chosen. Since only the EMG signal and motions of the dominant right hand was measured, the left arm segment and both legs of the entire AMMR human body model were omitted for this simulation to reduce the computational time.

Because a strong synergy of muscles within the hand for gross motor skills was assumed (Israely et al. 2018), a polynomial muscle recruitment criterion with a power of $p = 5$ was chosen, and simple muscle models are applied. The polynomial describes the objective function G , which has to be minimized by the algorithm.

$$G = \sum_i \left(\frac{f_i}{N_i} \right)^p$$

with f_i is the applied force and N_i is the strength of a muscle (see Chapter 3). The higher the polynomial coefficient p , the more the load is distributed between the individual muscles. All trials were calculated with 40 simulation steps per second. Prior to each motion simulation, a calibration of the skin resistance (see Figure 6.3) according to the anthropometrics of the subject was performed.

Compared to the original detailed hand model from Chapter 4, which was validated by moment arm studies and, therefore, simplified movements, smaller adjustments were made because of the complexity of the motions to assure a physiological pathing of the muscles. These adjustments mainly involved the initial wrapping vectors (like extensor pollicis brevis and extensor carpi radialis longus) and also the muscle path of the extensor carpi ulnaris muscle. Because the goal of this study was a real blind validation rather than just a calibration of the model (Lund et al. 2012), no further adjustments were made.

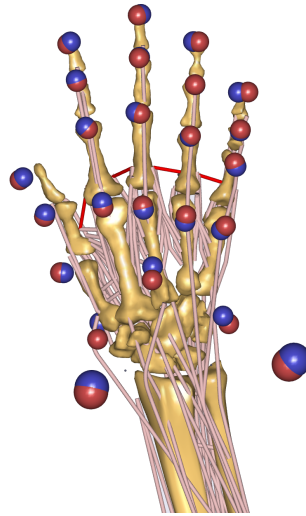


Figure 6.3: The new detailed hand model with measured markers (blue spheres) and markers fixed on the model (red spheres) within the AMS. The red lines between the fingers represent the purlicue skin resistance.

6.2.3 Data processing

For each EMG signal, the baseline off-set was subtracted, the root mean square with an applied window size of 50 ms was calculated, and the signal was normalized according to the MVC measurements (Konrad 2005).

To be able to compare the numerical with the experimentally measured muscle activity, simulated muscles were compiled and only the maximum value at each time step was taken into account. This compilation of muscles allows a numerical reproduction of the signal received by the EMG sensor. The exact list of enveloped muscles can be found in the Appendix - Table B.1.

The validation was quantified by the comparison of the on- and off-set time points of the numerical and measured muscle activities, which implies the time difference in which a muscle was activated/deactivated in reality and the simulation, respectively. There are numerous methods using computer analysis for determining the on- and off-sets, but little agreement regarding the most appropriate (Vannozzi et al. 2010, Lee et al. 2007, Solnik et al. 2010). Therefore, a MATLAB (The MathWorks Inc., Natick, USA) tool was designed through which a total number

of five trained biomechanical engineers were able to determine the various on- and off-set time points manually. Thereby, the graphs, as depicted in Figure 6.4 were displayed and the on- and off-set time point were selected and saved in a database. This method is also taken as the *gold standard* when comparing different numerical on- and off-set approaches by Tenan et al. (2017).

For the respective comparison of the EMG signal and the simulated muscle activity of each task, only muscles with a measured maximum EMG activity $>15\%$ in at least 50% of all performed movements were considered.

6.2.4 Statistical analysis

To determine to agreement between the model's prediction and measured EMG signal, the weighted kappa value for inter-rater agreement was calculated for all tasks and all muscles. Hence, the periods of time during which the muscles were active according to the experimental and numerical data were considered. The kappa value $\kappa \in [0, 1]$ represents the agreement between the two raters: $\kappa \in [0, 0.2]$ slight, $\kappa \in]0.2, 0.4]$ fair, $\kappa \in]0.4, 0.6]$ moderate, $\kappa \in]0.6, 0.8]$ substantial, and $\kappa \in]0.8, 1.0]$ almost perfect agreement.

6.3 Results

From the 105 potential trials, 100 motion data sets as input for the inverse dynamic simulation could be reconstructed, and 100 numerical simulations were performed. Because the aim of this study was a general comparison of measured and simulated muscle activities, Figure 6.4 shows one example of the normalized EMG signal and the calculated muscle activity for the FDI and ADM muscles of a test subject for task 1 (ab-/adduction of the fingers). All other muscle activities of this trial can be found in the Appendix - Figure B.2.

The predicted progression of the muscle activity corresponded to the measured data, but a shift of the on- and off-set points could be observed. Additionally, for the ADM, the model appeared to overestimate the muscle activity, whereas the magnitude of the peak correlated with the abduction angle, which was not reflected in the experimental data.

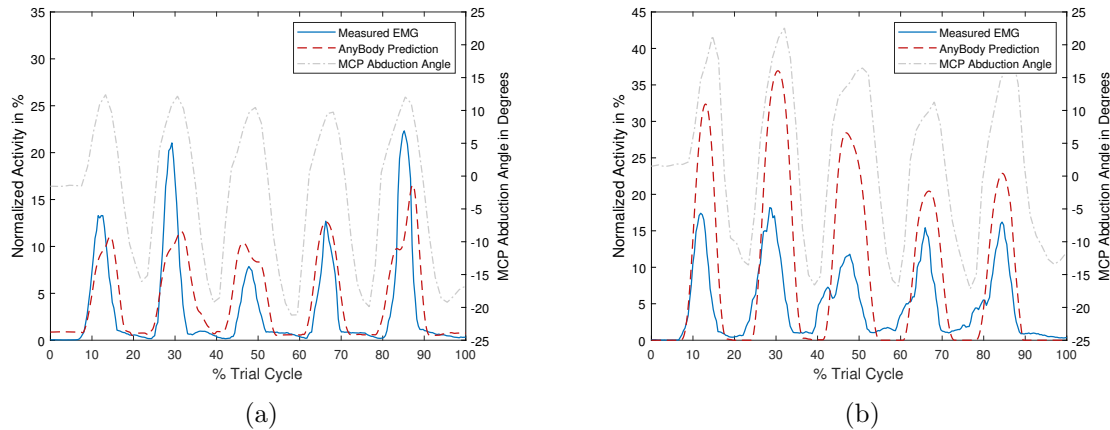


Figure 6.4: Muscle activity prediction from the model and measured EMG signal during the abduction of the fingers along the MCP joint five times in a row. (a) FDI muscle, (b) ADM muscle.

Regarding the on- and off-sets of the muscle activities of all tasks as well as the weighted kappa values, these are summarized in Table 6.4. An overall difference of 0.58 s between the estimated and measured muscle activities was computed. The lowest variation (0.19 s) was detected for the FPB muscle in task 4 (ab-/adduction of the thumb), while the highest (1.5 s) was found in the same task for the ECU muscle. Concerning the weighted kappa value, the average kappa value for all trials (0.48) and all muscles (0.46) show a moderate agreement.

Table 6.4 depicts which muscle was mostly active during the corresponding movement in the experiment. It is noticeable, for example, that the FDS muscles were not active in task 3 (flexion of the fingers), such that it can be assumed that most of the test subjects simply used gravity to flex their fingers or did not use their full ROM in the PIP and DIP joint to fulfill the task. The time difference between model and experiment was best for task 1 (ab-/adduction of the fingers), where a force against the resistance of the skin during the abduction had to be applied. This is also reflected in the highest kappa values for task 1, 2 and 4, in which all a passively acting force had to be overcome.

Table 6.4: Mean absolute difference of the measured and predicted muscle on- and off-set time points (\pm SD) for all tasks and muscles. Only muscles with a measured maximum EMG activity $>15\%$ in at least 50 % of all performed movements were considered. The weighted kappa values for the on- and off-set times. The on- and off-sets are given in seconds.

<i>Muscle</i>	<i>Task 1</i>		<i>Task 2</i>		<i>Task 3</i>		<i>Task 4</i>		<i>Task 5</i>		<i>Task 6</i>		<i>Task 7</i>		<i>Mean</i>	<i>Kappa</i>
	On-set	Off-set	On-set	Off-set	On-set	Off-set	On-set	Off-set	On-set	Off-set	On-set	Off-set	On-set	Off-set		
<i>ECU</i>	0.46 \pm 0.41	0.89 \pm 0.81	0.59 \pm 0.62	0.58 \pm 0.57	1.2 \pm 1.1	1.2 \pm 1.1	1.1 \pm 0.96	1.5 \pm 1.3	1.1 \pm 1.0	1.2 \pm 1.1	0.55 \pm 0.78	0.58 \pm 0.63	0.65 \pm 0.61	0.54 \pm 0.53	0.87	0.43
<i>FCU</i>	0.28 \pm 0.2	0.30 \pm 0.3	-	-	-	-	-	-	-	-	0.50 \pm 0.4	0.4 \pm 0.33	0.56 \pm 0.5	0.43 \pm 0.42	0.41	0.42
<i>ECR</i>	0.34 \pm 0.30	0.30 \pm 0.39	0.28 \pm 0.35	0.39 \pm 0.35	0.76 \pm 0.72	0.59 \pm 0.57	0.5 \pm 0.54	0.75 \pm 0.69	0.59 \pm 0.58	0.71 \pm 0.59	0.74 \pm 0.67	0.72 \pm 0.7	0.82 \pm 0.68	0.48 \pm 0.38	0.57	0.54
<i>FCR</i>	-	-	-	-	-	-	-	-	-	-	1.0 \pm 0.91	1.1 \pm 0.95	1.0 \pm 0.81	1.3 \pm 1.2	1.1	0.44
<i>ED</i>	0.20 \pm 0.21	0.26 \pm 0.24	0.34 \pm 0.37	0.38 \pm 0.36	-	-	-	-	0.45 \pm 0.56	0.46 \pm 0.48	0.41 \pm 0.41	0.43 \pm 0.46	0.72 \pm 0.68	0.75 \pm 0.71	0.44	0.48
<i>FDS</i>	-	-	-	-	-	-	-	-	-	-	0.73 \pm 0.7	0.63 \pm 0.6	0.6 \pm 0.54	0.49 \pm 0.43	0.61	0.51
<i>FDI</i>	0.62 \pm 0.61	0.63 \pm 0.58	-	-	-	-	-	-	-	-	-	-	-	-	0.63	0.27
<i>ADM</i>	0.47 \pm 0.4	0.91 \pm 0.9	-	-	-	-	-	-	-	-	0.60 \pm 0.5	0.42 \pm 0.4	-	-	0.60	0.36
<i>FPB</i>	0.23 \pm 0.22	0.21 \pm 0.26	-	-	0.51 \pm 0.58	0.6 \pm 0.59	0.19 \pm 0.33	0.24 \pm 0.32	0.32 \pm 0.38	0.35 \pm 0.32	0.53 \pm 0.57	0.55 \pm 0.55	-	-	0.37	0.54
<i>APB</i>	0.21 \pm 0.2	0.25 \pm 0.2	-	-	0.66 \pm 0.6	0.77 \pm 0.7	0.24 \pm 0.3	0.31 \pm 0.3	0.38 \pm 0.3	0.45 \pm 0.4	0.6 \pm 0.68	0.58 \pm 0.6	-	-	0.45	0.56
<i>Mean</i>	0.35	0.47	0.40	0.45	0.78	0.80	0.51	0.70	0.56	0.64	0.63	0.60	0.72	0.67		
<i>Kappa</i>	0.56		0.56		0.41		0.58		0.41		0.48		0.33			

6.4 Discussion

The aim of this study was an experimental validation of a recently developed detailed hand model by an overall comparison between the computed muscle activities of the hand model and the experimentally derived EMG activities. Therefore, the on- and off-sets and the corresponding kappa values of the muscle activities were investigated. Because these two approaches bring their own advantages and limitations, first the model and then the validation process will be examined more closely.

6.4.1 The hand model

For skilled movements, the AMS assumes the muscles to be recruited using more and fewer muscle synergies. Because hand movements are quite trained motions, this study used a strong criterion for the minimization of the muscles' efforts, which also previously showed good results for cycling, gait, and biting (Prilutsky and Zatsiorsky 2002, De Zee et al. 2007).

The current model has the limitation that the entire wrist is modelled as one rigid body, not including any ligaments within the wrist and hence lacking any passive forces, which might explain the divergence in the computed and experimentally derived activities of the ab-/adduction and the extension/flexion of the wrist (tasks 6 and 7). An implementation of such a detailed wrist model, like the one of Eschweiler et al. (2016), could provide a solution to address this issue.

Using a simple muscle model, additional passive forces from the muscle tendons are also omitted. The muscle model, which includes these forces, is the Hill-type model. Aurbach et al. (2020b) recently showed that using the Hill-model could be one key modelling parameter for simulation of the joint reaction forces within the shoulder. Particularly for the extrinsic muscles with long tendons, using the Hill-model could be an essential part, which, however, offers significant possibilities for additional uncertainties within the model.

6.4.2 Validation

Validating a musculoskeletal model is a necessary, albeit difficult step to take to determine when the model should be used for answering upcoming research questions.

Because there are no available datasets of instrumentalyzed prostheses and thus available joint reaction forces for the hand – compared to other joints (Bergmann 2008) – only indirect validation remains, in which muscle activities and moment arms are compared. This validation method is based on the assumption that when the muscle activities match, the joint reaction forces are also acceptable.

The validation in this study should be accomplished through the comparison of the time difference of numerically determined and experimentally measured on- and off-set time points. With regard to the EMG measurements, it can be stated, that the wrist extensors were more active than the wrist flexors for most of the tasks (which is indicated by the fact that they more frequently overcome the 15% activity threshold), which correlates well with the findings of Forman et al. (2019). When considering Figure 6.4, the EMG signal and the numerically calculated muscle activity displayed similar progressions. The on- and off-sets as well as magnitudes alternated in the same dimensions.

However, when considering and evaluating the results of Table 6.4, one must also always keep in mind which muscles should be primarily addressed in the respective task (see Table 6.2). For example, ab-/adduction and flexion of the thumb (tasks 4 and 5) mainly address the intrinsic muscles of the thumb, for which the on-/off-set time differences were much smaller than for the stabilizing muscles of the wrist, which are less affected by the movement.

Nevertheless, there are some uncertainties within the comparison which have to be born in mind. One major issue within EMG signals is cross-talk – neighboring muscles also produce an EMG signal, which is recorded by the sensor (Konrad 2005). Particularly in the forearm/hand, which contains 39 muscles, cross-talk is a systematic bias of the EMG signals (Kong et al. 2010), but not in the simulation. The lower the activity of the considered muscle is in comparison to the surrounding ones, the more pronounced the effects of the cross-talk become, which results in a lower signal-to-noise ratio (Kasprisin and Grabiner 1998). Therefore, only mus-

cles mainly targeted for the respective movement were compared to each other, and envelopes were introduced. Concerning at the individual tasks 1 - 7, it can be stated that cross-talk mainly influences tasks 2, 3, 6, and 7 since these task mainly involved extrinsic muscles which are bundled in the forearm. In contrast, the intrinsic muscles in the hand are in a more exposed position, which should reduce the influence of cross-talk in task 1, 4, and 5.

Additionally, the displacement of the innervation zones can produce some artifacts when considering dynamic movements (Rainoldi et al. 2000). An example in the collected data is the activity of the FDI during finger abduction. Only two of five subjects were able to abduct the index finger by more than 10° , but for all five subjects EMG deflections during movement were detected. When only the two indicated test persons were included in the data evaluation, the on-/off-set was reduced to 0.39/0.42 s (in contrast to 0.62/0.63 s). This improvement clearly demonstrates the influence that interference signals can have in EMG.

Jungtäubl et al. (2018) earlier introduced a method demonstrating how the numerical signal of a simulation can be contaminated with cross-talk and showed a positive effect on the corresponding Person correlation coefficient between measured and numerical obtained muscle activities. Contaminating the numerical outcome with synthetically generated cross-talk could help achieve a better comparison of experimental data and the model.

As the results of task 1, 2, and 4 (ad-/abduction of the fingers, extension of the fingers, abduction of the thumb) indicated, the EMG signal and simulated muscle activity became more distinctive when the movement was performed against a force (passive stiffness). All other tasks were performed with gravity as the only prevailing external force. For other scenarios, like measuring EMG in the lower limb, gravity as an additional force might be sufficient by using the body-weight. However, for the movement of the hand weighing only a few hundred grams (0.575% body weight for the average hand (Plagenhoef et al. 1983)), the on- and off-sets of the muscle activities were not as distinctive, which makes it complicated to assume the correct on- and off-set timing. The results from task 1 also show that the model is much more consistent with the measured data in that loaded case.

Another limitation, which might explain the differences between reality and the model predictions, is that the models were scaled only to the anthropometric data and were not exact patient-specific models. The lengths of the single finger bones were gained by an optimization process of the adjustment to the defined markers. Because of the relative sliding of the skin and bones along the finger joints, a particular inaccuracy regarding the hand anthropometrics may have occurred.

In future studies, it would also be of interest to morph subject based bone geometries (from CT data) into the model to make the outcome even more patient-specific. In this way, it would even be possible - also by scaling the strength of different muscle/muscle groups - to map any pathologies and accordingly obtaining even more realistic muscle activities in the numerical model.

A similar musculoskeletal validation study is the one by Wibawa et al. (2013) for the lower limb. In this study, it was not the time difference between experimental and numerical data that was determined, but the number of on and off set points during lower limb movements. Here, the AnyBody model of the lower extremity (De Pieri et al. 2018), which has been validated in several studies, showed a slight agreement between the measured EMG and predicted muscle activity data (kappa was up to approximately 0.3). The average kappa for all muscles presented in this study were even slightly higher (0.46).

Apart from all this, the experimental set-up restricted the comparison to only four intrinsic and six extrinsic muscles, which are not all, but the dominating hand muscles for most movements. Therefore, the question occurs whether the remaining muscle activity also fits quite well with reality. For this reason, this study attempted to perform a trend rather than an absolute validation. As a consequence, it should be expected that the underlying conceptual model is physically correct, although this is difficult to prove. One way could be the comparison of joint reaction forces to data obtained by an instrumentalized wrist or finger prosthesis in the future.

In general, a validation process based on the measurement of EMG is also restricted to the limitations of EMG. The major limitation of EMG signals in validation is that EMG is only able to reject models with a clearly wrong result (Lund et al. 2012), which according to the data of this study, is not the case for this hand model.

6.5 Conclusion

The study presented the comparison of a musculoskeletal hand model recently developed within the AMS with experimentally obtained data of muscle activities. The alignment of on- and off-set timings provides good initial agreement, also emphasized by kappa values between 0.27 and 0.56 for the muscles. Further studies might increase the accuracy of the validation by addressing external load cases. Nevertheless, the model provides a good basis to analyze future musculoskeletal research questions regarding the hand.

The presented generic model will become available in the AMMR and can be used for the biomechanical investigation of critical clinical problems affecting the human forearm.

Chapter 7

Hand model: sensitivity analysis

A part of the following chapter has been published in a similar form in the Journal for Computer Methods in Biomechanics and Biomedical Engineering under Melzner, Süß and Dendorfer (2022).

7.1 Introduction

The outcome of musculoskeletal models, e.g., joint moments and forces, is mostly reported as single values with a deterministic character. The incorporation of any uncertainties within the model is often left unexamined (Cook et al. 2014). When inaccuracies associated with model development are taken into considerations, simulation results have to be interpreted as a single case out of many possible outcomes. These uncertainties may arise either from simplifications in the model (Gagnon et al. 2011) or inaccuracies in underlying input variables as a function of data extraction (Žuk and Pezowicz 2016). The process of identifying such parameters is usually associated with complex measurements (Taddei et al. 2012, Scheys et al. 2009), which are based on an average error greater than zero (Scheys et al. 2008).

Critical variables for modeling are the muscle parameters, such as the line of action (Raikova and Prilutsky 2001), PCSA, and thus the maximum force capacity of muscles (Herzog 1992). These are crucial parameters for determining muscle activities and joint reaction forces. Maury et al. (1995) has already shown that

such uncertainties in the muscle line of action result in a change of more than 100 N in the joint reaction force within the spine.

If the model to be analyzed is based only on a single anatomical data set, the inaccuracy in the determination of muscle parameters is reduced to measurement errors as the data is not diversified. This lack of diversity may also lead to a systematic error if the subject's anatomical preconditions in patient-specific modeling deviate significantly from the cadaver, which the model is based on. To achieve ideal population-based models, a more comprehensive anatomical data set is necessary, which can be gained by including a large number of different cadavers when determining muscle parameters. The advantage of including a larger number of cadavers increases the representativeness of the sample means and reduces their susceptibility to be skewed by outliers. However, scattering of the respective parameters also leads to considerable uncertainties in parameters. Another disadvantage depicts the fact that there is high variability within human performance measures within a population, and hence only a few people can be defined as an average person (Smith et al. 2014). However, generalized musculoskeletal models' overall purpose should not be the ability to represent only an average person but to be applicable to a large number of subjects with idiosyncratic characteristics through patient-specific scaling.

The developed hand model from Chapter 4 is based on a general data set, which includes data of 16 donors (Havelková et al. 2020). This model consists of 80 extrinsic and intrinsic hand muscles with 31 DOFs and has been shown to correlate highly with moment arm studies from prior literature (see Chapter 5). Since this model's anatomical data has some unavoidable known indeterminacy, the outcome sensitivity of subject-specific model predictions (muscle activities and joint reaction forces) compared to the input parameters should be researched. Thus, this study aimed to investigate the sensitivity and stability of the model and at the same time determine whether the model can be applied to a broad population beyond the average hand. Due to its increasing importance in using various modern technologies, such as smartphones (Gustafsson et al. 2010), attention was focused in particular on the thumb.

7.2 Materials and Methods

The PCSA and the muscles' line of action are crucial parameters in determining acting muscle forces and hence the acting joint reaction forces. In order to evaluate the sensitivity of the recently developed musculoskeletal hand model from Chapter 4 to these parameters, the underlying anatomical data (Havelková et al. 2020) was varied according to their known measurement uncertainties – see Appendix Table C.1 and C.2.

Subsequently, the simulated on- and off-set time points of the muscle activities were compared with experimentally derived EMG activities. Further, the effects on the change of joint reaction forces within the hand were investigated.

7.2.1 Experiment set-up

The test subject (weight = 78.3 kg, hand length = 20.5 cm) was informed about the measurement procedure in advance and provided written consent confirming voluntary participation. Then, the test subject performed one trial with the abduction of all fingers, one trial with the abduction of the thumb, and one trial with the flexion of the thumb. Each trial consisted of five repetitive movements, where the hand was in pronation for the abduction of the fingers and neutral position otherwise.

The movements' kinematics were captured with a camera-based motion capture system (Vicon©, Vicon Motion Systems Ltd., UK) using a marker-set including the upper arm, forearm, and all fingers. The EMG activities of 10 extrinsic and intrinsic muscles were captured analog to Chapter 6 via surface EMG (Delsys Trigno IM and Delsys Trigno Mini, Delsys® Inc., MA, US.) following the recommendation of sensor placement according to Criswell (2011) and Barbero et al. (2012) (see Table 6.1 and Figure 6.2). Prior to the sensor placement, the skin was cleaned with an alcoholic solution to minimize the acquired signal's influences due to dead skin cells, salt, or grease. The muscles were selected according to the movements to be investigated (abduction of all fingers/ thumb and flexion of the thumb), such that in addition to the primarily active intrinsic muscles, extrinsic muscles stabilizing the wrist were also covered. For normalization of the EMG data, MVC measurements following Kendall et al. (1993) were performed beforehand analog to Chapter 6.

7.2.2 Simulation

The gathered kinematic data was fed into the musculoskeletal simulation software AnyBody™ (AnyBody Technology A/S, Aalborg, Denmark, V. 7. 3). Then, the model was scaled according to the anthropometric data of the test subject to allow for patient-specific simulation, and simple muscle models are applied. The change of input parameters and the simulation were performed externally using the python module AnyPyTools (Lund et al. 2019) to conduct the subsequent sensitivity study. The PCSA and the origin, as well as the insertion points of all extrinsic and intrinsic hand/wrist muscles were amended according to their measurement inaccuracies published by Havelková et al. (2020) – see Appendix Table C.1 and C.2.

A modification in the PCSA is directly incorporated into the cost function G , which has to be minimized by the algorithm

$$G = \sum_i \left(\frac{f_i}{N_i} \right)^p$$

whereby p is the polynomial coefficient symbolizing the muscle synergy, f_i is the applied force, and N_i is the strength of a muscle, which is linear proportional to the PCSA. Hence, the magnitude of the PCSA influences muscle recruitment and, thus, the joint reaction forces to be determined. The outputs are also influenced by changing the muscles' origin and insertion points, resulting in a resulting alteration in the moment arm.

For the PCSAs, origin, and insertion points, a normal distribution (with the expectation value μ being the value of the standard model and SD of the anatomical data (see Appendix Table C.1 and C.2) was assumed. Further, the following assumptions regarding origin and insertion points were made:

- The origin and insertion area was split up according to the number of the muscle representatives within the model.
- Since the anatomical data-set provided only the area in a two-dimensional plane, the SD in the third dimension was assumed to be 1 mm.

- To not exceed the limits of the origin and insertion areas while randomly creating input parameters, the boundaries of the area were set to ± 3 SDs. This restriction assures that origin and insertion points stay at 99,7% within the anatomical area.

Based on this set-up, 1.000 simulations were calculated for each trial. The Latin-Hypercube sampling (LHS) technique (Helton and Davis 2003) was used to perform sensitivity analysis, which is a standard method in biomechanics as it provides improved sampling efficiency compared to the otherwise commonly used Monte Carlo analysis (Valero-Cuevas et al. 2003, Reinbolt et al. 2005).

7.2.3 Data processing

For the EMG signal, a root mean square with a window size of 50 ms was applied, the baseline offset was subtracted, and the signal was normalized according to the MVC measurements. To compare the numerical with the experimentally measured muscle activity, a compilation of corresponding representatives of a muscle was created whereby only the maximum value at each time step of the grouped muscle elements was taken into account. A detailed list of enveloped muscles can be found in the Appendix - Table B.1.

Following prior research, which has used an evaluation of on- and off-set timing of muscle activities to validate musculoskeletal models (De Pieri et al. 2018), the on- and off-set time points of the experiment, the standard model, and all simulations run by the LHS method were compared. This comparison is particularly interesting since a larger variation of the on- and off-set timing would imply a questionable experimental validation or instability of the model.

For automatization of on- and off-sets detection, change point detection (Killick et al. 2012) as implemented by the MatLab (The MathWorks Inc., Natick, USA) *FindChangePts()* function was used. Based on this output, the difference between each simulation and the experiment was evaluated. Next, the joint reaction forces acting on the wrist and all finger joints were calculated using the inverse dynamic approach of the AMS. This inverse dynamic approach provides a computation of the muscle forces and the resulting joint reaction forces, but it can not be used directly for motion prediction. Since a relatively small ROM in the DIP and PIP

joint took place during the conducted movements, only the CMC and the MCP joint were considered in the investigation of the joint reaction forces.

For analysis of the model output and measured data, (Rebba and Mahadevan 2008) showed that a metric r

$$r = P(-\epsilon < m - c < \epsilon)$$

where $m - c$ is the difference between experimental data and numerical simulation, and ϵ is the accuracy requirement, which is more suitable than the hypothesis testing using the p -value. Therefore, the r metric was used for comparing the experimental data, the standard model, and the outcome of all LHS simulations regarding the on- and off-set time points. This metric was also applied to comparing joint reaction forces, although the model cannot be checked against experimental data. Instead, the results of the LHS simulations were compared to the standard model.

7.3 Results

As the aim of this study was to test the sensitivity and stability of the musculoskeletal hand model, Figure 7.1 exemplifies the extent to which variation in input parameters can affect changes in muscle activity (Figure 7.1(a)) and joint reaction forces (Figure 7.1(b)). Figure 7.1 displays the activity of the FDI muscle and the joint reaction force of the thumb's CMC joint during the abduction of all fingers. In both cases, the standard model is within the range of one SD of the LHS simulations. It can be stated that the variation in the joint reaction force is higher than that of the individual muscle activities. All muscle activities and joint reaction forces of each motion can be found in the Appendix - Table C.3 - C.5.

The mean values of the difference between all calculated on and off time points for each movement are displayed in Table 7.1. In contrast to the fingers' abduction, during movements of the thumb, mainly FPB and APB muscles were addressed. Hence, only these muscles were taken into account for calculating the on and off times. Comparing the mean values of the LHS simulations and the standard model, only a slight shift of the on-off times can be observed.

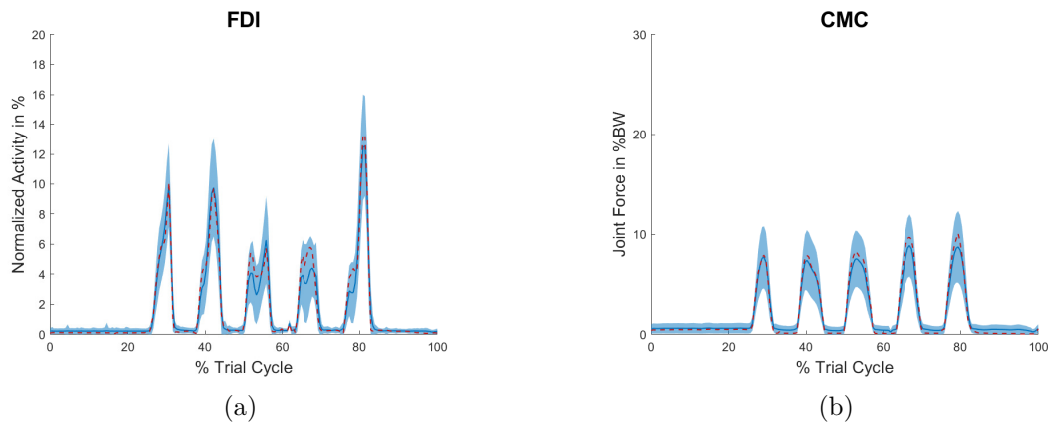


Figure 7.1: (a) Muscle activity of the FDI muscle and (b) the joint reaction force of the CMC joint of the thumb during the abduction of the fingers. The standard model is provided by the red dashed line, the mean of the LHS simulation by the blue line, and its corresponding SD (shaded area). The force of (b) is given in percent body weight (BW).

The joint reaction forces (normalized to the body weight) acting on the wrist and finger joints for each movement are shown in Table 7.2. When determining the joint reaction forces, only times when the muscles of the standard model were active were taken into account and averaged. The highest acting forces were found in the wrist joint, whereby the CMC joint of the index finger was also exposed to high loads during thumb movements. Considering the joint reaction forces, the standard model also stays within one SD of the LHS simulations except for the index finger's MCP joint during the abduction of the thumb. The coefficient of variation (CV) – which is defined as the ratio of SD and mean - varies between 9% (MCP_{thumb} – abduction thumb) and 56% ($CMC_{finger4}$ – abduction thumb) for individual joints.

The results for applying the metric proposed by Rebba and Mahadevan (2008) to the outcome of the on- and off-set time difference and the joint reaction forces, respectively, are shown in Figure 7.2 - 7.4 for each movement. Subfigures 7.2(a) - 7.4(a) show the probability of finding an outcome of the predicted joint reaction forces of the LHS simulations within a specific interval around the calculated value of the standard model (all forces were normalized to the standard model). Subfigures 7.2(b) - 7.4(b) show the probability that the time difference be-

tween the experimental and numerically calculated data is within a specified time interval for the standard model and the LHS simulations. Considering the joint reaction forces, almost 70% of all simulations stay within a 30% interval around the standard model for the abduction of all fingers. Notable exceptions are the CMC joint of the thumb and index finger, for which only 60% of results occur within this interval (Figure 7.2(a)).

Regarding the thumb flexion, approximately 60% of simulation outcomes stay within a 30% interval around the standard model (Figure 7.3(a)); whereas for the thumb abduction, it is about 70% except for the joints of finger 4 and 5 (Figure 7.4(a)). Regarding the probabilities of finding an on- or off-set point in a specific time interval, the results of the LHS simulations follow the trend of the standard model (see Figure 7.2(b) – 7.4(b)).

Table 7.1: The average time difference of the on- and off-set time points of the muscles between the experimental measured and simulated predictions during (a) the abduction of all fingers, (b) the flexion of the thumb, and (c) the abduction of the thumb. The standard model is compared to the mean value of the LHS simulations with modified input parameters and its SD. The on- and the off-sets time difference is given in millisecond.

(a)

On-/Off-Sets	ED	ECR	FCR	FCU	FDI	ADM	APB	FPB	FDS	ECU
<i>Standard model</i>	160	185	181	136	190	178	90	106	283	100
<i>Mean-LHS</i>	167	258	209	170	194	201	88	121	276	100
<i>SD-LHS</i>	39	180	173	177	169	213	27	63	245	25

(b)

On-/Off-Sets	APB	FPB
<i>Standard model</i>	309	258
<i>Mean-LHS</i>	311	269
<i>SD-LHS</i>	26	61

(c)

On-/Off-Sets	APB	FPB
<i>Standard model</i>	204	224
<i>Mean-LHS</i>	203	225
<i>SD-LHS</i>	7	22

Table 7.2: The average joint reaction forces of the wrist, CMC, and MCP finger joints during the (a) the abduction of all fingers, (b) the flexion of the thumb, and (c) the abduction of the thumb. The reaction force of the standard model is compared to the mean value of the LHS simulations with modified input parameters, its SD, and corresponding CV. The joint reaction forces are given in percent body weight.

	Wrist	CMC thumb	CMC finger2	CMC finger3	CMC finger4	CMC finger5	MCP thumb	MCP finger2	MCP finger3	MCP finger4	MCP finger5
<i>Standard model</i>	35.4	6.1	14.0	5.2	2.8	14.0	1.2	3.5	5.0	4.5	9.3
<i>Mean-LHS</i>	31.8	5.7	11.4	5.3	2.7	13.1	1.3	3.4	4.6	4.1	9.2
<i>SD-LHS</i>	9.4	2.4	4.8	2.2	0.5	2.5	0.3	1.2	1.4	0.6	1.7
<i>CV-LHS</i>	0.29	0.42	0.42	0.41	0.19	0.19	0.23	0.34	0.3	0.14	0.18

	Wrist	CMC thumb	CMC finger2	CMC finger3	CMC finger4	CMC finger5	MCP thumb	MCP finger2	MCP finger3	MCP finger4	MCP finger5
<i>Standard model</i>	31.6	4.1	14.6	6.4	4.1	7.8	2.5	4.0	5.4	6.8	7.8
<i>Mean-LHS</i>	30.2	4.0	11.6	8.4	4.4	8.0	2.5	4.0	5.0	5.8	8.0
<i>SD-LHS</i>	10.2	1.6	3.9	3.3	1.6	2.9	0.4	1.0	1.7	2.4	2.9
<i>CV-LHS</i>	0.34	0.39	0.33	0.39	0.37	0.36	0.15	0.24	0.35	0.42	0.37

	Wrist	CMC thumb	CMC finger2	CMC finger3	CMC finger4	CMC finger5	MCP thumb	MCP finger2	MCP finger3	MCP finger4	MCP finger5
<i>Standard model</i>	56.8	12.6	33.6	7.3	1.7	6.0	11.5	14.9	7.4	2.8	5.8
<i>Mean-LHS</i>	57.9	13.7	33.6	7.7	2.8	5.1	11.7	18.6	7.8	3.8	4.9
<i>SD-LHS</i>	8.9	2.3	4.2	2.3	1.6	2.1	1.0	2.8	2.3	1.6	2.1
<i>CV-LHS</i>	0.15	0.17	0.12	0.3	0.56	0.42	0.09	0.15	0.29	0.43	0.42

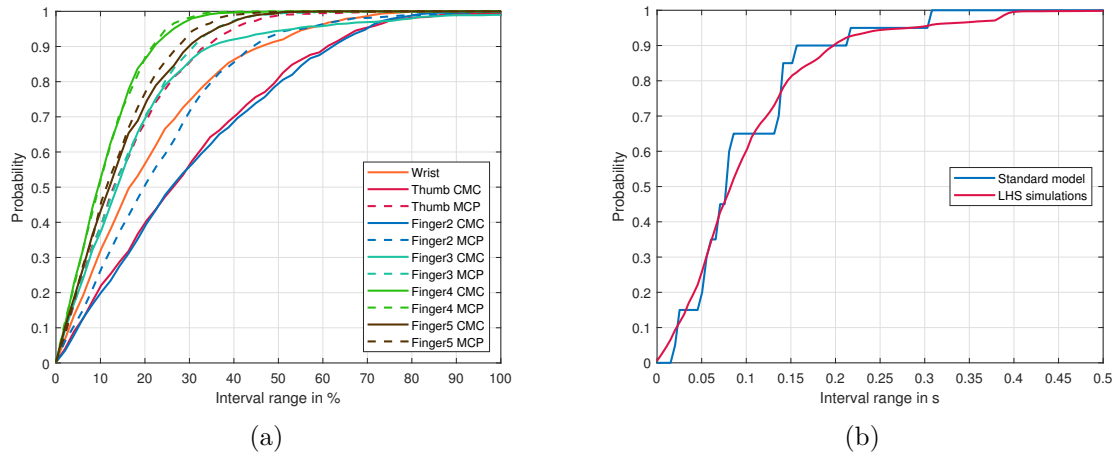


Figure 7.2: Probability for the abduction of all fingers (a) to find an outcome of the predicted joint reaction forces of the LHS simulations within a specific interval around the calculated value of the standard model (all forces are normalized to the standard model) (b) that the time difference between the experimental and numerical calculated data is within a specific time interval for the standard model and the LHS simulations.

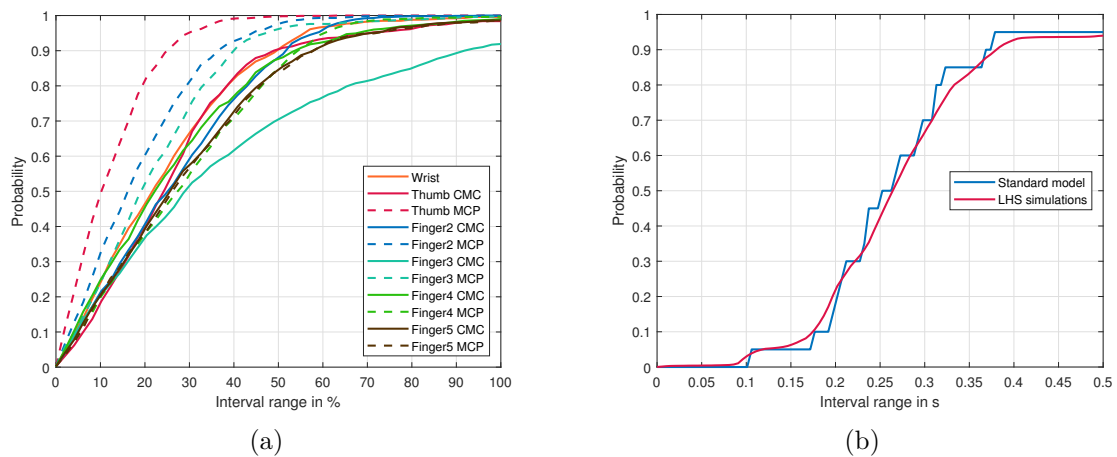


Figure 7.3: Probability for the flexion of the thumb (a) to find an outcome of the predicted joint reaction forces of the LHS simulations within a specific interval around the calculated value of the standard model (all forces are normalized to the standard model) (b) that the time difference between the experimental and numerical calculated data is within a specific time interval for the standard model and the LHS simulations. Only the APB and FPB muscles were considered.

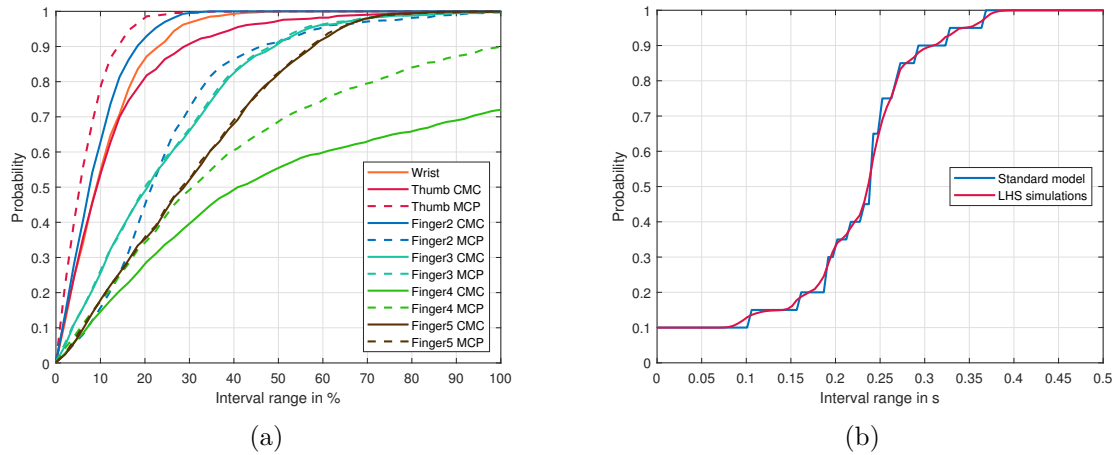


Figure 7.4: Probability for the abduction of the thumb (a) to find an outcome of the predicted joint reaction forces of the LHS simulations within a specific interval around the calculated value of the standard model (all forces are normalized to the standard model) (b) that the time difference between the experimental and numerical calculated data is within a specific time interval for the standard model and the LHS simulations. Only the APB and FPB muscles were considered.

7.4 Discussion

The aim of this study was to examine the sensitivity and stability of the musculoskeletal hand model from Chapter 4 and thus to determine whether the model can be applied to a broad population outside the average hand for patient-specific modeling. Examining the comparison between experimental data, the standard model, and LHS simulations suggests that the hand model is able to provide convergence for a broad range of input data and, therefore, can be considered relatively stable.

Combining all joints' CV values results in an average scattering of 30% around the expected value. The probability that the calculated joint reaction forces of the LHS simulations are located within an interval of $\pm 30\%$ around the value of the standard model is about 60% for the three investigated movements. Even when comparing the experimental data with the numerical models, the highest deviation between the prediction of the standard model and the mean value of the LHS simulations is 73 ms (abduction of all fingers - ECR muscle) and the probability curves of Figure 7.2(b) - 7.4(b) show no substantial deviations. Further, all SDs

are smaller than equal to approximately 250 ms, which is within an acceptable range once electromechanical delays (which are about 75 ms, according to Seth and Pandy (2007)) are taken into account.

Investigating joint reaction forces, the level of particular forces within the hand during the different movements is of particular interest. Especially in the abduction of the thumb, the wrist, and the index finger's CMC joint seem to be exposed to high forces (Table 7.2(c)). These increased forces are especially interesting, as this movement is mainly used in the operation of modern multimedia devices. However, because there are no in vivo measured force data of these joints - compared to other joints like the shoulder (Bergmann 2008) - these results cannot be validated quantitatively.

Taking a closer look at the outliers in the probability metrics of Figure 7.2 - 7.4, it is evident that outliers are mainly finger joints that were rarely involved in the respective movement, such as the CMC and MCP joint of fingers 3-5 for the abduction of the thumb or the CMC joint of finger 3 for the flexion of the thumb. Only the MPC joint of the index finger (during the abduction of the thumb) and the CMC joints of the thumb and index finger (during the abduction of all fingers) seemed to be sensitive to changes in input parameters, although the movements addressed these joints. One possible reason for these joints' increased sensitivity could be the large number of intrinsic muscles running through the area between the index finger and the thumb.

When evaluating the scattering of the model's outcome, the distribution of input parameters needs to be considered. The scattering magnitude is difficult to quantify in terms of the muscles' insertion/origin area, but for PCSA, this is quite manageable. The anatomical data set from Havelková et al. (2020) can be used to recalculate the average CV of PCSA values for all hand muscles, which is 38% of the corresponding mean. Weighting the individual muscles according to their size results only in a slightly smaller weighted average CV of 36.5%. Assuming a normal distribution of the underlying PCSA values, roughly 68% of the values are within an interval of $\pm 36.5\%$. Comparing this measure of dispersion to that of the numerical outcomes shows that the model predictions do not scatter more than the input parameters (with the limitation of reference to the PCSA).

The LHS method used in this study has improved sampling efficiency compared to the Monte Carlo analysis, which has the disadvantage of requiring a large number of simulation runs. Accordingly, the number of 1.000 simulations seems to be sufficient compared to the Monte Carlo studies of Valente et al. (2014) and Myers et al. (2015) with 500 and 3.000 simulations, respectively.

Although the results show that the model seems to be relatively stable concerning changes in input parameters, this stability depends on the type of movement performed, which should also be considered in future analyses. Therefore, an attempt was made to depict a correspondingly comprehensive range of relevant movements being essential for modern everyday life.

This study has important implications for patient-specific scaling of musculoskeletal models. A common approach to patient-specific modeling is to scale the model's force-specifically, which is analogous to changing the PCSA. Alternatively, it is also possible in the AMS to morph patient-specific bone geometries, which results in a shift of the muscle attachment points. The effects of both methods were illustrated in this study.

However, some limitations of this research need to be noted. The comparison of experimentally gained and numerically determined muscle activities introduces cross-talk, which is associated with the measurement of EMG signals (Konrad 2005). The kinematic inaccuracies that inevitably occur during the measurement can also impact model predictions (Myers et al. 2015).

Further, some assumptions about the distribution of input parameters had to be made when the anatomical data set did not provide exact data (e.g. for the SD of the third dimension of the origin/insertion area). In addition, it must be taken into account that this study did not investigate the direct effect of a change in muscle moment arms and thus the resulting variation in joint reaction forces. Rather, a change in the muscle line of action indirectly caused changes in the muscle moment arms. Finally, it is challenging to derive generally valid data from the measurement of only three different movements of a single person. However, these results provide valuable preliminary information, which can be useful to future investigations.

7.5 Conclusion

The study presented a sensitivity and stability analysis of the musculoskeletal hand model from Chapter 4 by changing the input parameters of the muscles' line of action. The results indicate the model's corresponding stability, which provides a reasonable basis for the patient-specific simulation of a broad population regarding the hand.

Chapter 8

Hand model: clinical application - simulation of the manual perineal protection

A part of the following chapter has been published in a similar form in the European Journal of Obstetrics & Gynecology and Reproductive Biology under Melzner et al. (2021). Parts of this chapter were created in collaboration with the project partners Vladimír Kališ, Zdeněk Rušavý, and Khaled Ismail from the Charles University in Pilsen.

8.1 Introduction

In spite of ongoing advances in medical care, clinical obstetrics still remains a high-risk practice. For centuries, childbirth posed life-threatening risks for both mother and child. These were markedly reduced in recent decades by progress in maternity care and the assistance of an experienced accoucheur (King 2013). Even though the lives of the mother and child are no longer threatened to the same extent, some complications during natural childbirth may have a lasting life-long impact on the woman's health and quality of life (Abedzadeh-Kalahroudi et al. 2019). Facilitating childbirth with the least consequences for the mother and child is the main priority, yet, remains to be one of the major challenges in

obstetrics. There are several interventions and maneuvers that are routinely used in obstetrics; operative vaginal deliveries (Yeomans 2010), manual perineal protection (MPP) (Kleprlikova et al. 2020), special maneuvers during breech or twin births are examples of some of them (Blickstein et al. 2000). For the purpose of this study the focus was set on MPP as a surrogate for such interventions.

Childbirth-related perineal trauma may lead to perineal pain (Åhlund et al. 2019) interfering with nursing and other activities shortly after birth while incontinence (LaCross et al. 2015) and other pelvic floor disorders can have long-term consequences (Mehrvarz et al. 2015). Therefore, the correct execution of interventions that can increase or reduce the risk of such injuries is of utmost importance to maternal outcomes. Indeed, the rate of these types of injuries varies across countries and institutions and obstetric practice seems to be a very important determining factor (Laine et al. 2013). Nevertheless, the maneuvers performed for the reduction of childbirth trauma may have a detrimental effect on the accoucheurs' health. Lower back pain is a common complaint amongst maternity care providers (doctors and especially midwives) (Karahana et al. 2009, Hougbedji et al. 2017). Back diseases represent one of the leading causes (71%) of musculoskeletal morbidity related to the work of accoucheurs. It is reported that about 30% of midwives have taken sick leave due to musculoskeletal disorders (Okuyucu et al. 2019). Inappropriate body postures have been widely associated with a high prevalence of such injuries more than other factors (Anita et al. 2014, Ezugwu et al. 2020). Therefore, the correct execution of these maneuvers is, not only important for mother and baby, but also of crucial importance for the healthcare professional. Depending on the particular posture during such maneuvers, the strain on the musculoskeletal system, particularly the critical stress peaks, may result in long-term consequences and disabilities to the accoucheur.

The most effective MPP techniques have been described and validated both theoretically (Jansova et al. 2017, 2014), and clinically (Laine et al. 2008). However, there is paucity of information regarding the most healthy posture for the accoucheur. In general, the postures adopted by accoucheurs in everyday clinical practice for assisting birth differ fundamentally.

For the purpose of this study, two completely different postures for comparison were selected:

- the accoucher being in an upright position and performing an MPP while bending slightly to the side – referred to in this study as standing technique (ST)
- the obstetrician kneeling (on one knee) and supporting the birth process in this position – referred to in this study as kneeling technique (KT)

Musculoskeletal simulations are increasingly used in biomechanical analyses. Using the kinematics of the human body, musculoskeletal simulations are able to analyze different loading situations and provide internal biomechanics. This is of particular interest since in-vivo measurements of the human body - like joint forces - are challenging to assess. These simulations are already used in numerous applications, e.g. orthopaedic research (Putzer et al. 2016, Dendorfer et al. 2014, Weber et al. 2014) sports (Nakashima et al. 2013, Kwan et al. 2011), and show good agreement compared to in-vivo data (Andersen et al. 2014). To my knowledge, no biomechanical analyses regarding the musculoskeletal load on obstetricians and midwives have been reported in the medical literature. Therefore, the feasibility of undertaking these measurements should be evaluated and the effect of the accoucheur's posture on their musculoskeletal system should be investigated.

8.2 Materials and Methods

Studied postures

To facilitate the reproducibility of the experiment all deliveries were conducted in a semi-recumbent maternal position. Two fundamentally differing accoucheurs' postures were selected for analysis, ST and KT, during real life and simulated deliveries. One obstetrician was in the standing position, bending slightly towards the perineum and the side, pivoting his elbow on his right thigh (Figure 8.1(a)), whereas the other obstetrician was supporting the perineum while kneeling on the right knee (Figure 8.1(b)).

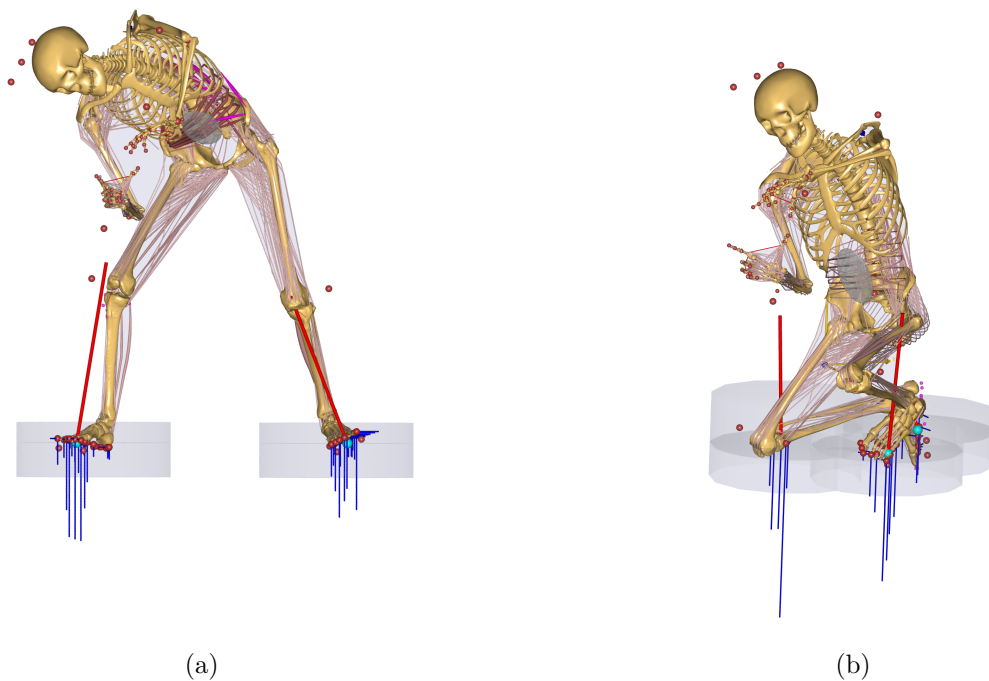


Figure 8.1: Musculoskeletal simulation of the loads acting on the accoucheur within the AMS while performing an MPP using (a) the ST and (b) the KT. The blue lines on the feet show the acting ground reaction force. The different shades of red indicate the various muscle activities - the redder, the more active the muscle.

Experiment set-up

To create the reference data set for the musculoskeletal analysis of the accoucheur's joint loads, a study containing the measurements of two obstetricians (both male, right handed) were conducted with one obstetrician always used ST and the other one KT (anthropometrics: ST 1.83 m and 95.0 kg; KT 1.95 m and 92.5 kg). For both obstetricians, three trials using the birthing simulator (BS) (Sophie and Sophie's Mum Birth Simulator, MODEL-med, Melbourne, Australia) and one trial of a real-life delivery (RD) were measured.. For the birth simulator measurements, the device was placed on a table (height 72 cm), whereas the bed height for the real births was adjusted at 85 and 90 cm, respectively.

To determine the movement of the obstetricians, an Xsens IMC System (Xsens Link, Xsens Technologies BV, Enschede, Netherlands) was applied to the test subjects (Figure 8.2(a)). This system uses inertial measurement units (17 sensors, measurement frequency 240 Hz) to gain joint angles during any motion.

Two gloves, on top of each other, were placed on the accoucheur's hand - one glove to obtain the kinematics of all fingers of each hand (Prime I Xsens, Manus VR, Geldrop, Netherlands) and one glove, measuring the forces acting on the thumb, index, and middle finger of the right hand. The latter glove is a bespoke custom-made glove which was previously described (Kalis et al. 2020). Three force sensor (sensitive resistors Tekscan FlexiForce A201) are used, which recorded the data with a frequency of 100 Hz. The measurement of these forces and the correct application of them via the hand model developed in Chapter 4 is necessary to set the correct boundary conditions for the subsequent musculoskeletal simulations.

After the test subjects were prepared accordingly, the measurements were recorded using a birth simulator (Figure 8.2(b)) and real-life deliveries. Women involved in the real life births were informed in advance about the procedure of the measurement, and informed consent was obtained concerning their voluntary participation. The study was approved by the Ethics committee of the University Hospital in Pilsen, Charles University.



Figure 8.2: (a) Fully equipped obstetrician – including Xsens IMU sensors, Manus VR glove and force measurement glove developed by the New Technologies Research Centre (University of West Bohemia). (b) Performing a delivery using the birth simulator

Simulation

Only the final contraction's time interval was considered for the analysis of the loads acting on the accoucheur's musculoskeletal system. The musculoskeletal simulation software AnyBody (AnyBody Technology A/S, Aalborg, Denmark, V.7.3.1) was used as a modeling environment.

Prior to the simulation, the model was scaled according to the anthropometric data of each test subject. The kinematic data of the experiments were introduced into the simulations as boundary conditions. Kinematic mismatches of the fingers caused by pressure artefacts due to the multiple layers of gloves on the right hand were improved in advance.

To reduce computational time, the muscles of the left (non-dominant) arm were omitted as the loads acting on the left hand were not of interest for this study. The detailed hand model from Chapter 4 was used in the simulation to best illustrate the loads acting on the hand and wrist. The forces measured on the glove were then applied to the corresponding fingers.

The missing boundary conditions of the ground reaction forces were included by using the ground reaction force prediction implemented within the AMS. This method uses the individual segments' acceleration to obtain the acting ground forces (Fluit et al. 2014). One exemplary simulation is shown in Figures 8.1(a) and 8.1(b) for the standing and the kneeling postures respectively. Following the simulations, joint forces were analysed.

For the ST, it is possible that the resting of obstetrician's right elbow on his thigh may have caused some force transmission between those two segments, which could not have been measured. To evaluate how far this possible force transmission affected the load on individual joints, a *spring* was implemented in the simulation model – meaning the closer the two segments get, the more force would have been transmitted. Depending on this spring's stiffness, some (k) or no (k_{zero}) force is transmitted between two segments being in contact. Based on these simulations, the effects of MPP on the accoucheur's musculoskeletal load were determined.

8.3 Results

With the different postures of the two obstetricians, the musculoskeletal system's whole kinematic chain was shifted. This variation was reflected in a corresponding change in the joint reaction forces along the upper extremity and lower back, listed in Figures 8.3 and 8.4. A corresponding table with all exact values (including the applied finger forces) is shown in the Appendix - Table D.2.

Regarding the intra-operator reliability for KT, an average deviation around the mean value of 10.5% was obtained in the maximal forces. The lower back's medio-lateral force components were a noticeable outlier (in the range of $\pm 25\%$). For ST the deviation was about 15.5% for the maximum force - without stronger outliers. When comparing KT and ST with regards to inter-operator stability using the respective mean values, there were comparable maximum and mean values for the upper extremity, although the obstetrician using ST applied on average less force to the perineum via the fingers.

However, this was no longer the case for the lower back. The average maximum total load between the lower back segments increased by 677 N (mean force 638 N) from KT to ST. Also, the shear forces showed a mean rise of the maximum force of 295 N (276 N) and 92 N (66 N) for the anteroposterior and the mediolateral directions respectively.

Hence it can not be excluded that there was any force transmission between the obstetrician's right elbow and his thigh during ST, an exemplary BS-trial (BS-01) was also simulated, using the *spring*. This transmitted force between the two segments was within a range of maximal 90 N.

Only joint loads on the musculoskeletal chain from the elbow upwards were changed by this procedure; therefore, only joints from the shoulder to the L5-Sacrum joint are shown in Figure 8.5. A corresponding table with all exact values can be found in the Appendix - Table D.1.

Based on the results in Figure 8.5, forces in the lower back can be considerably reduced by supporting the elbow. However, within the shoulder, the maximal and mean acting joint reaction forces were almost doubled and quadrupled respectively. Compared to the average force of KT, the shoulder was subjected to a much higher load. While the maximum load between the lumbar vertebral bodies were below the level of KT by the force transmission.

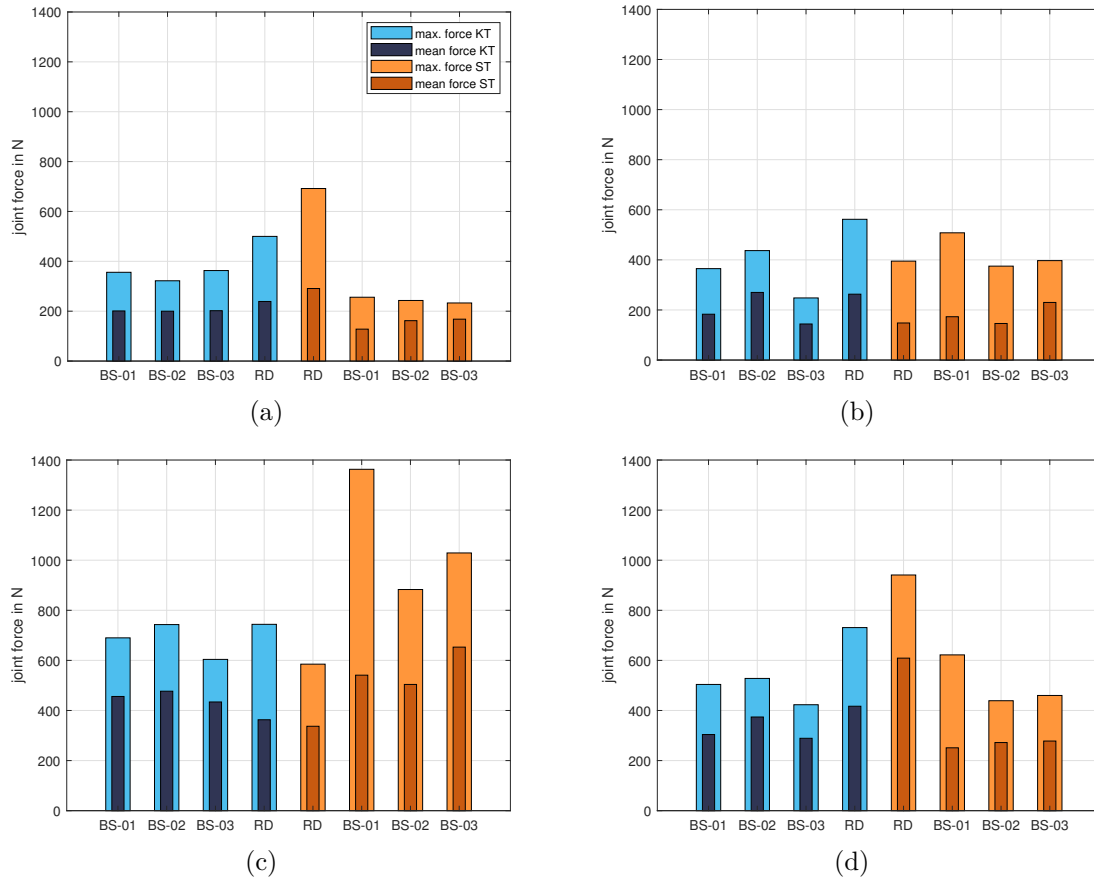


Figure 8.3: Maximal and mean forces (brighter outer or darker inner area) acting on the upper extremity ((a) wrist, (b) elbow – humeroulnar, (c) elbow – radiohumeral, and (d) shoulder joint) during the BS - 01-03 trials and the RD trial for KT 1 (blue) and ST 2 (orange). The results for ST were gained using zero stiffness of the spring between the elbow and the thigh (k_{zero}).

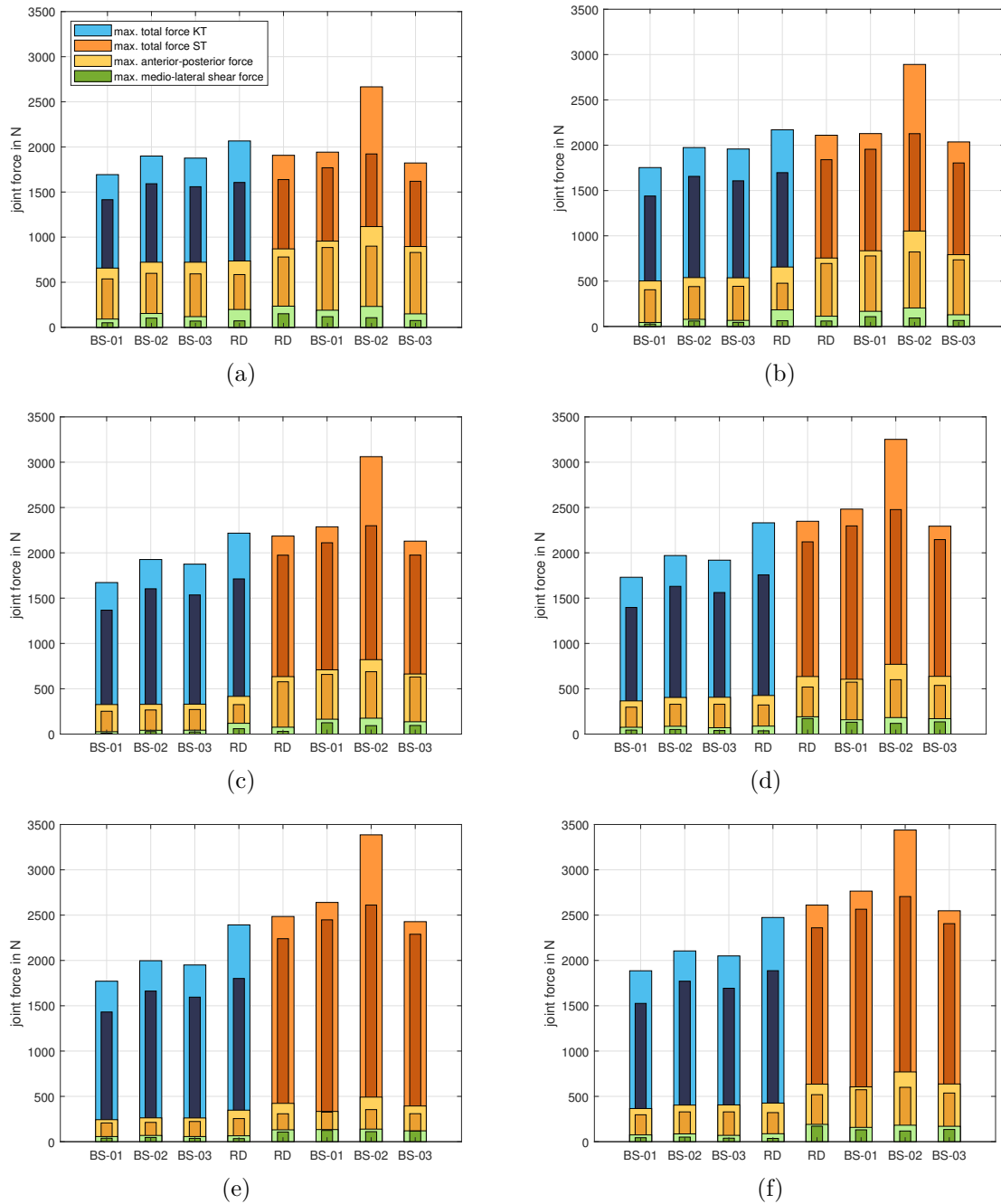


Figure 8.4: Maximal and mean forces (brighter outer or darker inner area) acting on the lumbar spine ((a) T12L1, (b) L1L2, (c) L2L3, (d) L3L4, (e) L4L5, and (f) L5Sacrum joint) during the BS - 01-03 trials and the RD trial for KT (blue) and ST (orange). The overall bar indicates the total acting force, whereas the yellow and green bar indicates the shear forces acting in the anterior-posterior and medio-lateral direction. The results for ST were gained using zero stiffness of the spring between the elbow and the thigh (k_{zero}).

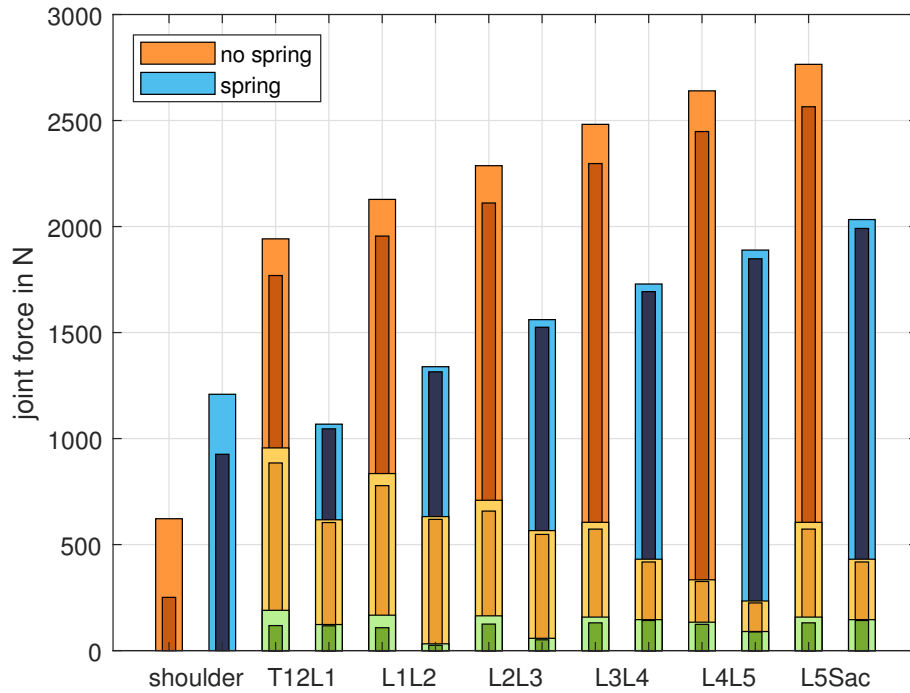


Figure 8.5: Maximal and mean forces (brighter outer or darker inner area) acting on the respective joint during BS - 01 trial for ST using a spring with k_{zero}/k (orange/blue). The overall bar indicates the total acting force, whereas the yellow and green bar indicates the shear forces acting in the anterior-posterior and medio-lateral direction.

8.4 Discussion

This study assessed the feasibility of measuring accoucheur's musculoskeletal joint loads during an obstetric intervention and explored the effect of change in the accoucheur's posture on these loads during real life and simulated vaginal deliveries. With the gained kinematics, the musculoskeletal loads between segments was determined using musculoskeletal simulations. A comparison of the musculoskeletal load of the two techniques used indicates that, regardless of the uncertainty of how much support was provided by the thigh during the standing posture, the kneeling position puts less strain on the musculoskeletal system than the standing position. Moreover, the intra-operator variability of the forces between the individual segments was more scattered in the standing posture compared to the kneeling position (15.5% to 10.5%). If the variability is recalculated with the loads' deviation weighted linearly in relation to the acting force, the intra-operator variability even shifts to 17.6% and 7.2%, respectively. A possible explanation for this is the restriction of the human body's kinematic chain due to the knee's additional fixation on the floor. Thus, higher stability is achieved, allowing less movement variability. This is also reflected in the kinematic data due to the local stronger fixation of the pelvis. Therefore, the intra-operator variability is probably more pronounced in ST than in KT.

If the load on the two test subjects' musculoskeletal system is compared, the loads on the upper extremity were similar, but the radio-humeral joint load is slightly higher in ST. Even if the loads between the two techniques do not differ significantly for the upper extremity, it can be stated that forces up to 146% of the body weight (see BS-01 for subject 02 - radiohumeral force) can appear during perineal support. These high forces, in combination with the nature of the repetitive task of obstetricians, have the potential to cause musculoskeletal disorders, according to Gallagher and Heberger (2013). Higher forces mean a higher risk, and this is the case for the accoucher.

Therefore, using the standard detailed hand model of the AMS in the simulation instead of the hand model developed in Chapter 4 would possibly underestimate this risk. Compared to the hand model developed in this thesis, the simulation of the birth process with the AMS hand model shows a lower maximum and average

force in the area of the upper extremity (wrist: 10% max., 20% mean; elbow-humeroulnar: 20% max., 29% mean; elbow-radiohumeral: 41% max., 45% mean; shoulder: 13% max., 16% mean). This underestimation of the acting forces is most likely due to the lack of detail of the AMS model. The synergy of the muscles distributes the load among several muscles - including those with a lower moment arms. Thus, in order to apply the same moment, higher forces are required in the muscle, which in turn increases the joint reaction forces. However, if some of these muscles are not present at all (as in the AMS hand model), the acting force is automatically reduced compared to the hand model developed in Chapter 4 and validated in Chapters 5, 6, and 7. Thus, the potential risk of musculoskeletal disorders in the upper extremity of the obstetricians is more accurately represented by the newly developed and validated hand model.

Regarding the lower back load during the birth process, forces are, approximately, equivalent to carrying a 20 kg box in a bent-over position if other studies are used for classification (Lee et al. 2013). However, these forces were much higher in the upright position. According to Gallagher and Marras (2012), occasional exposures to antero-posterior shear loadings up to 1000 N are acceptable, and a limit of 700 N is appropriate for repetitive work. This 1000 N limit was exceeded twice in the standing posture (BS-02 T12/L1 and L1/L2) and the 700 N limit was exceeded constantly at the T12/L1, the L1/L2 and partly at the L2/L3 joint or are even close to this limit for the other joints considering the maximum values. But the mean values for the first two joints are also above the 700 N limit.

In contrast, during KT the 1000 N mark was never broken, and the 700 N limit was only slightly broken for the maximum values of the T12/L1 joint. Regardless of whether the limits used in the literature can be considered to be absolutely valid, it can be seen that peak loads are significantly less pronounced in KT than in ST.

However, an unknown parameter in the simulations is the extent to which the right elbow during ST transfers force to the thigh. A corresponding absorption or redirection of force could relieve the lower back. Therefore, the spring was included in the simulation, and an exemplary case (BS-01) was calculated, which demonstrated that up to 90 N could be transferred. Indeed, the comparison of Figure 8.3 - 8.5 shows that the force transmission is capable of reducing the load (total and shear forces) of the lower back in general for the standing posture.

Interestingly, the maximum acting force was even lower than the average maximal force acting during KT (for example, -755 N at T12/L1 and -566 N at L1/L2). However, when assessing the average acting force, there was a reduction at T1/L1 and L1/L2 but an increase at L2/L3 - L5/Sac.

Nonetheless, most of the force transmitted via the elbow seems to increase the load on the shoulder where the mean and maximal acting forces acting were almost tripled compared to the average forces during KT. These findings suggest that a higher force transfer to the distal thigh protects the lower back (about the same extent as the KT) but makes musculoskeletal injuries in the shoulder area much more likely.

When considering the differences between the birthing simulator and real delivery, there are slight deviations for the lower back and the upper extremity. On average, the lumbar spine's maximal forces deviate only 17% and 13% for KT and ST, respectively (mean force 10% for both) during the birth simulator measurements compared to real birth values. However, for the upper extremity, the deviation increased to 27% and 54% in the maximal (mean forces 23% and 54%) respectively. Exploring the reasons for these variations was outside the remit of this study, however, there are several possible reasons. First, the increased elbow pronation and ulnar abduction of the wrist during real birth compared to BS-01-03. Second, the difference in table/bed heights, which also contributes to the kinematic movement chain. Third, ST transferred a below average amount of force in simulated birth, which could possibly be due to a non-optimal haptic of the birth simulator. These are all important points that need to be addressed in further studies.

This study has some limitations. Firstly, only data from two male obstetricians performing MPP in two postures were captured. However, the primary intention was to assess the strain on the musculoskeletal system in general and determine if there is a significant difference depending on accoucheur's posture. Additionally, this allowed evaluation of the intra-practitioner variability. Secondly, one real life delivery per posture is insufficient to draw conclusions, however, due to the nature of a vaginal birth, motion capture is extremely challenging. This is also the reason why these were compared to birth simulations as these are much easier, safer and more controlled to organize and perform. Nonetheless, the development and application of a specifically designed integrated system to capture the required data

and the fact that this is the first report of such measurements are major strengths to this study.

This feasibility study enabled us to test the protocol and optimize data collection that will inform future larger studies, in which the number of obstetricians should be increased and the influence of additional parameters, such as the influence of altering the table height, should be examined more closely.

8.5 Conclusion

In this study an extremely high strain on the musculoskeletal system of an accoucheur during manual perineal protection was demonstrated using kinematic measurement of birth processes conducted with the assistance of a birth simulator, as well as recordings of real deliveries. The results of this study point to an unstudied aspect of a vaginal delivery. Optimizing practitioners' posture during labor may significantly contribute to the increase in the quality of life of obstetricians and midwives and reduce the cost burden of staff sickness leave secondary to musculoskeletal problems. Finding the optimal posture for the accoucheur remains a challenge for future research.

Furthermore, the results of this study demonstrated that the hand model developed in this thesis is suited to assess the risk of potential musculoskeletal disorders regarding the upper extremity. Moreover, the hand model developed in Chapter 4 enables the correct application of external forces into the system and thus ensures a realistic musculoskeletal analysis of the lower back.

Chapter 9

Elbow model: model development

9.1 Introduction

The elbow joint, which connects the two forearm bones (ulna and radius) with the humerus, consists of two joints, namely a hinge (i.e., humeroulnar joint) and a socket and ball joint (i.e., radiohumeral joint). While the former allows flexion/extension, the latter only allows two degrees of freedom (flexion/extension and pronation/supination of the hand) due to the fact that there is a fixation between the ulna and radius. Thus, the elbow joint ensures that the hand can be precisely spatially aligned as a grasping mechanism allowing for interactions with the external world. This ROM of the elbow joint is enabled by a total of four main muscle groups (m. biceps brachii, m. brachialis, m. brachioradialis, m. triceps brachii), which span the joint. The joint itself is also enclosed by a joint capsule and the medial and lateral collateral ligaments, which provide additional stability to the elbow (see Chapter 2.2).

In recent years, extensive work has already been done in the Laboratory for Biomechanics at the Ostbayerische Technische Hochschule in Regensburg on advancing a musculoskeletal shoulder model in the AnyBody simulation software (Aurbach et al. 2020a,b). Additionally, a new musculoskeletal hand model was developed and validated (see Chapters 4 - 7) in this thesis. Therefore, investigating elbow joint – arguably the most important joint of the upper limb (Morrey 2009) – was the logical next step of research as it links the shoulder joint and the hand. This

step will complete the development of an entire detailed model of the upper extremity in the Laboratory for Biomechanics in Regensburg.

Such a model is of high practical importance and contributes to the literature in manifold ways. To elaborate, the elbow is the most or second most commonly dislocated joint (following the shoulder) in children and adults, respectively (Litin and Nanda 2018). Specially, the action of intercepting of falls and the resulting high varus/valgus moments causes not only numerous injuries of the ligaments but also fractures of the bones in the elbow area. A loss of elbow functionality as a consequence often results in a very severe limitation of mobility and incapability to interaction with the environment effectively.

Musculoskeletal simulation models are an effective tool for investigating the effects of such injuries/damage to the soft tissues or bony structures of the elbow joint and their downstream consequences for elbow functionality and stability. Numerous research groups conducted musculoskeletal simulations of the human elbow over recent decades. In addition to the model of Holzbaur et al. (2005), which was already addressed in Chapter 4, there are many other musculoskeletal models that are concerned with the biomechanics of the elbow (Gonzalez et al. 1996, Lemay and Crago 1996, van der Helm et al. 2001, Garner and Pandy 2001). However, all these studies consider the elbow joint merely as a simplified hinge joint and neglect the ligamentous components. Of note, though, Tanaka et al. (1998) showed that the elbow joint reveals instability in relation to valgus and varus moments. Thus, previous models miss a crucial part, which is foundational to the stability of the elbow and of high relevance to clinical questions. Another limitation of the research mentioned above is that all developed models are stand-alone models without being embedded in a holistic body model and thus cannot properly reflect the complexity of the human body.

Furthermore, the model developed in the research mentioned above are advanced by the work of Fisk and Wayne (2009), who developed a musculoskeletal elbow model, in which the joint behaviour was determined by ligament constraints. However, their model is based on several strong assumptions that do not correspond to reality. That is, the ligaments were modeled as linear springs, the muscle forces were modeled as constant force vectors, and only *m. triceps*, *m. brachialis*, and *m. biceps* were considered, while neglecting that the path of the muscles and ligaments is influenced by different obstacles.

While some of these shortcomings have already been addressed through more realistic modeling by Rahman et al. (2018), their model is also a stand-alone model, which only contains the three main muscles that span the elbow (m. triceps, m. brachialis, and m. biceps).

To the best of my knowledge, no musculoskeletal model of the elbow exists that 1. can be embedded in a holistic body model, 2. can be scaled patient-specifically, 3. does not represent the elbow as a simplified hinge joint, and 4. includes both the ligamentous apparatus and all the muscles spanning/passing the elbow. Therefore, this thesis aims to create a more detailed model of the human elbow based on literature data and validates it using experimental data (muscle moment arms, ligament elongation during flexion, ligament tautness, and acting moment within the elbow during valgus/varus moments). The elbow model will be developed in the simulation software AnyBody in a similar fashion to the hand model to benefit from all the advantages of the inverse dynamic approach and the scaling functions already mentioned in Chapter 4. As with the hand, the elbow cannot be considered in isolation, but must be integrated into a holistic body model, which is implemented by the generic human body model in the AMS.

Subsequently, this model will be used in Chapter 11 to evaluate clinical issues of elbow stability after different elbow stabilization failures from a biomechanical point of view.

9.2 Elbow model

The elbow model was embedded in the AMS Version 7.3 and AMMR 2.2.2 (Lund et al. 2019). The AMMR full-body model including the detailed hand model was used as a basis. The fact that many of the extrinsic muscles of the hand model originate in the elbow area is particularly relevant in this context, as the use of the detailed hand model also allows for a more accurate calculation of the forces acting on the elbow. For the elbow joint, the revolute joint implemented as standard in the AMS was used allowing only one DOF (flexion and extension). In contrast to the standard model, the new elbow model allows an adjustment of the cubital angle (formed between the axis of a radially deviated forearm and the axis of the humerus). In the AMS standard model, this angle is set to 0° , which corresponds

to a cubitus varus deformity; a deformity in which the extended forearm is deviated towards the midline of the body (see Figure 9.1(a)). However, since the literature (Waldt and Woertler 2014) assumes that a normal cubital angle is between 5° ($<5^\circ$ cubitus varus deformity) and 15° ($>15^\circ$ cubitus valgus deformity), a cubital angle of 10° was defined as standard in the new elbow model (see Figure 9.1(b)).

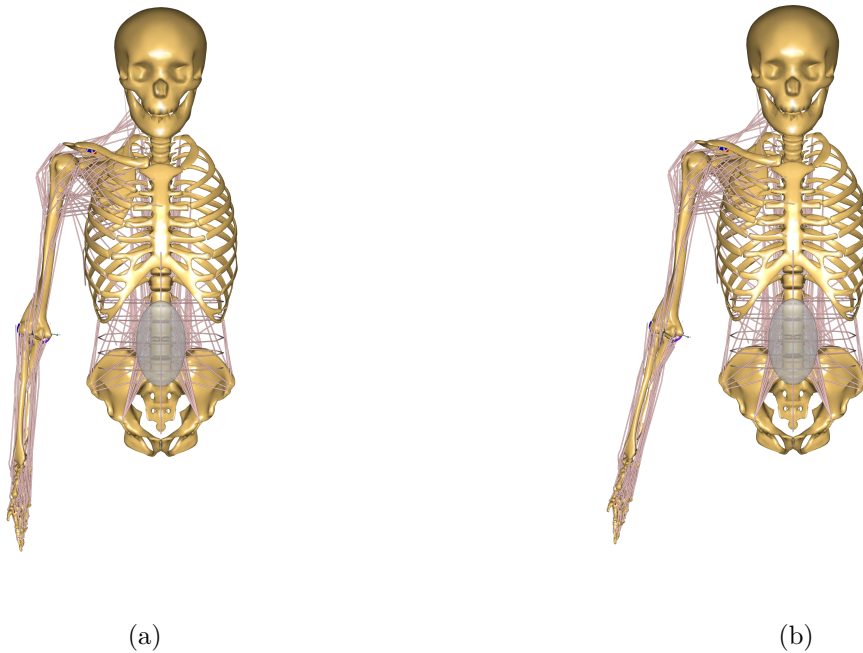


Figure 9.1: Implementation of the cubital angle in the AMS. Figure (a) shows the formerly default cubital angle of 0° within AMS, whereby Figure (b) depicts the basic angle of 10° defined for the new elbow model.

9.2.1 Muscles

As part of the same anatomical study conducted at the University of Pilsen to determine the muscle parameters of the ex- and intrinsic hand muscles in the forearm region (see Chapter 4), detailed maps of the upper arm muscles were created as well (Havelková et al. 2020). These data, which include the muscle origin and insertion points, as well as the muscle cross-sectional areas, were implemented in the new elbow model.

9.2.2 Ligamentous apparatus

For the ligamentous apparatus, the medial and lateral collateral ligament complexes were implemented using data from prior literature. According to Morrey and An (1985), the lateral ligament complex is composed of the radial collateral ligament (RCL) as well as the medial ligament complex of the anterior and posterior medial collateral ligaments (AMCL and PMCL). The origin and insertion points of these three ligaments, based on a dissection of ten fresh cadaver specimens, were taken from Morrey and An (1985) for the new elbow model. To be able to distangle the occurring forces in more detail, each band complex was divided into three parts - an anterior, middle, and posterior portion.

Unlike muscles, ligaments cannot actively generate forces themselves. They only passively introduce forces into the multi-body system like a spring. Therefore, the force applied to the system depends strongly on the specific stiffness of the ligaments. Regarding the AMCL, PMCL, and RCL ligaments, Regan et al. (1991) measured corresponding force-strain curves of up to seven specimens and representative curves were determined (see Figure 9.2). These curves are used for the analysis of the load acting within the model.

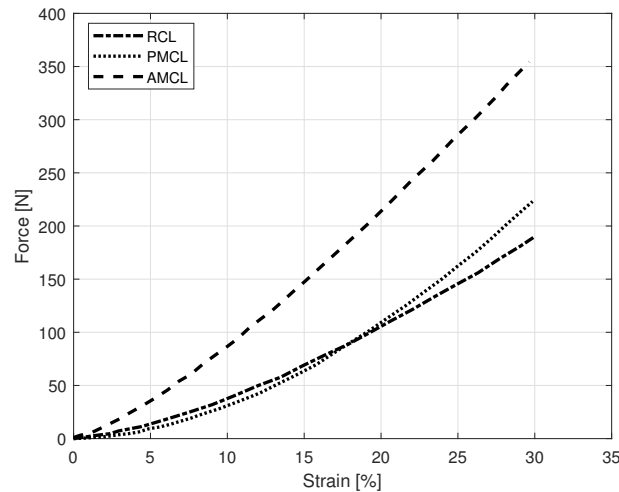


Figure 9.2: Experimental data from Regan et al. (1991) regarding the force-strain relationship of the different elbow ligament complexes.

In addition to the stiffness of the ligaments, the length (or the positions of the elbow) at which the ligaments are in a taut state, and thus introduce passive forces to the system, is also essential. The ligament position at which the different parts (anterior, middle, posterior) of the ligaments can be considered taut in the neutral state (without additional valgus or varus moments) was also taken from the experimental study of Regan et al. (1991). All ligaments were calibrated according to the individual zero-load length l_0 to best fit the tautness-range within the neutral position.

9.2.3 Varus-Valgus motion

Within the AMS, all joints are defined as ideal joints allowing a certain number of DOFs. However, many biomechanical joints are not ideal and allow small motions between the bones based on acting forces from muscles or ligaments. One example of such a motion is the varus-valgus motion of the elbow joint.

On the one hand, as discussed in Chapter 3, the inverse dynamics approach requires motion of the entire system in order to compute the muscle forces. On the other hand we need the acting forces to compute the according motion, which leads to a chicken-and-egg problem. This issue is solved by means of the force-dependent kinematics (FDK) approach (Skipper Andersen et al. 2017), which allows a small rotational deviation for the elbow joint in this case. The passive force created by the ligaments of the elbow stabilizes the joint against free rotation. Therefore, the ligamentous apparatus contributes crucially to resistance against applied valgus/varus moments (though the stabilizing function of capsule and articulation ought to be acknowledged - see Morrey and An (1983)). Morrey and An separated the elbow joint from four cadaver specimens, leaving only the bone, ligamentous apparatus and capsule. The joints were then fixed in a corresponding testing machine and the moment acting in the elbow was recorded both for the extension and the 90°-flexion for different displacements in the valgus and varus directions. These displacement-load curves were obtained for the intact condition as well as for the complete transection of the lateral and medial ligament apparatus. This data was incorporated into the new elbow model to determine the rotational resistance of the joint in the intact case. This resistance, which results from the capsule and the

articulation, was then simulated in the new elbow model by a torsion spring in the elbow joint. Since only the values for extension and 90° flexion were determined in the experiment, and thus experimental values for the interval between the two values were missing, the model was based on the assumption of a linear progression between the two interval limits and beyond.

Chapter 10

Elbow model: validation

In order to validate the new elbow model, a comparison of the data calculated by the model with experimental literature data was conducted with regard to the following variables, which are elaborated in the subsequent chapter.

- muscle moment arms (section 10.1.1)
- ligament elongation (section 10.1.2)
- ligament tautness (section 10.1.3)
- elbow moment (section 10.1.4)
- change of cubital angle/rotation axis during flexion (section 10.1.5)

Since prior literature does not provide precise anthropometric data of cadaver specimens, all following simulations were performed using the anthropometrics of an average 50 percentile male person (body height: 1.75 m; body weight: 75 kg). All other segment lengths and segment masses were scaled according to Winter (2009).

10.1 Validation

10.1.1 Muscle moment arms

As mentioned in Chapter 5, the line of action and moment arms are critical parameters in predicting muscle and joint reaction forces according to Raikova and Prilutsky (2001). Therefore, a comparison of the numerically determined moment arms with experimental data was performed for the elbow model as well. The comparison was based on a study conducted by Murray et al. (1995) in which the moment arm of *m. brachioradialis*, *m. brachialis*, *m. biceps*, *m. triceps*, and *m. pronator teres* during elbow flexion and of *m. pronator teres*, *m. biceps*, and *m. brachioradialis* during elbow pronation of two alcohol-preserved cadaver specimens was measured using the tendon excursion method (see also Chapter 5).

10.1.2 Ligament elongation

Ligaments cannot actively generate forces. However, they act as passive elements whose forces depend on stiffness and the range of the respective strain/elongation. In order to determine the distance between the origin and the insertion of the different bands as a function of the angle of flexion, Morrey and An (1985) conducted a study in which five specimens were measured accordingly. The resulting data were normalized to the magnitude at 0° flexion (= full extension). This change in band length will be compared with data collected numerically analogous to the study for validation purposes. Since the study by Morrey and An did not contain any information on the position of the hand (supination/neutral/pronation) during the collection of the data, a neutral position was assumed for the collection of the numerical data.

10.1.3 Ligament tautness

The range during the flexion of the elbow in which the anterior, middle, and posterior parts of the ligaments are to be considered taut was also addressed by Regan et al. (1991). In his study, this range was determined both without valgus/varus displacement and for the position under valgus and varus moments. Unfortunately, however, it is not further defined which excursion was considered as valgus or varus deviation. Due to this lack of information, the following parameters were assumed for the comparison of the model with the experimental data from Regan et al. (1991). A varus/valgus deviation was defined as a deflection of the cubital angle by 5° in each case, allowing the cubital angle of the model to reach the marginal ranges (5° or 15°) at which deformity is not yet considered to exist. Since the underlying study did not contain any information about the position of the hand in this case either, a neutral position was assumed.

As mentioned in Chapter 9, the data without occurring valgus-varus-deviation were used to define the zero-load length and thus the values with occurring deviation could subsequently be used for validation purposes.

10.1.4 Elbow moment

The resistance of the elbow regarding an acting moment is an essential parameter when assessing the stability of the elbow (see Chapter 11). Consequently, the moment acting on the elbow and the corresponding change in the cubital angle is compared with experimental data from Morrey (2009), both in the intact state and in the case of various ligament injuries/ruptures. Morrey has exposed the elbow joint of four cadaver specimens and mounted them in a material testing machine. A force was applied at a distance of 12 cm from the joint center in the medial and lateral direction for extension as well as 90° flexion. The corresponding shift the cubital angle was detected. This procedure was performed for the intact case as well as a complete cut of the medial and lateral ligament apparatus. The experimental setup was simulated using the musculoskeletal simulation model without any acting muscles and the corresponding measurement series were recreated.

10.1.5 Change of cubital angle/rotation axis during flexion

In the previous validation steps, the ligamentous apparatus and the muscles (more precisely, their moment arms) were considered separately. In a final validation step, the acting ligamentous apparatus will be tested in conjunction with all muscles. A study by Van Roy et al. (2005), who measured the change in the cubital angle of 20 subjects (10 male and 10 female subjects) during elbow flexion from 0° to 120° , was used for this purpose. Therefore, a flexion of 0° to 120° was simulated in the model and the change in the cubital angle was measured.

Furthermore, according to Bottlang et al. (2000), the flexion axis of the elbow joint is not a fixed rotation axis (as specified in the previous AMS model), but shows a tilt during flexion. Thus, it should also be examined whether and to what extent the flexion axis rotates during flexion.

10.2 Results

10.2.1 Muscle moment arms

Figure 10.1 and 10.2 show the comparison of the experimentally gathered literature data (Murray et al. 1995) and the numerically calculated muscle moment arms of the m. brachioradialis, m. brachialis, m. biceps, m. triceps, and m. pronator teres. For the elbow flexion, all muscles follow the trend of the experimental data and remain mostly within the SD. Only two out of three branches of the m. brachioradialis show an offset (see Figure 10.1). Regarding the pronation of the elbow, the model prediction shows a progression comparable to the data from literature. However, a deviation from the literature data with regard to m. brachioradialis can be observed for the pronation as well (see Figure 10.2).

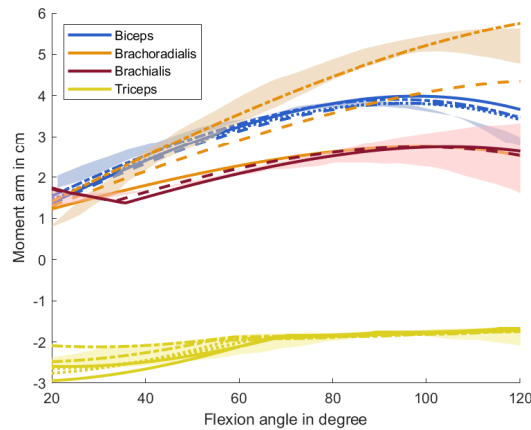


Figure 10.1: Progression of the moment arms for the elbow regarding the most dominant muscles during the flexion of the elbow joint. Lines represent the simulated results, whereas the shaded areas highlight the experimental data from Murray et al. (1995). Positive moment arms indicate flexion, negative moment arms indicate extension and 0° flexion angle represents full extension.

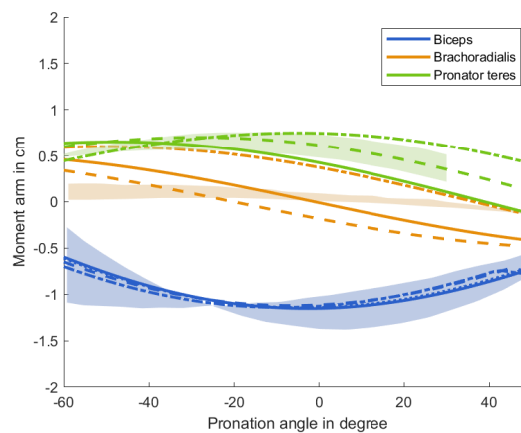


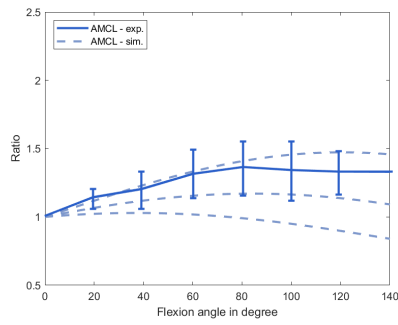
Figure 10.2: Progression of the moment arms for the elbow regarding the most dominant muscles during the pronation/supination of the forearm. Lines represent the simulated results, whereas the shaded areas highlight the experimental data from Murray et al. (1995). Negative angles and moment arms indicate supination, positive angles and moment arms indicate pronation.

10.2.2 Ligament elongation

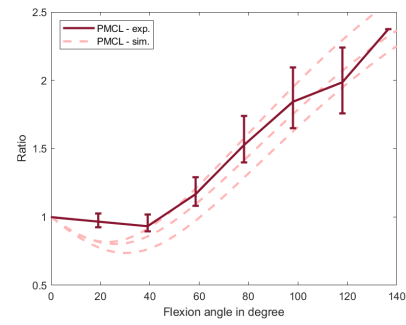
The experimentally gathered length difference between the origin and insertion points of the three ligaments (including SD) is compared with the numerically determined length difference in Figure 10.3(a) - 10.3(c). Throughout elbow flexion, two of three strands of AMCL always remain within the range of experimental data (\pm SD). The third, however, exhibits a significant lower elongation. For the PMCL, the band is initially compressed more in the model than in the experimental data. However, starting from a flexion angle of approximately 60° the band length change of the numerical model is within the range of the experimental values. In contrast, the RCL shows a larger distance between origin and insertion points in the model. Especially in the range from 100° flexion, only one portion is within the SD.

10.2.3 Ligament tautness

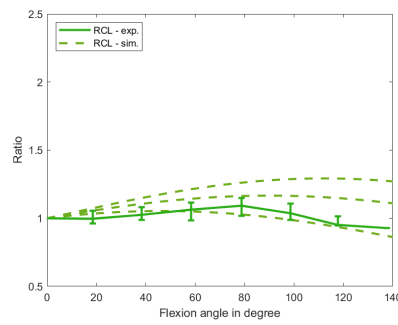
Figure 10.4(a) - Figure 10.4(c) show the area in which the different ligaments can be considered taut with and without valgus or varus deviation. The darker bars represent the experimental data from Regan et al. (1991), whereas the brighter bars represent the numerical data for the anterior (blue), middle (red), and posterior (yellow) parts. For the AMCL, all three portions of the ligament follow the trend of a decreasing area of stiffness from valgus to varus. Furthermore - except for the anterior part in neutral position, which is slightly outside the SD - all stiffness ranges of the bands agree very well with the experimental data. The same is true for the PMCL, which also shows good agreement between literature and numerical data and reflects the trend of reduced tautness range from valgus to varus. Especially in the case of valgus deviation, the RCL shows larger deviations from the experimental data for the medial (no stiffness in the range between 0° and 30° flexion) and posterior (no stiffness in the range between 120° and 140° flexion) ligament part. However, the anterior ligament part also shows slightly increased stiffness range in the numerical model.



(a) Elongation of AMCL

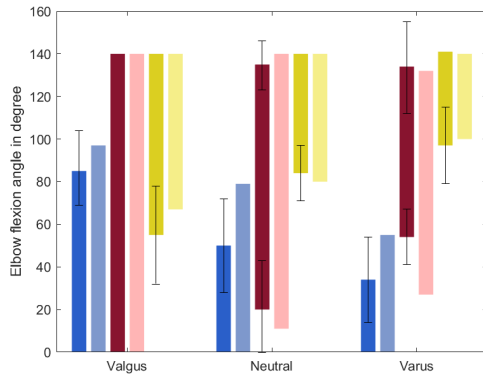


(b) Elongation of PMCL

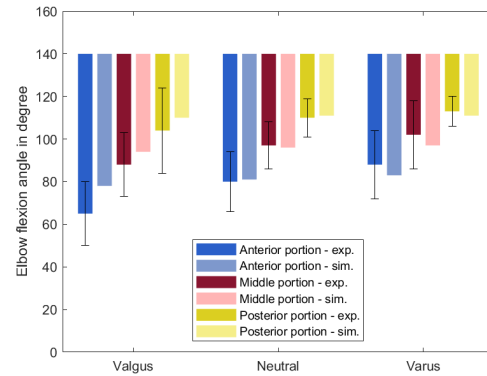


(c) Elongation of RCL

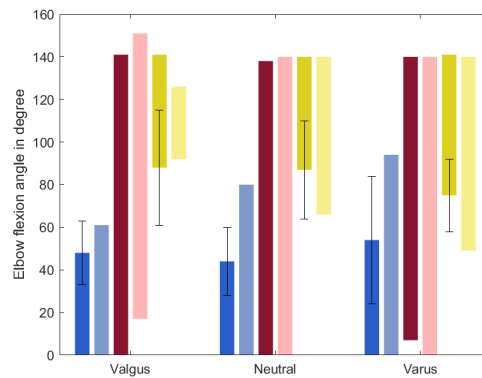
Figure 10.3: Comparison of ligament elongation for (a) the AMCL, (b) the PMCL, and (c) the RCL ligament between AMS (dashed lines) and experimental data (solid lines) according to Morrey and An (1985). All values were normalized to the initial value at 0° elbow flexion (= full extension).



(a) Tautness of AMCL



(b) Tautness of PMCL



(c) Tautness of RCL

Figure 10.4: Comparison of the mean and SD of the experimental data gained by Regan et al. (1991) and the AMS for the (a) AMCL, (b) PMCL, and the (c) RCL ligament. The bars indicate the areas during the elbow flexion (whereby 0° flexion represents full extension) in which die corresponding ligament is under tension or taut. These ranges were compared without deviation (neutral) and with valgus varus deviation.

10.2.4 Elbow moment

Using the FDK, the change of the cubital angle can be determined for different scenarios (failure of different ligaments) by applying a certain valgus and varus moment. The data obtained from the simulation are contrasted with the experimental data from Morrey (2009) in Figure 10.5 (extension) and Figure 10.6 (flexion).

For the extension, the two calculated scenarios - Intact and the failure of the ulnar collateral ligaments (UCL) (which corresponds AMCL and PMCL) - follow the trend of the experimental values. A UCL cut has a stronger effect on the lack of elbow stability in the experimental data than in the numerical one. Further, for the flexion, the trend of decreasing elbow stability against valgus moments from the intact case over the RCL cut to the UCL cut can be well represented by the model. For the varus area, the data is within the range of experimental values, whereby the stability of the model decreases from the intact case via UCL cut to RCL cut and slightly increases in the study of Morrey (2009).

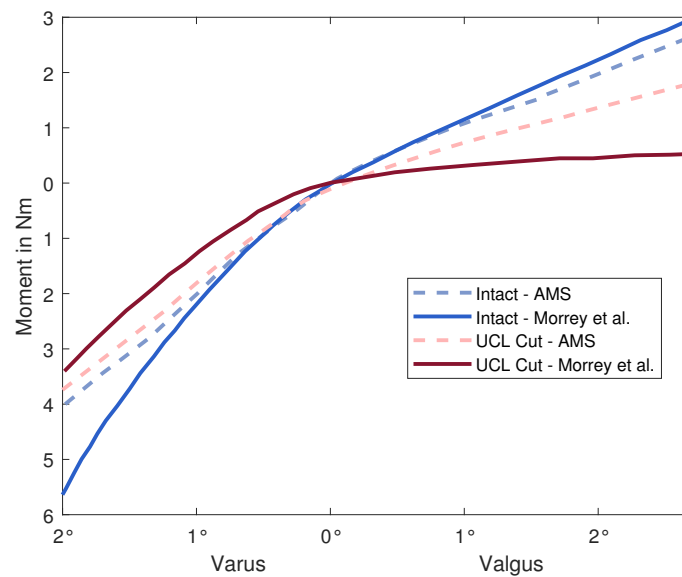


Figure 10.5: Compared load-displacement curves of the experimental data gained by Morrey (2009) (solid lines) and the AMS (dashed lines) for full extension.

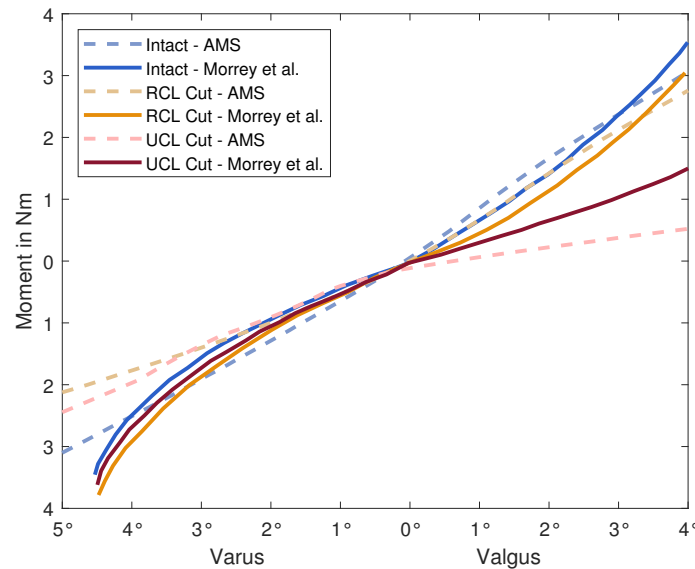


Figure 10.6: Compared load-displacement curves of the experimental data gained by Morrey (2009) (solid lines) and the AMS (dashed lines) for 90° flexion.

10.2.5 Change of cubital angle/rotation axis during flexion

During flexion from 0° to 120°, the cubital angle decreases continuously according to the experimental data from Van Roy et al. (2005). This reduction can also be identified in the model - see Figure 10.7. With the exception of the case of a 90° flexion, the values of the model remain within the SD of the data of Van Roy et al. (2005).

Similar to the experimental data from Bottlang et al. (2000), the new elbow model does not show a fixed flexion rotation axis for a performed flexion between 10° and 130° (see Figure 10.8). Rather, using the humerus bone as a reference system, a tilt of the rotation axis in the medial-lateral direction of up to 4.3° (Bottlang et al.: $5.7^\circ \pm 2.2^\circ$) and proximal-distal direction of up to 3.5° (Bottlang et al.: $2.6^\circ \pm 1.0^\circ$) can be identified.

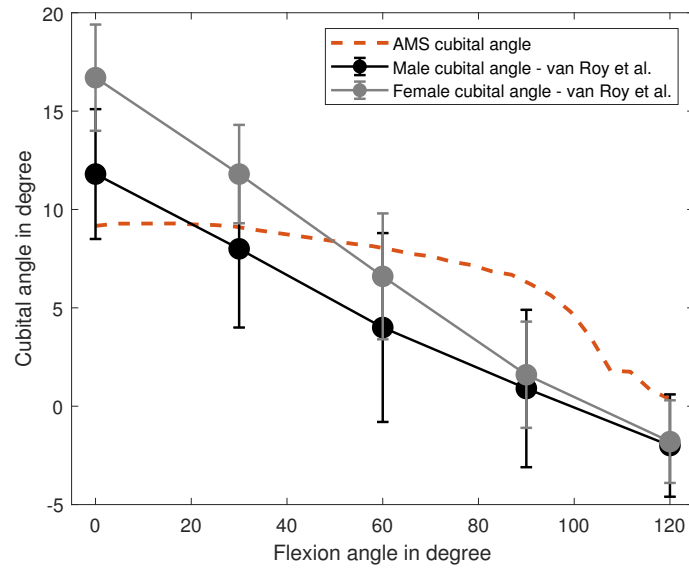


Figure 10.7: Comparison of the change in the cubital angle during elbow flexion of experimental data gained by Van Roy et al. (2005) and the AMS model. Positive cubital angle represents a rotation to the lateral side.



Figure 10.8: Visualization of the change in the rotation axis during elbow flexion of the new elbow model. The individual red lines correspond to the position of a rotation axis during flexion from 10° to 130°.

10.3 Discussion

The aim of this study was to validate the developed detailed elbow model from Chapter 9 by means of comparing the numerical gained quantities of the model with the experimentally gathered data from literature. Therefore, the muscle moment arms, the elongation of the different ligaments, the range in which the ligaments can be considered taut, the elbow stability against varus and valgus moments, and the change of the cubital angle/rotation axis during flexion were investigated. Since the model and the different validation steps come with idiosyncratic advantages and limitations, the validation process and then the model itself will be examined more closely in the following.

10.3.1 Muscle moment arms

With respect to flexion/extension and pronation/supination, muscle moment arm patterns of the elbow indicate a good alignment with data from the literature and are within the range reported by Murray et al. (1995). However, deviations from the experimental data can be observed for the m. brachioradialis whose representatives show an approximately larger variation. Only one of the three representatives of the muscle in the AMS is within the range of the literature data for the flexion/extension movement. For supination/pronation, the trend of a decreasing moment arm in the AMS can also be observed, but the sign changes from supination to pronation, which is not reflected in the experimental data. With respect to these deviations, however, it is important to note that the experimental study of Murray et al. is based on only two cadaveric subjects with unspecified anthropometric data.

10.3.2 Ligament elongation

Concerning the elongation of the ligaments, the progression of the ligaments implemented in the AMS essentially corresponds to that of the experimental data from Morrey and An (1985). However, a comparison of experimental and numerically calculated data is problematic, since the literature does not specify exactly which points were defined as origin and insertion points of the ligaments, from which

the distance was measured. Furthermore, it is important to consider to what extent certain deviations are relevant for numerical simulations. For example, in the range from 0° to about 40° , all three PMCL ligaments in the AMS deviate from the literature data (see Figure 10.3(b)). However, since the PMCL band can only be considered stiff above a much higher flexion angle and only from this point on passive forces would enter the system, such a deviation can be neglected.

10.3.3 Ligament tautness

The change in ligament length as well as zero-load length, essentially determine the range of stiffness and as a consequence determine when the ligaments apply passive forces to the system through their stiffness. The tautness of the ligaments determined by the elbow model is relatively consistent with the experimental data of Regan et al. (1991). The model also reflects potential trends - such as a decreasing tautness range from valgus to neutral position to varus in the PMCL and the AMCL ligament, respectively.

Any deviation from the experimental data can also be attributed to the fact that no precise data (i.e. applied moment or cubital deflection of the elbow joint) was found for varus/valgus deviation in the study from Regan et al. (1991) and therefore a change in the cubital elbow angle of $\pm 5^\circ$ for varus/valgus was assumed.

10.3.4 Elbow moment

The implementation of the FDK approach in combination with the ligaments and the additional stability provided by the articulation and the capsule modeled by the torsion spring seems to be able to reflect the trend of the experimental data well. However, it is worth mentioning that the data presented by Morrey is only a typical load-displacement curve and no exact measurement data is available. Furthermore, the underlying study is based on unembalmed and fresh frozen cadaver specimens. Studies, however, have shown that the freezing process can have a strong impact on the biomechanical properties of cadaver specimens (Clavert et al. 2001, Giannini et al. 2008). Consequently, the experimental data cannot be considered as absolute. Further, the fact that at 90° flexion at varus deviation for the intact case lower moments are necessary for the same cubital deflection as for the RCL and UCL Cut seems questionable.

10.3.5 Change of cubital angle/rotation axis during flexion

In the final validation step, the interaction of the FDK approach with the ligaments and all muscles was examined. By dissolving the simplified hinge joint in the elbow, the axis of rotation of the joint can change depending on the flexion angle. As a result, this axis may tilt slightly in the medial-lateral and proximal-distal directions, and thus the cubital angle may also change across flexion. Therefore, consistent with findings by Van Roy et al. (2005), a respective decrease of the angle is shown. Additionally, the corresponding tilt of the rotation axis agrees with the experimental data of Bottlang et al. (2000).

10.3.6 The model

As discussed in Chapter 4, a major advantage of the hand model is the consistency of the data set it is based on. Since not all parameters required for the elbow were recorded in the data set from Havelková et al. (2020), various literature data had to be used to create the elbow model. The muscle attachment points and strengths were taken from Havelková et al. (2020), the attachment points of the ligaments from Morrey and An (1985), and the stiffness and the zero-load length from Regan et al. (1991). Thus, the resulting model can be described as "Frankensteinian", as is often the case in the field of musculoskeletal simulation.

Since the underlying literature was limited to the AMCL, PMCL, and RCL ligaments, only these ligaments were implemented in the model while lateral ulnar collateral ligament and the annular ligament were omitted; since, to the best of my knowledge, there was no corresponding literature that included the necessary biomechanical properties of these ligaments. This approach can also be justified by the fact that, according to Morrey and An (1985), a lateral ulnar collateral ligament was found in only half of the cadaver specimens examined, indicating that this ligament need not necessarily be present. Furthermore, the annular ligament is mainly responsible for the stability of the radial head during supination/pronation movements (Alcid et al. 2004). However, since during the validation process (and also in the later application of the elbow model in Chapter 11) only elbow flexion in the neutral position of the hand was considered, the annular ligament does not play a noteworthy role as far as elbow stability is concerned; especially

since its contribution to elbow stability in the neutral position is represented by the additionally implemented torsion spring.

Despite the limitations mentioned above, the developed model provides innovative contributions, such as the implementation of the cubital angle, usage of the passive forces of the ligaments combined with the FDK approach, softening the flexion-rotation axis as a fixed hinge joint. These improvements are of high practical relevance in answering a number of clinical research questions, which will be discussed in the following chapter.

Chapter 11

Elbow model: clinical application - stability analysis

11.1 Introduction

The elbow is the most or second most commonly dislocated joint (following the shoulder) in children and adults, respectively (Litin and Nanda 2018). An elbow trauma can cause injury to the bony, ligamentous, and muscular stabilizers of the elbow joint, which interact in complex ways and are distinguished in primary and secondary stabilizers. Hence, special examination maneuvers, like the milking maneuver, valgus stress test, or the chair push-up test (Hausman and Lang 2014) must be performed to diagnose a resulting elbow instability. The stability of the joint is an important decision criterion for the subsequent treatment (e.g. non-operative vs operative) (van Riet 2017). Clinical applicability of these tests is often hindered due to pain or patient compliance. While some cases clearly fall in the non-operative or operative treatment categories, treatment selection for many cases is less clear due to the complex interaction of the stabilizers and the diverse injury patterns. In these cases, the decision regarding non-operative/operative care depends mostly on the subjective assessment of the medical expert.

Elbow stability is derived from a combination of muscular, ligamentous, and bony structures. Depending on their contribution and mechanism, they are divided into primary and secondary as well as static and dynamic stabilizers. In this context,

secondary stabilizers adopt a decisive function in the context of injury of the primary stabilizers. There are mainly three primary static structures that stabilize the elbow joint: the ulnohumeral articulation, the medial collateral ligament complex and the lateral collateral ligament complex (see also Chapter 2).

The majority of joint stability is provided by the ulnohumeral anatomy (Karbach and Elfar 2017). The anterior part of the medial collateral ligament complex provides stability in mediolateral direction and against valgus moments, whereas the posterior part is responsible for posteromedial rotatory elbow stability (Seiber et al. 2009, Floris et al. 1998, Hwang et al. 2018). Facing external rotation and varus moments, the lateral collateral ligament complex is the primary stabilizer (Singh et al. 2020). The muscles that span the elbow and compress the joint are secondary dynamic stabilizers (Ahmed and Mistry 2015, Safran and Baillargeon 2005). Other secondary, but static, stabilizers are the radial head and capsule of the elbow (Morrey and An 1983, 2005). When considering elbow stability, the influence of forearm rotation cannot be omitted, as it is of decisive importance for valgus-varus laxity. The elbow exhibits a maximum laxity throughout the elbow flexion during the position of the forearm in the neutral position (Safran et al. 2005).

As indicated above, the respective roles of individual primary and secondary stabilizers has been investigated in numerous studies. However, to the best of my knowledge, there exists no biomechanical analysis of how different combinations of failures of these stabilizers influence each other in the presence of valgus/varus moments and in which way this loss of stabilizing structures effects elbow stability. Musculoskeletal simulation platforms, such as the AMS provide the ability to analyze a variety of different injury patterns and thus can assist medical specialists in a more objective assessment through a numerical analysis of elbow stability.

Therefore, the aim of this study is to use musculoskeletal simulation in order to investigate the extent to which failure of different primary and secondary stabilizers affects the elbow stability in neutral position against valgus/varus moments from a biomechanical perspective and how these observations correspond to the assessment from clinical practice.

11.2 Materials and Methods

For the aim of this study the musculoskeletal simulation software AnyBody™ (AnyBody Technology A/S, Aalborg, Denmark, V.7.3.1) was used as a modeling environment including the developed elbow model presented in Chapter 9 and the detailed hand model presented in Chapter 4 with all its extrinsic hand muscles originating at the elbow. Both legs and the left arm were omitted for the simulation and the model was scaled using the default human model (50th percentile male anthropometrics) with a height of 1.75 m (and a corresponding upper arm length of 34.0 cm/forearm length of 26.9 cm) and 75 kg.

To investigate the stability of the elbow under the conditions of varus and valgus moments, the elbow was subjected to a corresponding force at the ulnar end in the neutral position of the hand. These moments were applied under 0°, 45° and 90° flexion while the respective cubital angle was analyzed. The graphical interface of the simulation is shown in Figure 11.1.

In close collaboration with experienced practicing physicians, various scenarios of ligament injuries, muscle and bone structures damages that occur in everyday clinical practice were identified. The resulting scenarios, which were investigated in this study using musculoskeletal simulation models, are summarized in Table 11.1.

For the realization of each scenario, the stiffness of the corresponding ligaments or the maximum muscle forces of the extensor/flexor muscles were set to zero, respectively. The fracture of the radial head was accomplished by adjusting the torsion spring present in the elbow joint (see Section 9.2.3) according to the data of Morrey (2009), in which the radial head was excised.

Data analysis

A total of 5.790 calculated models provide the basis for data analysis of this study. For each flexion angle, ten different parameter studies (intact case + nine scenarios according to Table 11.1) were performed; each with 193 simulation models, whereby the valgus-varus moments for each parameter study varied between 6 Nm in valgus and varus direction (± 0.0625 Nm between two simulations). For data

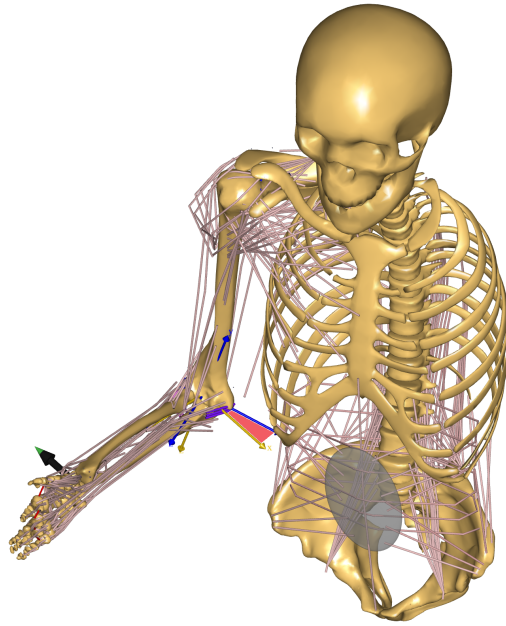


Figure 11.1: Graphical interface of the AMS simulation regarding the elbow stability testing. In this illustration, the stability testing under 90° flexion and application of a valgus force is shown (black arrow). The blue coordinate system is the reference frame of the elbow joint on the humerus and the yellow coordinate system is the corresponding frame on the ulna. The rotation of these coordinate systems corresponds to the cubital angle (red marked area).

analysis, the stability contribution to low (2 Nm) and high (4 Nm) moments of each scenario was calculated according to Frangiamore et al. (2018) for the three investigated flexion angles (0° , 45° , 90°).

For the intact case, the cubital angle was determined for 2 Nm and 4 Nm (based on the range of applied moments in the study of Morrey (2009)) and subsequently, the moment required for the individual scenarios to cause the same change in the cubital angle ($\Theta_{scenario}$) was analyzed. With the collected data the determination of the stability contribution to low (2 Nm) and high (4 Nm) ($StabCon_{low}$ and $StabCon_{high}$) valgus and varus moments for the individual scenarios was determined according to the following formulas.

Table 11.1: Overview of the different scenarios regarding elbow stability. On the horizontal axis, all possible injuries of the ligamentous apparatus or the radial head are displayed. Corresponding combinations were selected for the individual scenarios (vertical axis).

	lateral ligament failure	radial head fracture	medial ligament failure (posterior part)	medial ligament failure (complete)	extensor muscles failure	flexor muscles failure
Scenario 1	X					
Scenario 2	X	X				
Scenario 3	X	X			X	
Scenario 4			X			
Scenario 5				X		
Scenario 6				X		X
Scenario 7	X	X	X			
Scenario 8	X	X		X		
Scenario 9		X				

$$\text{StabCon}_{low} = \frac{2.0 \text{ Nm} - \Theta_{scenario} \text{ Nm}}{2.0 \text{ Nm}} \quad (11.1)$$

$$\text{StabCon}_{high} = \frac{4.0 \text{ Nm} - \Theta_{scenario} \text{ Nm}}{4.0 \text{ Nm}} \quad (11.2)$$

The data calculated in equations 11.1 to 11.2 were then used to evaluate the stability of the elbow joint under conditions of valgus and varus moments.

This objective evaluation based on musculoskeletal simulation models was compared with the experience-based assessment of professional practicing specialists. Therefore, a survey was conducted among a total of 19 physicians, who were asked to evaluate the individual scenarios (in a randomized order) according to their stability. The basis for the evaluation was the Mayo Elbow Performance Score (MEPS) according to Broberg and Morrey (1987), which is commonly used among professionals. In this context, stability is assessed in three sub-classes and assigned a corresponding score (gross instability (0), moderate instability (5), stable (10)). The total questionnaire of the survey can be found in Appendix E.

11.3 Results

Musculoskeletal simulation

Figure 11.2 and 11.3 show the stability contribution of the respective scenarios to varus and valgus moments (low and high) for the flexion angles of 0° , 45° , and 90° degrees. The higher the contribution for the particular scenario, the more unstable the elbow joint becomes when the respective injury occurs. An overview of which scenario represents which specific injury can be found in Table 11.1.

In this context, it should be noted that the stability contribution can range up to 72.8% in individual cases (scenario 7 for 90° flexion). While certain injuries (such as those occurring in scenario 5 and 6) affect elbow stability only at moments in certain directions (valgus moment in this case), other injury patterns affect the stability against valgus and varus moments, such as scenario 2, 3, and 7 under high moments, as well as scenario 8 under low and high moments. Furthermore, there are also injury patterns whose stability influence depends more on the respective flexion angle (scenario 1) than those of others.

Considering the contribution to elbow stability across all three flexion angles for varus and valgus moments, it can be observed that on average the respective scenario contributes to the joint stability according to Table 11.2.

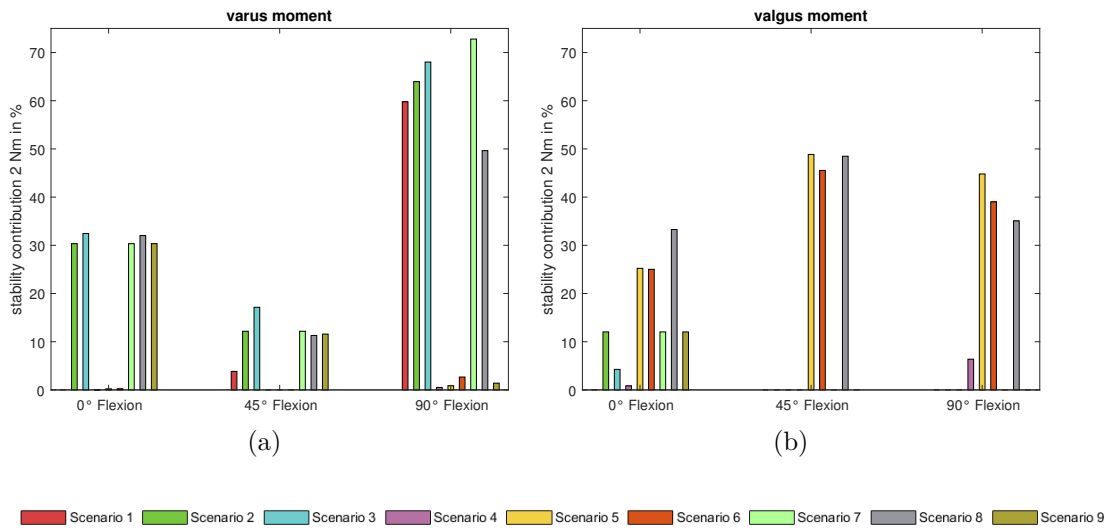


Figure 11.2: Comparison of the change in elbow stability contribution regarding low (2 Nm) valgus and varus moments of the different ligaments, muscles and bony structures with respect to the particular scenarios.

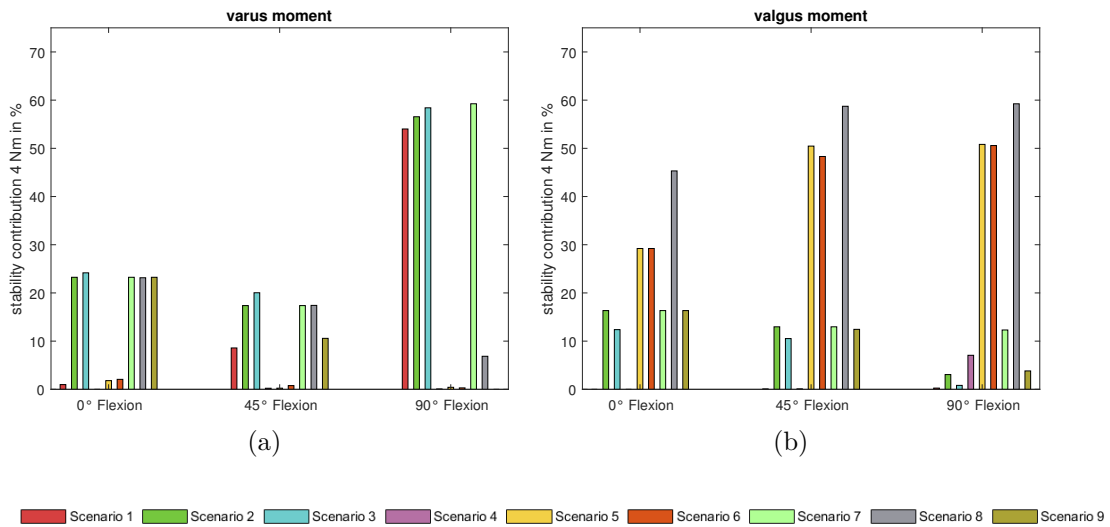


Figure 11.3: Comparison of the change in elbow stability contribution regarding high (4 Nm) valgus and varus moments of the different ligaments, muscles and bony structures with respect to the particular scenarios.

Survey among professionals

A total of 19 (3 female, 16 male) specialists participated in the survey. The average age of the participants was 39.8 (± 8.8 SD) years with an average professional experience as a practicing surgeon of 12.2 (± 7.4 SD) years. Table 11.2 contains the median and average MEPS score (\pm SD) of the respective scenarios in ranked order from a MEPS score of 10 to 0. According to the median, the elbow stability of the different scenarios can be evaluated as stable (intact, scenario 9), moderate unstable (scenario 1, 2, 4, 5, 6, and 7) and grossly unstable (scenario 3 and 8).

Table 11.2: The MEPS score (\pm SD) of the investigated scenarios according to the conducted survey among 19 physicians and average contribution of every scenario according to the musculoskeletal simulations. The different scenarios are ranked according to their MEPS score.

	median MEPS score	average MEPS score	(\pm SD)	sim. average contribution [%]
Intact	10	10.0	0.0	–
Scenario 9	10	8.7	2.3	10.1
Scenario 4	5	6.8	3.0	1.3
Scenario 1	5	6.3	2.3	10.6
Scenario 2	5	5.0	2.9	20.7
Scenario 5	5	5.0	0.0	21.1
Scenario 7	5	3.2	2.5	22.4
Scenario 6	5	2.9	2.5	20.3
Scenario 3	0	2.1	2.5	20.7
Scenario 8	0	1.3	2.8	35.0

Considering the Fleiss kappa κ , which determines the inter-rater stability between several raters (Fleiss 1971), the Fleiss kappa based on the survey is 0.39, which reflects a fair agreement ($\kappa < 0$ poor, $\kappa \in]0.0, 0.2]$ slight, $\kappa \in]0.2, 0.4]$ fair, $\kappa \in]0.4, 0.6]$ moderate, $\kappa \in]0.6, 0.8]$ substantial and $\kappa \in]0.8, 1.0]$ almost perfect agreement).

11.4 Discussion

The purpose of this study was to evaluate elbow stability to varus and valgus moments based on the calculations of a musculoskeletal model. Therefore, the deflection of the cubital angle under the effect of 2 Nm and 4 Nm valgus and varus moments was considered and the biomechanical effects of different injury patterns on elbow stability were determined. Different contribution behaviors to elbow stability are revealed depending on the failure of different stabilizers, which allows for the derivation of appropriate treatment procedures. Based on the numerical outcome, a comparison with the clinical experience of practicing physicians is made. As far as the musculoskeletal model is concerned, the new elbow model could only be used to evaluate elbow stability in the neutral position of the hand (see Chapters 9 and 10), and it was not possible to perform a corresponding investigation for supination/pronation. However, since according to Safran et al. (2005), the elbow exhibits a maximum laxity throughout the elbow flexion during the position of the forearm in the neutral position, the chosen approach is also the most relevant one. Another limitation of the musculoskeletal simulation represents the fact that the fracture of the radial head is only based on the adaptation of the torsion spring implemented in the elbow model based on data from the study by Morrey (2009). Furthermore, the outcomes based on the numerical simulation in this study are restricted to expected varus and valgus loads as they might appear during activities of daily living or sports. In these cases, muscles are capable of compensating some of the loads and therefore protect the passive structures. However, the muscle model used for the simulation does not take into account the passive structure of the muscles that serve as stabilizers in the stability of the elbow joint (Singh et al. 2020). In order to be able to represent these passive structures, the muscle model according to Hill would have to be considered (Hill 1938), but important parameters for the muscles of the upper extremity are still missing within the AMS. A future stability study based on a muscle model according to Hill, could therefore provide further insights.

Moreover, it is important to keep in mind that the AMS always assumes trained movements when determining the individual muscle forces and optimizes them accordingly (see Chapter 3). By changing the basic input parameters of the nu-

merical simulation (as it is the case in the simulation of the different scenarios), the muscles are recruited in a different order. To ensure that the occurring change in stability contribution is caused by the injuries specified in the respective scenario and not by a change in muscle recruitment, the muscle activities must be considered accordingly. If we consider the change in muscle activity of the upper extremity between the individual scenarios for one and the same muscle, a maximum deviation of 4.9% (m. deltoideus) for 0° flexion, 7.0% (m. pectoralis major) for 45° flexion, and 10.9% (m. brachialis) for 90° flexion can be determined. While the first two are less relevant for elbow stability in terms of the size change and the muscle concerned, this is certainly the case for 90° flexion. The m. brachialis shows very little to no activity in all cases except in scenario 8 under a 4 Nm varus moment where the activity is 10.9%. The resulting stabilization of the elbow joint by the m. brachialis may thus be the reason for the relatively low stability contribution of scenario 8 in Figure 11.3(a).

The presented results of this study allow detailed observations of different luxation patterns and their effects on elbow stability. The advantage of the elbow assessment based on musculoskeletal simulation is the investigation of the influence of different failure combinations of primary and secondary stabilizers. Nevertheless, in the context of this study, the failure of individual stabilizers was simulated as well. These outcomes can therefore be compared with the results of previous studies. According to Callaway et al. (1997), the failure of the posterior part of the medial ligament (scenario 4) has no effect on the valgus stability; only in the case of a section of the total medial ligament (scenario 5) a significant effect on valgus stability can be observed. The entire MCL contributes approximately one-third in extension and half in 90° flexion to elbow stability (Karbach and Elfar 2017). No significant valgus instability is observed after resection of the radial head (scenario 9); this only occurs if the medial ligament is also damaged (scenario 8) (Karbach and Elfar 2017). The simulation model accurately reproduced all these points.

Looking at the different combinations of the failures of the respective primary and secondary stabilizers, it can be seen that the structures responsible for the stability against varus moments show a slightly higher contribution to the elbow stability against low occurring moments than high occurring moments; in the case of valgus stability, however, this pattern is reversed. Furthermore, it is notable that certain

injury patterns, for the most part, only affect stability to varus (scenario 1) and valgus (scenario 5 and 6) moments, whereas others provide instability to all moments (scenario 7, 8 and 9).

While the comparison of the evaluation of elbow stability with that from the survey yields many parallels, some differences must be noted. For example, scenario 8 is the most unstable injury in both cases (average MEPS score 1.3; average stability contribution 35.0%), and scenarios 1 (average MEPS score 6.3; average stability contribution 10.6%), 4 (average MEPS score 6.8; average stability contribution 1.3%) and 9 (average MEPS score 8.7; average stability contribution 10.1%) the most stable. Only scenario 3, which has an average MEPS score of 2.1, shows an average stability contribution of 20.7%, which is comparable to scenarios 2, 5, and 6. However, the survey conducted with only 19 practicing physicians is not representative enough for a general statement. In addition, it is difficult to reduce such a highly complex topic as the assessment of elbow stability to an ordinal scale with only three values (gross instability (0), moderate instability (5), stable (10)). This conclusion is also supported when considering the Fleiss kappa κ , which determines the inter-rater stability between several raters (Fleiss 1971). The Fleiss kappa based on the survey is 0.39, which reflects a fair agreement ($\kappa < 0$ poor, $\kappa \in]0.0, 0.2]$ slight, $\kappa \in]0.2, 0.4]$ fair, $\kappa \in]0.4, 0.6]$ moderate, $\kappa \in]0.6, 0.8]$ substantial and $\kappa \in]0.8, 1.0]$ almost perfect agreement). Accordingly, a conclusion can be drawn that even among the surveyed physicians there was not always unanimous agreement on how to assess elbow stability. An objective basis for evaluation, as represented by the results from musculoskeletal simulations, can thus support physicians in such assessments in the future. Especially since detailed and objective stability evaluations are possible from the observations of Figure 11.2 and 11.3. From this stability analysis, appropriate rehabilitation interventions/exercises can be derived for the respective injury.

11.5 Conclusion

The study presented a numerical determination of elbow stability against varus and valgus moments with regard to clinical injury patterns, as well as a comparison of the numerical outcome with experience gained in clinical practice. The numerical predictions agree well with the assessments of the clinical specialists and differ slightly only in individual cases. Thus, the results from musculoskeletal simulation can make an important contribution to a more objective assessment of elbow stability. In further steps, the model could be used to simulate specific injuries of individual patients and to derive individualized rehabilitation interventions based on the results.

Chapter 12

Conclusion

Due to demographic changes, the significance of musculoskeletal disorders has steadily increased over the past decades and therefore the detailed understanding of the musculoskeletal system of the human body and the forces acting within is of increasing relevance. In vivo measurements that address the forces acting in the human body are often only feasible at great expense and are usually associated with ethical problems. For this reason, numerical models that allow calculation of individual muscle forces or even joint reaction forces and can also be adapted to specific patients have gained increasing relevance.

The aim of this thesis was to develop and validate a new musculoskeletal model of the hand and elbow and subsequently apply it to answer initial clinical research questions. A comparison between the hand model and prior literature, as well as experimentally collected data showed no major inconsistencies between model and corresponding comparison values (see Chapter 5 and 6). Results show that the hand model provides stable output data compared to the input data (see Chapter 7) and thus can be patient specifically adjusted without major concerns. Furthermore, the results of the first clinical application (the simulation of the perineal protection) demonstrated that the hand model developed in this thesis is suited to assess the risk of potential musculoskeletal disorders regarding the upper extremity. The next step in the further development of the hand model could be the integration of all carpal bones as separate rigid bodies and their kinematic relationship by means of implemented ligaments. As far as the elbow is concerned,

the implemented ligament apparatus and FDK approach was able to realistically represent the anatomical characteristics of the elbow from the literature data (see Chapter 10). Thus, in a first clinical application, it was possible to investigate different injuries of the primary and secondary stabilizers of the elbow joint for their stability against valgus and varus moments and to compare them with the clinical evaluation by practicing physicians (see Chapter 11). The results from musculoskeletal simulation demonstrated to be an important contribution to a more objective assessment of elbow stability.

Upon completion of this work, a validated elbow and hand model will thus be available (whereby the latter is already in the process of being integrated into the AnyBody simulation software), which represent anatomical features of the upper extremity that have not yet been realized in musculoskeletal simulation. These include:

- the implementation of the ligamentous apparatus at the elbow and the resulting dependence of the cubital angle on the forces applied using the FDK approach.
- modeling of the hand based on a consistent data set and representation of all DOFs.
- patient-specific scaling of the hand.
- movement of the DIP joint as a function of the PIP joint.
- representation of special features of the hand by means of newly developed classes (*muscle on a muscle*)

Therefore, in addition to the clinical applications presented in this underlying work, the represented models can be helpful in answering numerous other research questions in the future.

Appendix A

Supplementary material: Chapter 5

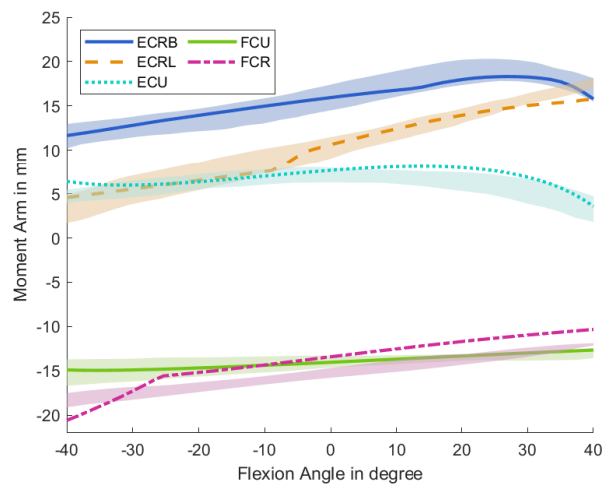


Figure A.1: Progression of the moment arms for the wrist regarding the extensor and flexor muscles during the extension/flexion phase. Negative angles represent the extension of the wrist, and positives the flexion. Lines represent the simulated results, whereas the shaded areas are the experimental results with SD from Loren et al. (1996).

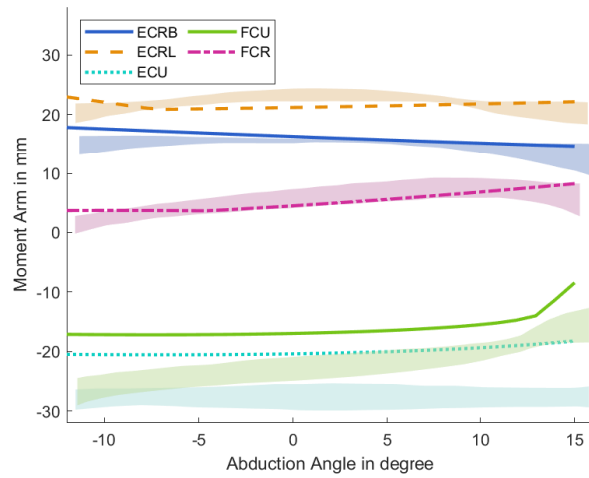


Figure A.2: Progression of the moment arms for the wrist regarding the extensor and flexor muscles during the radial/ulnar abduction phase. Negative angles represent the radial, and positives the ulnar abduction. Lines represent the simulated results, whereas the shaded areas are the experimental results with SD from Loren et al. (1996).

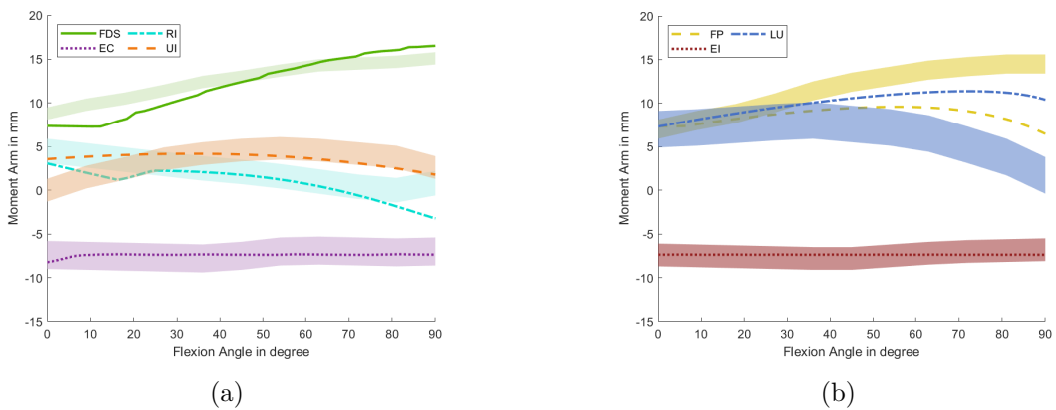


Figure A.3: Progression of the moment arms for the index finger regarding extrinsic and intrinsic hand muscles during the flexion of the MCP joint. Lines represent the simulated results, whereas the shaded areas highlight the experimental data with SD from An et al. (1983).

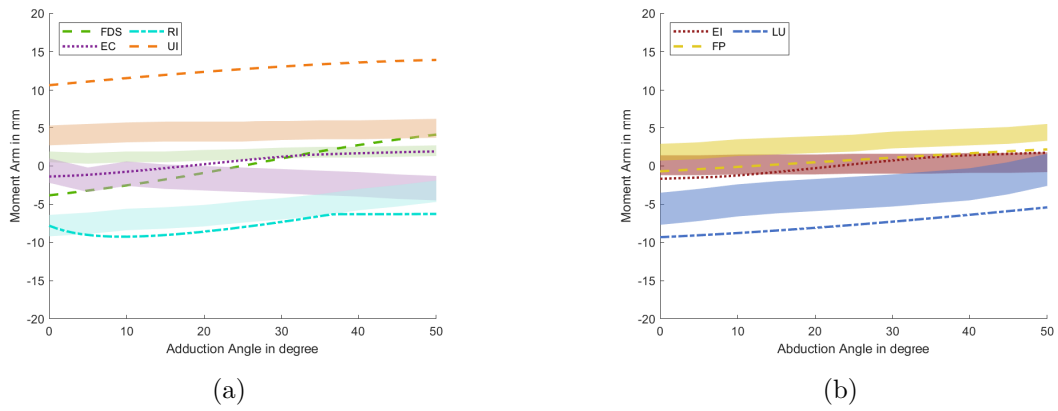


Figure A.4: Progression of the moment arms for the index finger regarding extrinsic and intrinsic hand muscles during the adduction of the MCP joint. Lines represent the simulated results, whereas the shaded areas highlight the experimental data with SD from An et al. (1983).

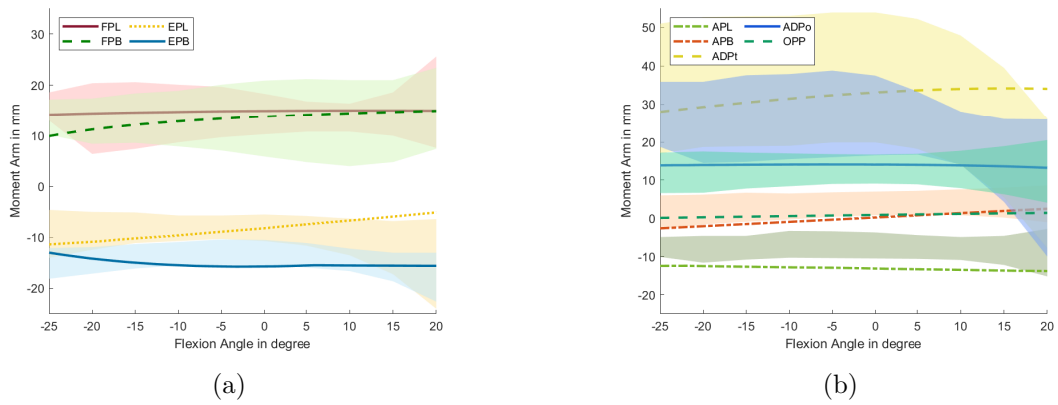
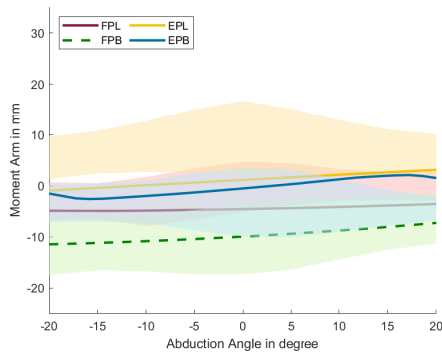
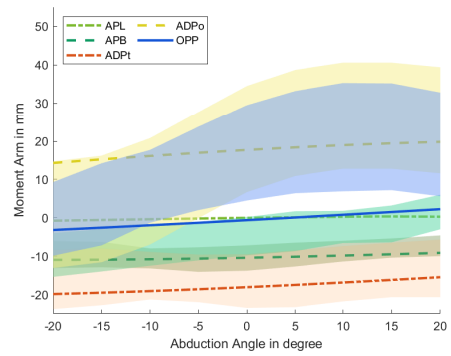


Figure A.5: Progression of the moment arms for the thumb regarding extensor and flexor muscles during flexion around the CMC joint. Negative angles represent the extension of the CMC joint, and positives the flexion. Lines represent the simulated results, whereas the shaded areas highlight the experimental data with SD from Smutz et al. (1998).

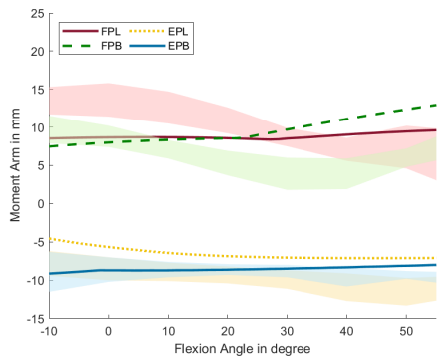


(a)

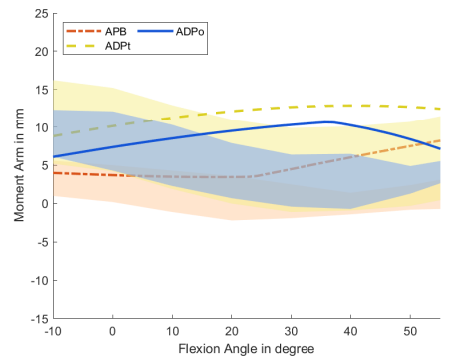


(b)

Figure A.6: Progression of the moment arms for the thumb regarding extensor and flexor muscles during abduction/adduction around the CMC. Negative angles represent the adduction of the CMC joint, and positives the abduction. Lines represent the simulated results, whereas the shaded areas highlight the experimental data with SD from Smutz et al. (1998).



(a)



(b)

Figure A.7: Progression of the moment arms for the thumb regarding extensor and flexor muscles during flexion around the MCP joint. Negative angles represent the extension of the MCP joint, and positives the flexion. Lines represent the simulated results, whereas the shaded areas highlight the experimental data with SD from Smutz et al. (1998).

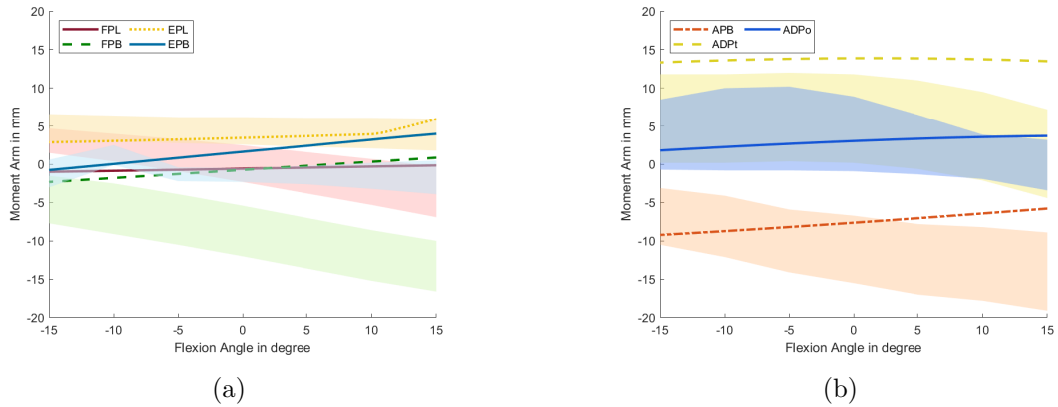


Figure A.8: Progression of the moment arms for the thumb regarding extensor and flexor muscles during abduction/adduction around the MCP. Negative angles represent the adduction of the MCP joint, and positives the abduction. Lines represent the simulated results, whereas the shaded areas highlight the experimental data with SD from Smutz et al. (1998).

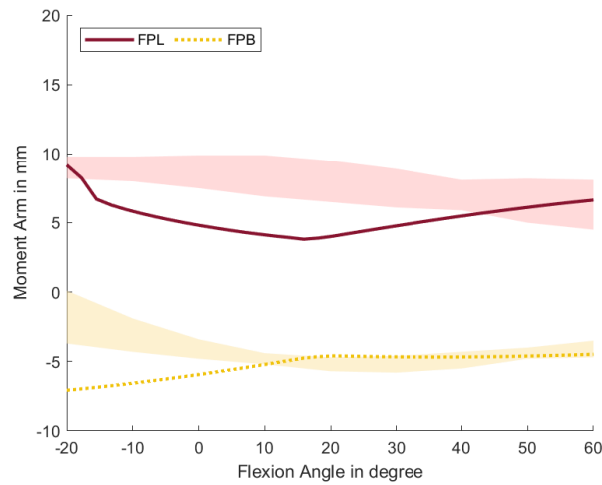


Figure A.9: Progression of the moment arms for the thumb regarding extensor and flexor muscles during flexion around the DIP joint. Negative angles represent the extension of the DIP joint, and positives the flexion. Lines represent the simulated results, whereas the shaded areas highlight the experimental data with SD from Smutz et al. (1998).

Appendix B

Supplementary material: Chapter 6

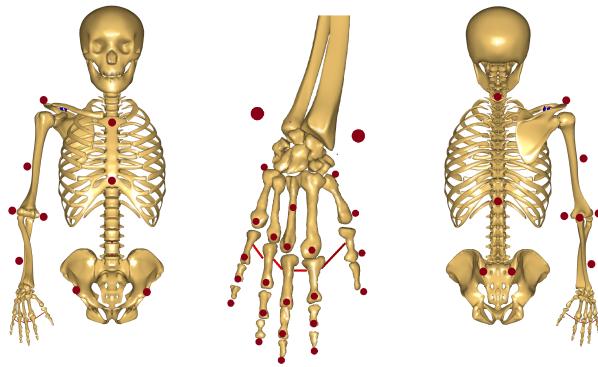


Figure B.1: The location of all markers used for gaining the motion capture data.

Table B.1: EMG sensor and envelope of corresponding AnyBody muscles.

<i>EMG signal</i>	<i>AnyBody Muscles</i>
Extensor digitorum	Extensor_Digitorum_Finger2_1 Extensor_Digitorum_Finger3_1 Extensor_Digitorum_Finger4_1 Extensor_Digitorum_Finger5_1
Extensor carpi radialis	Extensor_Carpi_Radialis_Brevis_1 Extensor_Carpi_Radialis_Longus_1 Supinator_humerus_part_2 Supinator_ulna_part_1
Flexor carpi radialis	Flexor_Carpi_Radialis_1
Flexor carpi ulnaris	Flexor_Carpi_Ulnaris_1 Flexor_Digitorum_Profundus_Finger5_1 Flexor_Digitorum_Superficialis_Finger5_1
First dorsal interosseus	Lumbricales_I Interossei_Dorsales_I_Finger2_1 Interossei_Dorsales_I_Finger1_2 Interossei_Dorsales_I_Finger1_1 Interossei_Dorsales_I_Finger2_2 Interossei_Dorsales_I_Finger2_3
Abductor digit minimi	Abductor_Digiti_Minimi_1 Flexor_Digiti_Minimi_Brevis Opponens_Digiti_Minimi_1 Opponens_Digiti_Minimi_2
Abductor pollicis brevis	Abductor_Pollicis_Brevis_1 Abductor_Pollicis_Brevis_2 Abductor_Pollicis_Brevis_3 Abductor_Pollicis_Brevis_4 Abductor_Pollicis_Brevis_5 Flexor_Pollicis_Brevis_Caput_Superficiale_1 Flexor_Pollicis_Brevis_Caput_Superficiale_2 Flexor_Pollicis_Brevis_Caput_Profundum Opponens_Pollicis_1 Opponens_Pollicis_2 Opponens_Pollicis_3 Opponens_Pollicis_4
Flexor pollicis brevis	Flexor_Pollicis_Brevis_Caput_Profundum Adductor_Pollicis_Caput_Obliquum_1 Adductor_Pollicis_Caput_Obliquum_2 Adductor_Pollicis_Caput_Obliquum_3 Opponens_Pollicis_1 Opponens_Pollicis_2 Opponens_Pollicis_3 Opponens_Pollicis_4
Flexor digitorum superficialis	Flexor_Digitorum_Superficialis_Finger2_1 Flexor_Digitorum_Superficialis_Finger3_1 Flexor_Digitorum_Superficialis_Finger4_1 Flexor_Digitorum_Superficialis_Finger5_1
Extensor carpi ulnari	Extensor_Carpi_Ulnaris_1

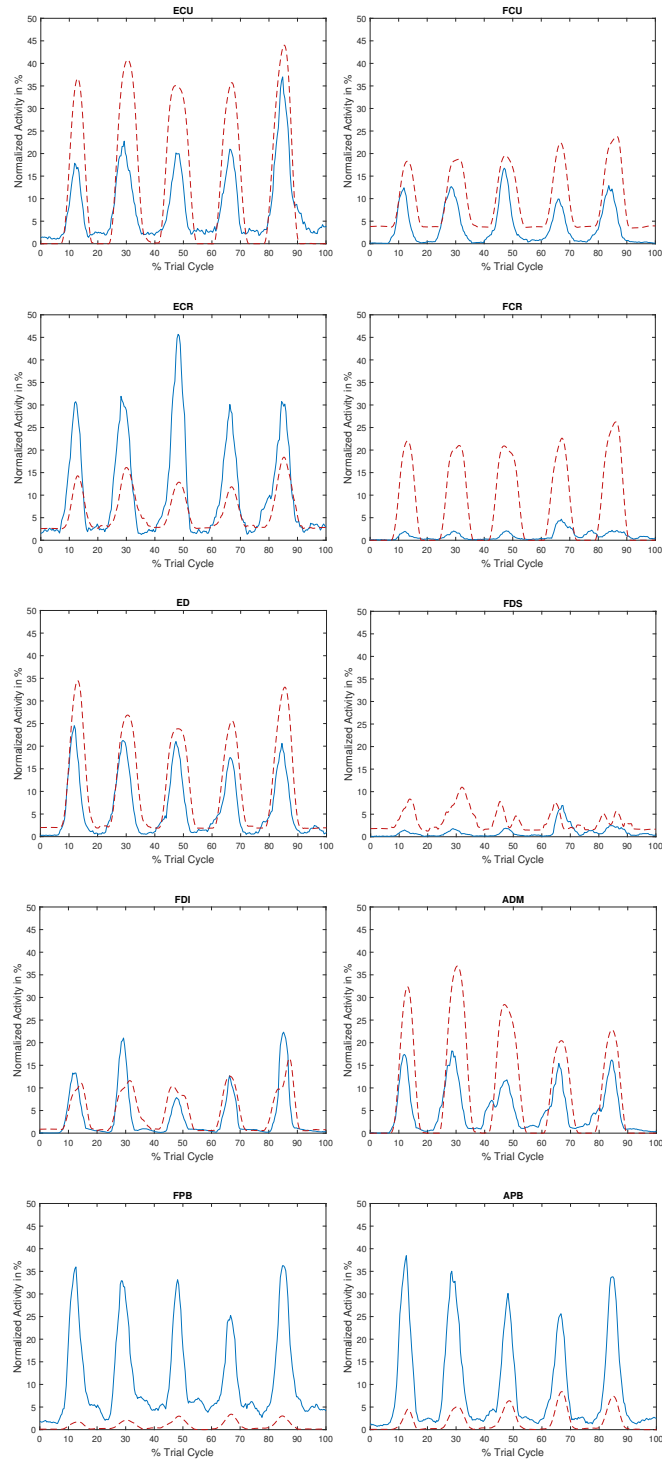


Figure B.2: All measured (blue) and simulated (dashed red) muscle activities of task 1 (five times abduction of the fingers) from one test subject.

Appendix C

Supplementary material: Chapter 7

Table C.1: The dimensions of insertion, origin area as well as the PCSA (height x width of an approximated ellipse \pm SD, respectively) for the extrinsic muscles according to Havelková et al. (2020). All lengths given are in millimeters.

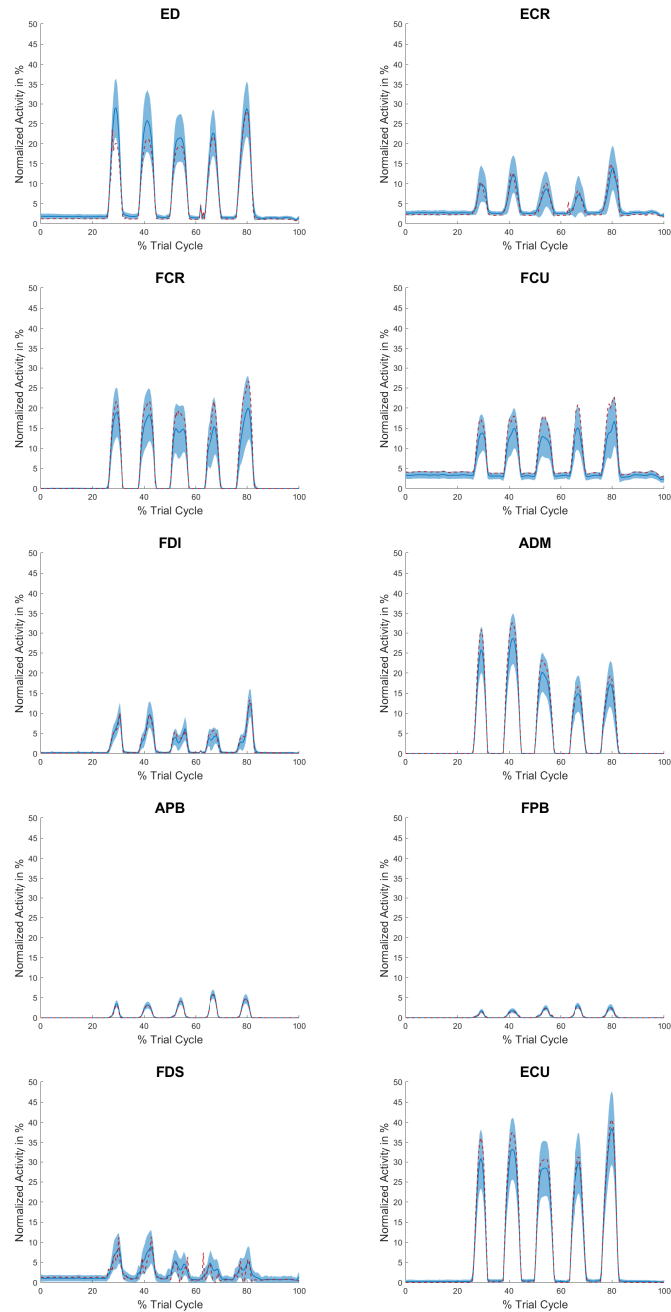
Name	Origin	Insertion	PCSA
<i>Flexor carpi ulnaris</i>	19.2 (\pm 2.28) x 14.6 (\pm 3.38)	6.0 (\pm 0.82) x 3.0 (\pm 0.95)	18.0 (\pm 2.95) x 7.0 (\pm 1.95)
<i>Flexor carpi radialis</i>	19.2 (\pm 2.28) x 14.6 (\pm 3.38)	7.0 (\pm 0.6) x 3.0 (\pm 0.2)	17.0 (\pm 2.35) x 9.0 (\pm 1.6)
<i>Flexor pollicis longus</i>	84.0 (\pm 8.01) x 17.0 (\pm 3.8)	4.0 (\pm 0.69) x 3.0 (\pm 0.91)	22.0 (\pm 1.8) x 11.0 (\pm 1.05)
<i>Flexor digitorum superficialis – humeroulnar head</i>	19.2 (\pm 2.28) x 14.6 (\pm 3.38)	3.0 (\pm 0.2) x 2.0 (\pm 0.3)	32,0 (9,7) x 20,5 (3,0)
<i>Flexor digitorum superficialis – radial head</i>	44.5 (\pm 5.51) x 3.8 (\pm 0.84)		
<i>Flexor digitorum profundus</i>	96.0 (\pm 9.2) x 16.0 (\pm 3.2)	3.0 (\pm 0.82) x 4.1 (\pm 0.5)	26.0 (\pm 2.4) x 12.1 (\pm 1.8)
<i>Palmaris longus</i>	19.2 (\pm 2.28) x 14.6 (\pm 3.38)	6.0 (\pm 0.28) x 3.0 (\pm 0.95)	6 (\pm 1.26) x 4 (\pm 0.8)
<i>Extensor carpi radialis longus</i>	46.67 (\pm 1.15) x 8.5 (\pm 1.29)	4.75 (\pm 0.96) x 4.0 (\pm 1.83)	19.25 (\pm 4.11) x 11.5 (\pm 1.91)
<i>Extensor carpi radialis brevis</i>	23.0 (\pm 2.58) x 9.25 (\pm 1.5)	4.88 (\pm 0.85) x 2.0 (\pm 0.82)	18.5 (\pm 3.42) x 9.0 (\pm 1.41)
<i>Extensor carpi ulnaris</i>	23.0 (\pm 2.58) x 9.25 (\pm 1.5)	3.38 (\pm 0.48) x 3.25 (\pm 0.96)	17.25 (\pm 3.59) x 6.5 (\pm 1.29)
<i>Extensor digitorum</i>	23.0 (\pm 2.58) x 9.25 (\pm 1.5)	proximal insertion: 2.55 (\pm 0.58) x 1.88 (\pm 0.63) distal insertion: 4.0 (\pm 0.71) x 2.5 (\pm 0.5)	27.25 (\pm 4.11) x 13.0 (\pm 0.71)
<i>Extensor digiti minimi</i>	23.0 (\pm 2.58) x 9.25 (\pm 1.5)	proximal insertion: 2.5 (\pm 0.58) x 1.88 (\pm 0.63) distal insertion: 2.88 (\pm 0.25) x 2.63 (\pm 0.75)	6.88 (\pm 0.85) x 4.63 (\pm 0.95)
<i>Extensor indicis</i>	72.75 (\pm 8.58) x 5.7 (\pm 1.7)	proximal insertion: 1.67 (\pm 0.58) x 1.5 (\pm 0.5) distal insertion: 2.25 (\pm 0.5) x 2.0 (\pm 0.82)	12.67 (\pm 1.15) x 8.0 (\pm 2.0)

Table C.2: The dimensions of insertion, origin area as well as the PCSA (height x width of an approximated ellipse \pm SD, respectively) for the intrinsic muscles according to Havelková et al. (2020). All lengths given are in millimeters.

Name	Origin	Insertion	PCSA
<i>Abductor pollicis brevis</i>	13.3 (\pm 2.8) x 2.4 (\pm 1.1)	8.8 (\pm 1.3) x 2.2 (\pm 0.2)	22.6 (\pm 3.7) x 3.5 (\pm 1.2)
<i>Flexor pollicis brevis - superficial head</i>	5.5 (\pm 0.71) x 1.5 (\pm 0.3)	8.5 (\pm 2.65) x 2.5 (\pm 0.58)	9.5 (\pm 0.71) x 3.0 (\pm 0.4)
<i>Flexor pollicis brevis - deep head</i>	5.33 (\pm 1.04) x 2.1 (\pm 0.8)		7.5 (\pm 1.32) x 3.0 (\pm 0.4)
<i>Opponens pollicis</i>	22.0 (\pm 2.16) x 4.0 (\pm 0.82)	39.0 (\pm 1.1) x 18.0 (\pm 1.1)	16.0 (\pm 1.63) x 4.0 (\pm 1.41)
<i>Adductor pollicis - oblique head</i>	12.0 (\pm 3.16) x 4.2 (\pm 1.3)	9.1 (\pm 1.8) x 4.0 (\pm 1.1)	12.5 (\pm 2.52) x 3.6 (\pm 1.3)
<i>Adductor pollicis - transverse head</i>	40.2 (\pm 2.99) x 4.8 (\pm 1.64)		18.8 (\pm 2.41) x 3.5 (\pm 1.29)
<i>Flexor digiti minimi brevis</i>	4.0 (\pm 1.41) x 2.5 (\pm 1.0)	4.0 (\pm 2.0) x 2.33 (\pm 0.58)	6.0 (\pm 1.83) x 1.5 (\pm 0.5)
<i>Abductor digiti minimi</i>	9.5 (\pm 1.29) x 4.2 (\pm 0.86)	9.1 (\pm 1.63) x 3.0 (\pm 1.1)	13.5 (\pm 3.56) x 7.6 (\pm 1.29)
<i>Opponens digiti minimi</i>	8.0 (\pm 1.83) x 2.5 (\pm 1.29)	13.3 (\pm 1.92) x 3.0 (\pm 0.9)	10.7 (\pm 2.4) x 3.5 (\pm 1.1)
<i>Abductor pollicis longus</i>	58.0 (\pm 2.38) x 21.0 (\pm 1.41)	4.67 (\pm 0.58) x 2.67 (\pm 1.15)	2.0 (\pm 2.0) x 7.0 (\pm 1.0)
<i>Extensor pollicis longus</i>	72.75 (\pm 8.85) x 8.25 (\pm 3.32)	2.5 (\pm 0.71) x 1.33 (\pm 0.58)	10.75 (\pm 2.99) x 6.5 (\pm 1.29)
<i>Extensor pollicis brevis</i>	27.0 (\pm 1.83) x 5.5 (\pm 1.91)	2.25 (\pm 0.5) x 2.25 (\pm 0.96)	8.0 (\pm 2.0) x 4.3 (\pm 0.58)
<i>Lumbrical I</i>	15.2 (\pm 2.38) x 1.3 (\pm 0.4)	2.2 (\pm 0.6) x 2.4 (\pm 0.54)	5.0 (\pm 1.1) x 1.3 (\pm 0.5)
<i>Lumbrical II</i>	14.6 (\pm 2.2) x 1.9 (\pm 0.5)	2.3 (\pm 0.5) x 2.5 (\pm 0.48)	5.0 (\pm 1.0) x 2.3 (\pm 0.56)
<i>Lumbrical III</i>	11.9 (\pm 2.1) x 1.8 (\pm 0.6)	2.4 (\pm 0.48) x 2.3 (\pm 0.48)	5.1 (\pm 1.0) x 2.3 (\pm 0.58)
<i>Lumbrical IV</i>	11.6 (\pm 2.0) x 2.3 (\pm 0.4)	2.2 (\pm 0.36) x 2.3 (\pm 0.3)	4.3 (\pm 0.58) x 1.3 (\pm 0.5)
<i>Palmar interossei I</i>	21.2 (\pm 3.4) x 8.3 (\pm 1.82)	2.3 (\pm 0.6) x 2.4 (\pm 0.53)	7.0 (\pm 0.8) x 4.0 (\pm 0.82)
<i>Palmar interossei II</i>	20.4 (\pm 1.6) x 8.6 (\pm 0.95)	2.2 (\pm 0.4) x 2.6 (\pm 0.7)	9.0 (\pm 1.0) x 3.0 (\pm 0.8)
<i>Palmar interossei III</i>	18.6 (\pm 2.8) x 8.0 (\pm 1.3)	2.0 (\pm 0.4) x 2.5 (\pm 0.56)	6.8 (\pm 0.6) x 2.9 (\pm 0.8)
<i>Dorsal interossei I.1</i>	33.0 (\pm 2.94) x 10.1 (\pm 1.83)	7.0 (\pm 1.58) x 3.1 (\pm 0.87)	19.0 (\pm 1.83) x 10.0 (\pm 0.8)
<i>Dorsal interossei I.2</i>	48.0 (\pm 2.94) x 9.21 (\pm 1.86)		
<i>Dorsal interossei II.1</i>	40.0 (\pm 3.81) x 6.0 (\pm 1.7)	6.2 (\pm 1.71) x 3.0 (\pm 0.82)	16.1 (\pm 1.82) x 9.0 (\pm 1.1)
<i>Dorsal interossei II.2</i>	32.0 (\pm 2.6) x 6.1 (\pm 1.1)		
<i>Dorsal interossei III.1</i>	36.1 (\pm 2.8) x 6.5 (\pm 1.1)	6.3 (\pm 1.8) x 3.1 (\pm 0.6)	15.8 (\pm 1.6) x 9.1 (\pm 1.7)
<i>Dorsal interossei III.2</i>	30.8 (\pm 3.0) x 6.0 (\pm 1.3)		
<i>Dorsal interossei IV.1</i>	32.8 (\pm 2.6) x 5.6 (\pm 0.8)	5.8 (\pm 0.3) x 3.0 (\pm 0.4)	15.5 (\pm 2.0) x 8.1 (\pm 1.4)
<i>Dorsal interossei IV.2</i>	26.6 (\pm 2.38) x 5.0 (\pm 1.1)		

Table C.3: Variation of muscle activities and joint reaction forces during the abduction of all fingers.

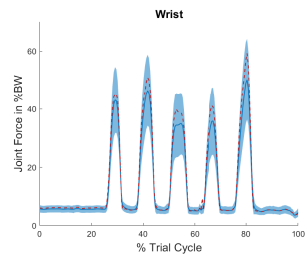
Muscle activities



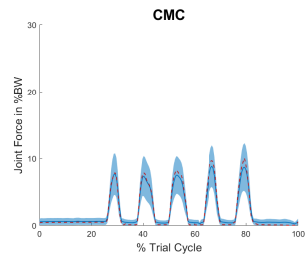
Continued on next page

Table C.3 – continued from previous page

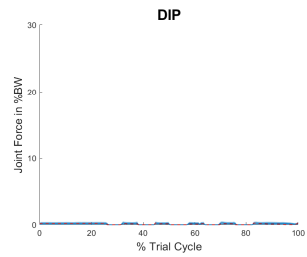
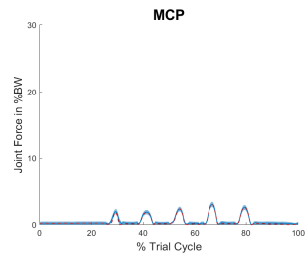
Wrist



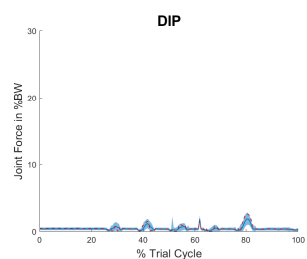
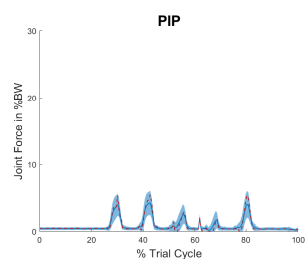
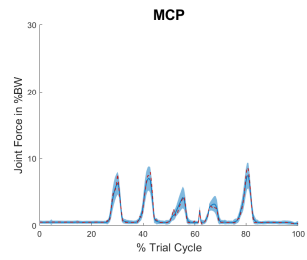
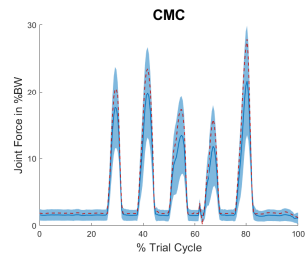
Thumb



Thumb



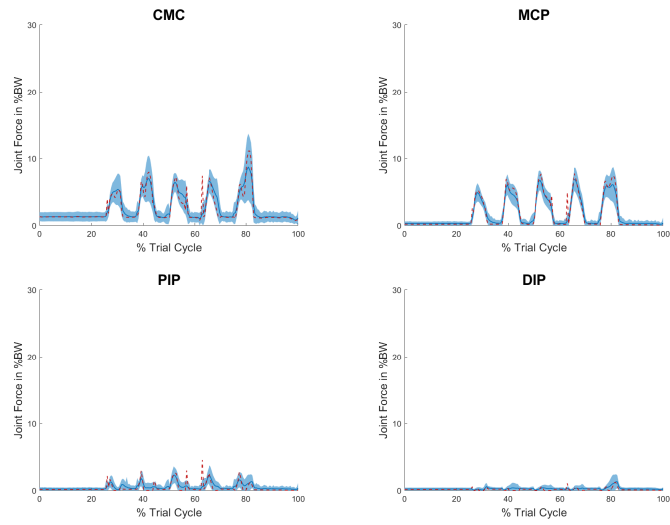
Finger 2



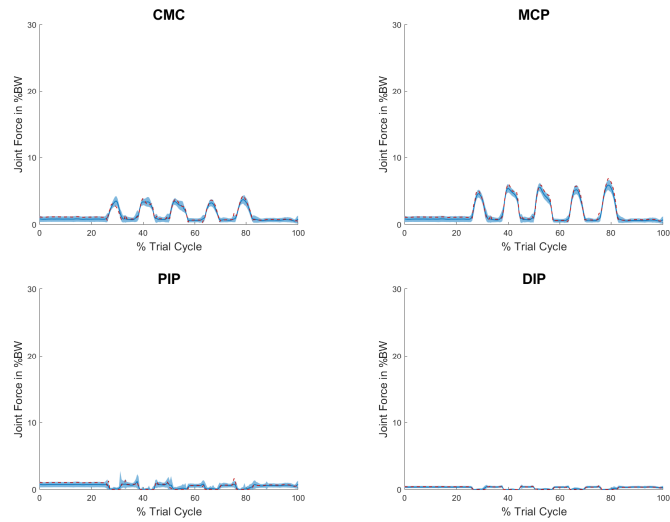
Continued on next page

Table C.3 – continued from previous page

Finger 3



Finger 4



Continued on next page

Table C.3 – continued from previous page

Finger 5

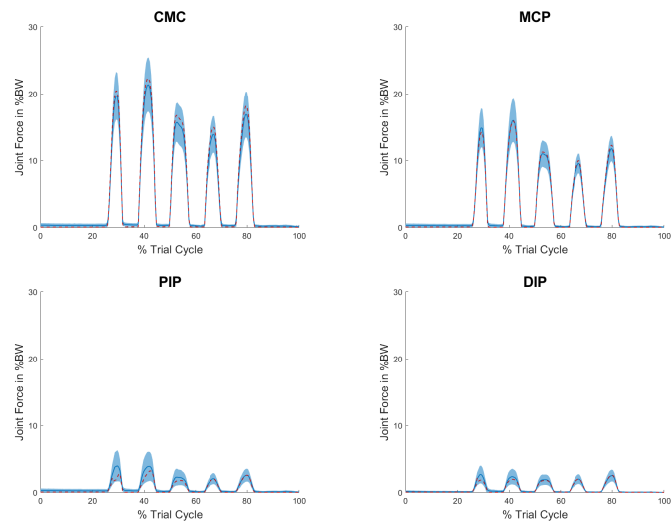
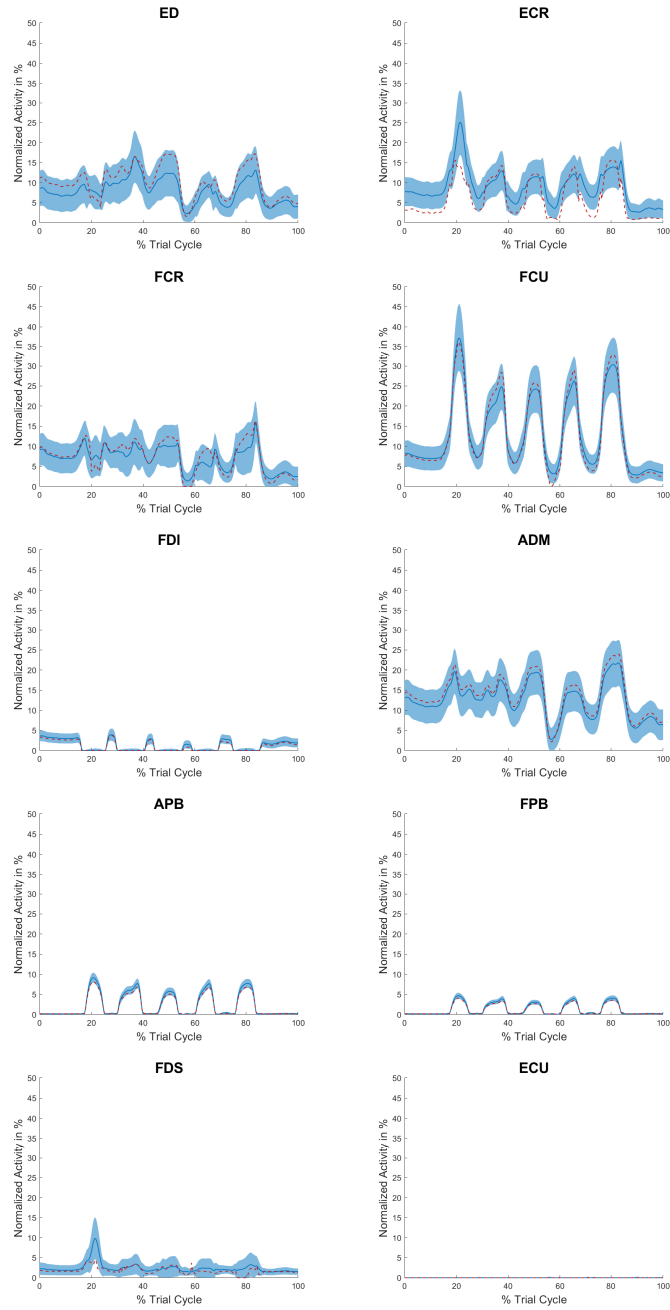


Table C.4: of muscle activities and joint reaction forces during the flexion of the thumb.

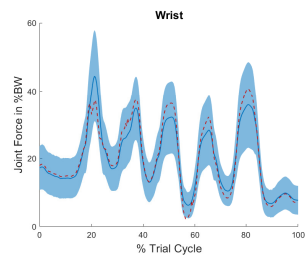
Muscle activities



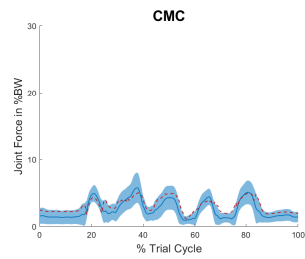
Continued on next page

Table C.4 – continued from previous page

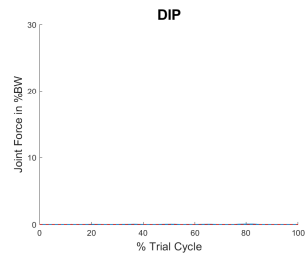
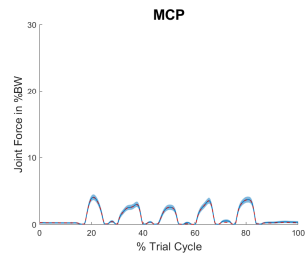
Wrist



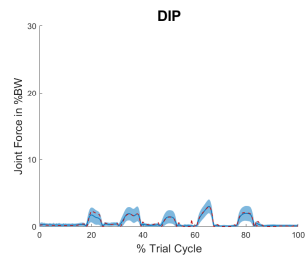
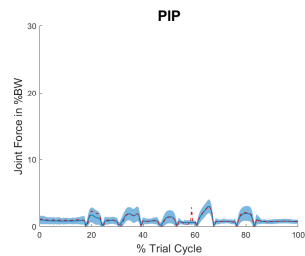
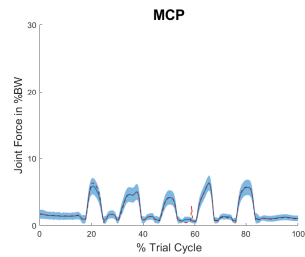
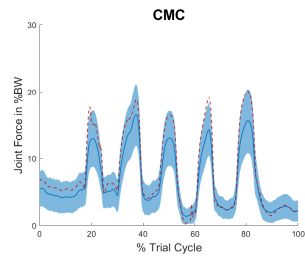
Thumb



Thumb



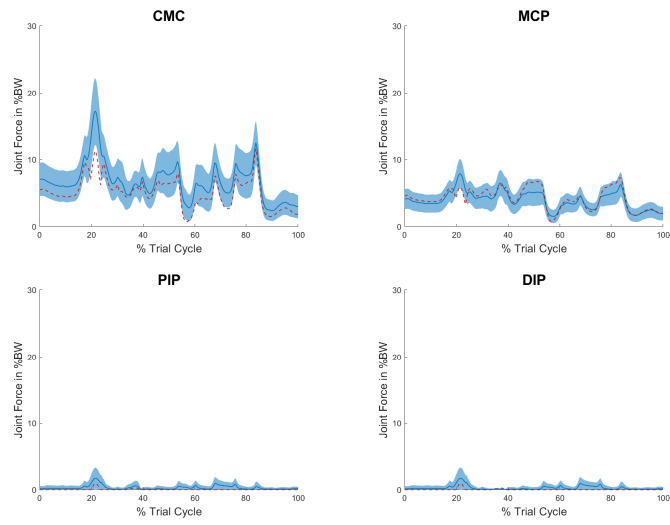
Finger 2



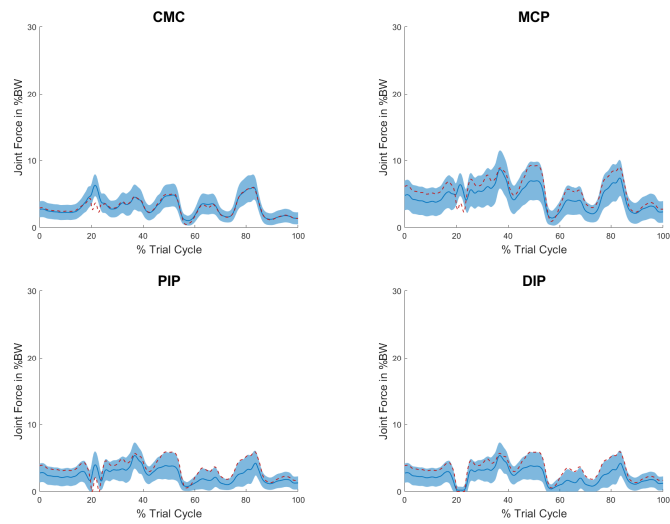
Continued on next page

Table C.4 – continued from previous page

Finger 3



Finger 4



Continued on next page

Table C.4 – continued from previous page

Finger 5

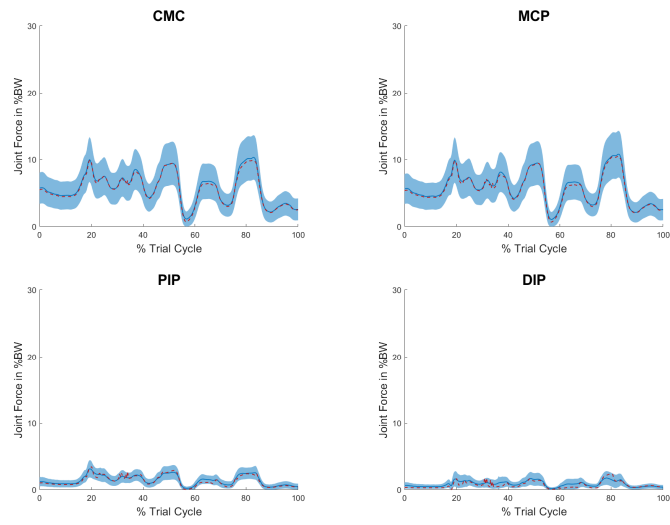
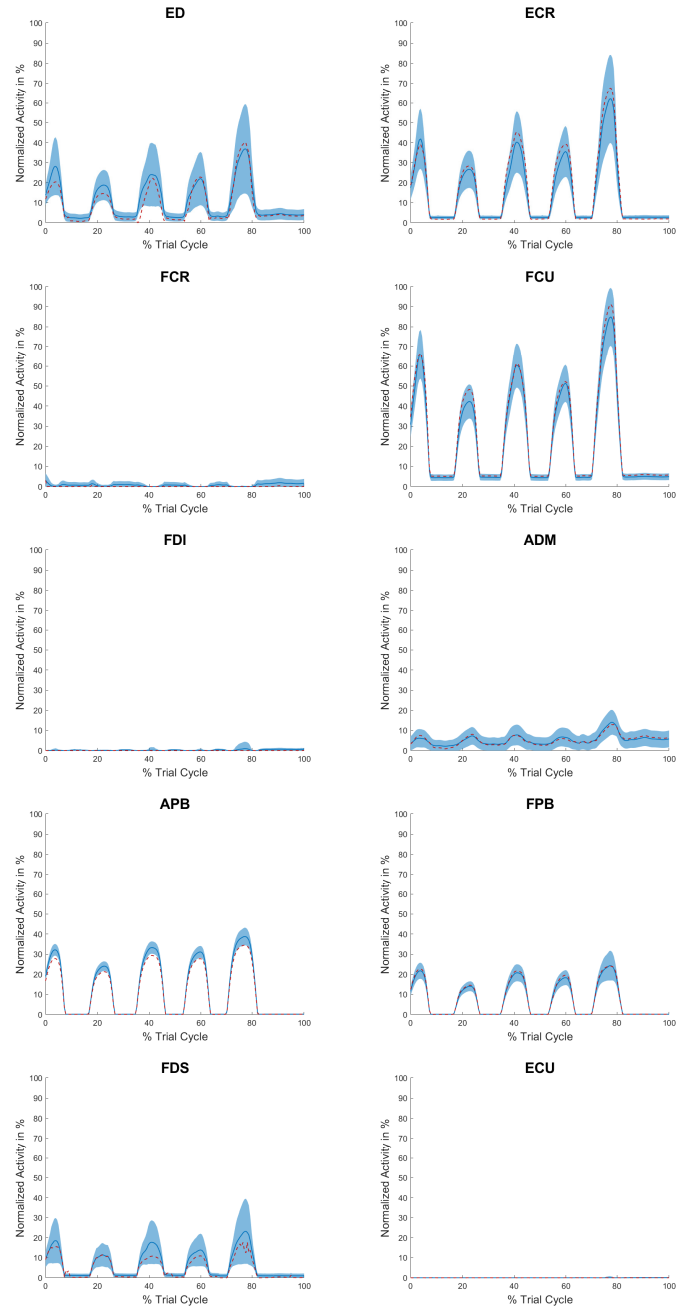


Table C.5: Variation of muscle activities and joint reaction forces during the abduction of the thumb.

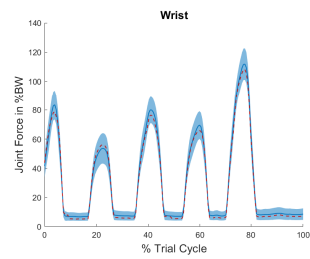
Muscle activities



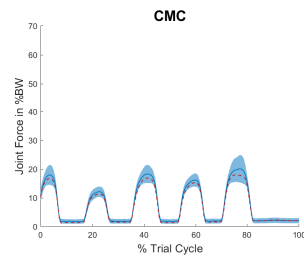
Continued on next page

Table C.5 – continued from previous page

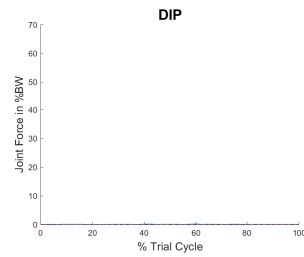
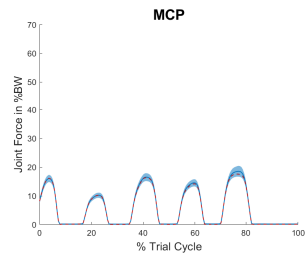
Wrist



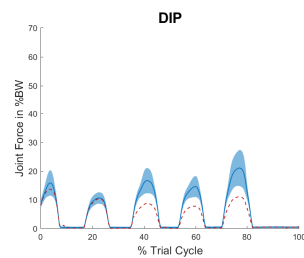
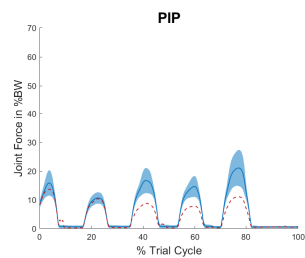
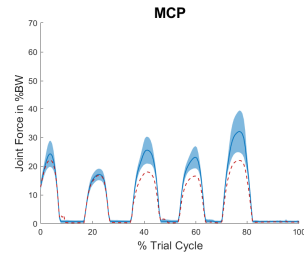
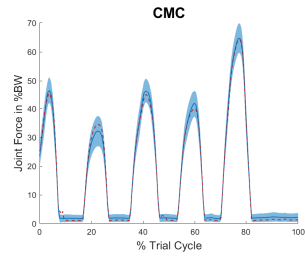
Thumb



Thumb



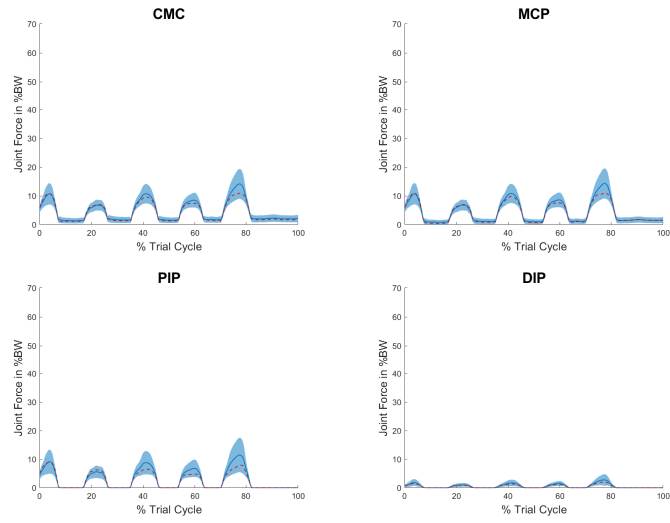
Finger 2



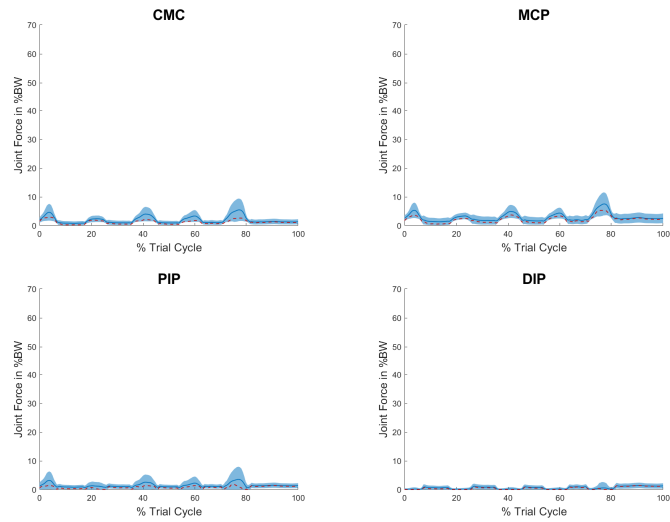
Continued on next page

Table C.5 – continued from previous page

Finger 3



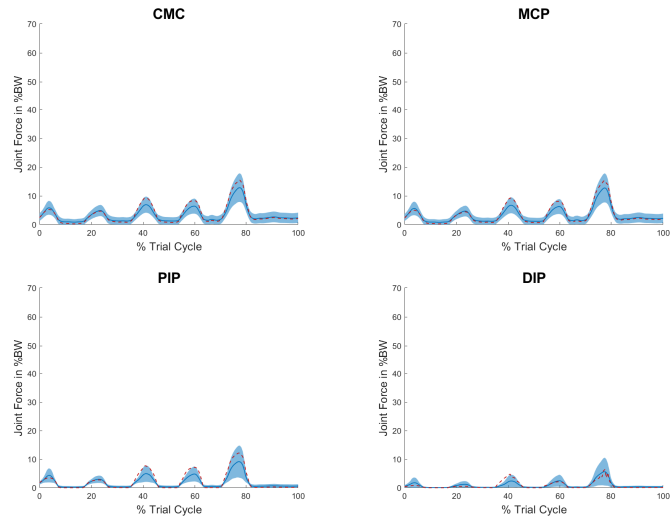
Finger 4



Continued on next page

Table C.5 – continued from previous page

Finger 5



Appendix D

Supplementary material: Chapter 8

Table D.1: Maximal and mean forces (in brackets) in Newton acting on the respective joint during BS-01 trial for the standing technique using a spring with k_{zero}/k .

	BS-01			BS-01	
	k_{zero}	k		k_{zero}	k
<i>shoulder</i>	622 (251)	1209 (926)	<i>L3L4 total</i>	2482 (2297)	1729 (1693)
<i>T12L1 total</i>	1942 (1769)	1068 (1046)	<i>L3L4 anteroposterior</i>	605 (573)	431 (418)
<i>T12L1 anteroposterior</i>	956 (885)	617 (604)	<i>L3L4 mediolateral</i>	158 (131)	146 (142)
<i>T12L1 mediolateral</i>	190 (118)	123 (117)	<i>L4L5 total</i>	2640 (2448)	1889 (1848)
<i>L1L2 total</i>	2128 (1955)	1339 (1315)	<i>L4L5 anteroposterior</i>	334 (326)	234 (225)
<i>L1L2 anteroposterior</i>	835 (778)	632 (619)	<i>L4L5 mediolateral</i>	134 (124)	90 (88)
<i>L1L2 mediolateral</i>	167 (108)	32 (25)	<i>L5Sac total</i>	2765 (2565)	2033 (1991)
<i>L2L3 total</i>	2287 (2111)	1561 (1525)	<i>L5Sac anteroposterior</i>	605 (573)	431 (418)
<i>L2L3 anteroposterior</i>	709 (658)	566 (548)	<i>L5Sac mediolateral</i>	158 (131)	146 (142)
<i>L2L3 mediolateral</i>	164 (125)	58 (51)			

Table D.2: Maximal (and mean forces) in Newton acting on the respective joint during the BS-01-03 trials, the average acting force of these three trials and the RD trial for the kneeling and standing technique. The results for the standing technique were gained using zero stiffness of the spring between the elbow and the thigh (k_{zero}).

	kneeling technique					standing technique				
	BS-01	BS-02	BS-03	mean	RD	RD	mean	BS-01	BS-02	BS-03
<i>thumb</i> (<i>measured</i>)	23 (15)	26 (18)	22 (15)	24 (16)	28 (17)	26 (14)	13 (6)	20 (9)	7 (3)	12 (7)
<i>index finger</i> (<i>measured</i>)	25 (10)	32 (12)	23 (7)	27 (10)	29 (15)	32 (19)	20 (8)	25 (6)	18 (9)	16 (8)
<i>middle finger</i> (<i>measured</i>)	17 (7)	19 (10)	15 (7)	17 (8)	20 (13)	27 (19)	11 (4)	17 (4)	7 (3)	9 (4)
<i>wrist</i>	356 (201)	322 (200)	363 (202)	347 (201)	500 (239)	692 (291)	244 (153)	256 (128)	243 (162)	233 (168)
<i>elbow</i> <i>humero ulnar</i>	365 (183)	437 (270)	248 (144)	350 (199)	562 (263)	395 (148)	427 (183)	508 (173)	375 (146)	397 (230)
<i>elbow</i> <i>radio humeral</i>	690 (456)	743 (477)	604 (434)	679 (456)	744 (363)	585 (337)	1092 (566)	1363 (541)	883 (504)	1029 (653)
<i>shoulder</i>	504 (304)	528 (374)	423 (289)	485 (322)	731 (417)	941 (609)	507 (267)	622 (251)	439 (272)	460 (278)
<i>T12L1</i> <i>total</i>	1693 (1415)	1899 (1592)	1876 (1559)	1823 (1522)	2066 (1606)	1907 (1638)	2143 (1770)	1942 (1769)	2666 (1922)	1822 (1619)
<i>T12L1</i> <i>anteroposterior</i>	657 (537)	722 (599)	722 (593)	700 (576)	736 (585)	870 (780)	990 (872)	956 (885)	1117 (900)	896 (830)
<i>T12L1</i> <i>mediolateral</i>	92 (51)	154 (103)	119 (70)	122 (75)	198 (72)	235 (151)	191 (100)	190 (118)	232 (107)	150 (76)
<i>L1L2</i> <i>total</i>	1753 (1439)	1974 (1656)	1958 (1607)	1895 (1567)	2170 (1697)	2110 (1840)	2352 (1962)	2128 (1955)	2891 (2127)	2036 (1804)
<i>L1L2</i> <i>anteroposterior</i>	502 (405)	539 (440)	537 (443)	526 (429)	656 (477)	755 (695)	893 (778)	835 (778)	1053 (822)	792 (735)
<i>L1L2</i> <i>mediolateral</i>	44 (27)	79 (60)	67 (45)	63 (44)	183 (63)	113 (60)	167 (89)	167 (108)	204 (93)	129 (66)
<i>L2L3</i> <i>total</i>	1672 (1367)	1926 (1603)	1875 (1535)	1824 (1502)	2217 (1712)	2185 (1974)	2492 (2128)	2287 (2111)	3061 (2299)	2129 (1975)
<i>L2L3</i> <i>anteroposterior</i>	326 (252)	328 (266)	330 (271)	328 (263)	416 (325)	634 (577)	731 (659)	709 (658)	821 (688)	663 (630)
<i>L2L3</i> <i>mediolateral</i>	26 (11)	42 (27)	43 (23)	37 (20)	119 (59)	76 (29)	158 (104)	164 (125)	175 (93)	136 (95)
<i>L3L4</i> <i>total</i>	1730 (1397)	1970 (1630)	1919 (1562)	1873 (1530)	2331 (1757)	2348 (2121)	2676 (2307)	2482 (2297)	3252 (2477)	2294 (2146)
<i>L3L4</i> <i>anteroposterior</i>	366 (297)	404 (329)	406 (329)	392 (318)	426 (321)	635 (519)	671 (570)	605 (573)	770 (600)	637 (537)
<i>L3L4</i> <i>mediolateral</i>	75 (44)	86 (51)	70 (39)	77 (45)	88 (36)	191 (171)	170 (128)	158 (131)	182 (118)	170 (135)
<i>L4L5</i> <i>total</i>	1771 (1431)	1997 (1662)	1950 (1595)	1906 (1563)	2392 (1801)	2485 (2240)	2818 (2449)	2640 (2448)	3386 (2611)	2428 (2289)
<i>L4L5</i> <i>anteroposterior</i>	243 (207)	263 (213)	262 (223)	256 (214)	348 (255)	423 (308)	407 (330)	334 (326)	492 (354)	394 (309)
<i>L4L5</i> <i>mediolateral</i>	57 (39)	69 (47)	57 (37)	61 (41)	65 (34)	131 (107)	131 (177)	134 (124)	139 (111)	120 (117)
<i>L5Sac</i> <i>total</i>	1886 (1526)	2105 (1771)	2050 (1693)	2014 (1663)	2474 (1887)	2611 (2360)	2917 (25589)	2765 (2565)	3439 (2705)	2548 (2406)
<i>L5Sac</i> <i>anteroposterior</i>	366 (297)	404 (329)	406 (329)	392 (318)	426 (321)	635 (519)	671 (570)	605 (573)	770 (600)	637 (537)
<i>L5Sac</i> <i>mediolateral</i>	75 (44)	86 (51)	70 (39)	77 (45)	88 (36)	191 (171)	170 (128)	158 (131)	182 (118)	170 (135)

Appendix E

Supplementary material: Chapter 11

In the following, the survey questionnaire concerning the elbow stability from Chapter 11 is listed. Starting with question 4, the questions were asked in randomized order.

Elbow stability

It takes about 5-10 minutes to complete the survey.

1. **Gender:** female male divers
2. **Age (in years):** _____
3. **How many years have you been a practicing surgeon?**
 <5 5 - 10 10 - 15 15 - 20 20 - 25 > 25
4. **How do you assess the stability of an elbow with the following symptoms¹?**
 - **no injury of the ligaments**
 - **no fractures**

MEPS: 0 5 10

¹according to MEPS (0 = severe instability; 5 = moderate instability ; 10 = stable) by Broberg and Morrey (1987)

5. How do you assess the stability of an elbow with the following symptoms¹?

- rupture of the lateral ulnar collateral ligament

MEPS: 0 5 10

6. How do you assess the stability of an elbow with the following symptoms¹?

- rupture of the lateral ulnar collateral ligament
- fracture of the radial head

MEPS: 0 5 10

7. How do you assess the stability of an elbow with the following symptoms¹?

- rupture of the lateral ulnar collateral ligament
- fracture of the radial head
- tear/damage of the radial muscle group (extensors)

MEPS: 0 5 10

8. How do you assess the stability of an elbow with the following symptoms¹?

- rupture of the posterior part of the medial ulnar collateral ligament

MEPS: 0 5 10

9. How do you assess the stability of an elbow with the following symptoms¹?

- rupture of the complete medial ulnar collateral ligament

MEPS: 0 5 10

¹according to MEPS (0 = severe instability; 5 = moderate instability ; 10 = stable) by Broberg and Morrey (1987)

10. How do you assess the stability of an elbow with the following symptoms¹?

- rupture of the complete medial ulnar collateral ligament
- tear/damage of the medial muscle group (flexors)

MEPS: 0 5 10

11. How do you assess the stability of an elbow with the following symptoms¹?

- rupture of the lateral ulnar collateral ligament
- fracture of the radial head
- rupture of the posterior part of the medial ulnar collateral ligament

MEPS: 0 5 10

12. How do you assess the stability of an elbow with the following symptoms¹?

- rupture of the lateral ulnar collateral ligament
- fracture of the radial head
- rupture of the complete medial ulnar collateral ligament

MEPS: 0 5 10

13. How do you assess the stability of an elbow with the following symptoms¹?

- fracture of the radial head

MEPS: 0 5 10

¹according to MEPS (0 = severe instability; 5 = moderate instability ; 10 = stable) by Broberg and Morrey (1987)

Bibliography

- Abé, H., Hayashi, K., Sato, M. et al. (1996), *Data book on mechanical properties of living cells, tissues, and organs*, Springer.
- Abedzadeh-Kalahroudi, M., Talebian, A., Sadat, Z. and Mesdaghinia, E. (2019), 'Perineal trauma: incidence and its risk factors', *Journal of Obstetrics and Gynaecology* **39**(2), 206–211.
- Åhlund, S., Rådestad, I., Zwedberg, S. and Lindgren, H. (2019), 'Perineal pain the first year after childbirth and uptake of post-partum check-up-a swedish cohort study', *Midwifery* **78**, 85–90.
- Ahmed, I. and Mistry, J. (2015), 'The management of acute and chronic elbow instability', *Orthopedic Clinics* **46**(2), 271–280.
- Alcid, J. G., Ahmad, C. S. and Lee, T. Q. (2004), 'Elbow anatomy and structural biomechanics', *Clinics in sports medicine* **23**(4), 503–517.
- An, K.-N., Chao, E. Y., Cooney III, W. P. and Linscheid, R. L. (1979), 'Normative model of human hand for biomechanical analysis', *Journal of biomechanics* **12**(10), 775–788.
- An, K.-N., Ueba, Y., Chao, E., Cooney, W. and Linscheid, R. (1983), 'Tendon excursion and moment arm of index finger muscles', *Journal of biomechanics* **16**(6), 419–425.
- Andersen, M. S., Marra, M., Vanheule, V., Fluit, R., Verdonschot, N. and Rasmussen, J. (2014), Patient-specific musculoskeletal modelling of total knee

- arthroplasty using force-dependent kinematics, *in* ‘7th World Congress of Biomechanics’.
- Anderson, F. C. and Pandy, M. G. (2001), ‘Static and dynamic optimization solutions for gait are practically equivalent’, *Journal of biomechanics* **34**(2), 153–161.
- Anita, A., Yazdani, A., Hayati, K. and Adon, M. (2014), ‘Association between awkward posture and musculoskeletal disorders (msd) among assembly line workers in an automotive industry’.
- Aurbach, M., Spicka, J., Süß, F. and Dendorfer, S. (2020b), ‘Evaluation of musculoskeletal modelling parameters of the shoulder complex during humeral abduction above 90°’, *Journal of biomechanics* **106**, 109817.
- Aurbach, M., Špička, J., Süß, F., Vychytil, J., Havelková, L., Ryba, T. and Dendorfer, S. (2020a), ‘Torus obstacle method as a wrapping approach of the deltoid muscle group for humeral abduction in musculoskeletal simulation’, *Journal of biomechanics* **109**, 109864.
- Bailly, F., Ceglia, A., Michaud, B., Rouleau, D. M. and Begon, M. (2021), ‘Real-time and dynamically consistent estimation of muscle forces using a moving horizon emg-marker tracking algorithm—application to upper limb biomechanics’, *Frontiers in bioengineering and biotechnology* **9**, 112.
- Barbero, M., Merletti, R. and Rainoldi, A. (2012), *Atlas of muscle innervation zones: understanding surface electromyography and its applications*, Springer Science and Business Media.
- Bergmann, G. (2008), ‘Orthoload.(ed.) charité universitaetsmedizin berlin (2008)’.
- Binder-Markey, B. I. and Murray, W. M. (2017), ‘Incorporating the length-dependent passive-force generating muscle properties of the extrinsic finger muscles into a wrist and finger biomechanical musculoskeletal model’, *Journal of biomechanics* **61**, 250–257.
- Blickstein, I., Goldman, R. D. and Kupferminc, M. (2000), ‘Delivery of breech first twins: a multicenter retrospective study’, *Obstetrics and Gynecology* **95**(1), 37–42.

- Bottlang, M., Madey, S., Steyers, C., Marsh, J. and Brown, T. D. (2000), ‘Assessment of elbow joint kinematics in passive motion by electromagnetic motion tracking’, *Journal of Orthopaedic Research* **18**(2), 195–202.
- Broberg, M. A. and Morrey, B. F. (1987), ‘Results of treatment of fracture-dislocations of the elbow.’, *Clinical orthopaedics and related research* (216), 109–119.
- Buchholz, B., Armstrong, T. J. and Goldstein, S. A. (1992), ‘Anthropometric data for describing the kinematics of the human hand’, *Ergonomics* **35**(3), 261–273.
- Callaway, G., Field, L., Deng, X.-H., Torzilli, P., O’BRIEN, S., Altchek, D. and Warren, R. (1997), ‘Biomechanical evaluation of the medial collateral ligament of the elbow’, *JBJS* **79**(8), 1223–31.
- Carbone, V. (2016), ‘Subject-specific lower extremity modeling: personalization of musculoskeletal models using medical imaging and functional measurements’.
- Carbone, V., Fluit, R., Pellikaan, P., Van Der Krogt, M., Janssen, D., Damsgaard, M., Vigneron, L., Feilkas, T., Koopman, H. F. and Verdonschot, N. (2015), ‘Tlem 2.0—a comprehensive musculoskeletal geometry dataset for subject-specific modeling of lower extremity’, *Journal of biomechanics* **48**(5), 734–741.
- Clavert, P., Kempf, J.-F., Bonnomet, F., Boutemy, P., Marcelin, L. and Kahn, J.-L. (2001), ‘Effects of freezing/thawing on the biomechanical properties of human tendons’, *Surgical and Radiologic Anatomy* **23**(4), 259–262.
- Cook, D., Julias, M. and Nauman, E. (2014), ‘Biological variability in biomechanical engineering research: Significance and meta-analysis of current modeling practices’, *Journal of biomechanics* **47**(6), 1241–1250.
- Criswell, E. (2011), *Cram’s introduction to surface electromyography*, Jones and Bartlett Publishers.
- De Monsabert, B. G., Edwards, D., Shah, D. and Kedgley, A. (2018), ‘Importance of consistent datasets in musculoskeletal modelling: a study of the hand and wrist’, *Annals of biomedical engineering* **46**(1), 71–85.

- De Pieri, E., Lund, M. E., Gopalakrishnan, A., Rasmussen, K. P., Lunn, D. E. and Ferguson, S. J. (2018), ‘Refining muscle geometry and wrapping in the tlem 2 model for improved hip contact force prediction’, *PloS one* **13**(9).
- De Zee, M., Dalstra, M., Cattaneo, P. M., Rasmussen, J., Svensson, P. and Melsen, B. (2007), ‘Validation of a musculo-skeletal model of the mandible and its application to mandibular distraction osteogenesis’, *Journal of biomechanics* **40**(6), 1192–1201.
- Dendorfer, S., Weber, T. and Kennedy, O. (2014), ‘Musculoskeletal modeling for hip replacement outcome analyses and other applications’, *JAAOS-Journal of the American Academy of Orthopaedic Surgeons* **22**(4), 268–269.
- Engelhardt, L., Melzner, M., Havelkova, L., Fiala, P., Christen, P., Dendorfer, S. and Simon, U. (2021), ‘A new musculoskeletal anybody™ detailed hand model’, *Computer Methods in Biomechanics and Biomedical Engineering* **24**(7), 777–787.
- Eschweiler, J., Stromps, J.-P., Fischer, M., Schick, F., Rath, B., Pallua, N. and Radermacher, K. (2016), ‘Development of a biomechanical model of the wrist joint for patient-specific model guided surgical therapy planning: Part 1’, *Proceedings of the Institution of Mechanical Engineers, Part H: Journal of Engineering in Medicine* **230**(4), 310–325.
- Ezugwu, U. A., Egba, E. N., Igweagu, P. C., Eneje, L. E., Orji, S., Ugwu, U. C. et al. (2020), ‘Awareness of awkward posture and repetitive motion as ergonomic factors associated with musculoskeletal disorders by health promotion professionals’, *Global Journal of Health Science* **12**(6), 128–128.
- Fisk, J. P. and Wayne, J. S. (2009), ‘Development and validation of a computational musculoskeletal model of the elbow and forearm’, *Annals of biomedical engineering* **37**(4), 803–812.
- Fleiss, J. L. (1971), ‘Measuring nominal scale agreement among many raters.’, *Psychological bulletin* **76**(5), 378.

- Floris, S., Olsen, B. S., Dalstra, M., Søjbjerg, J. O. and Sneppen, O. (1998), 'The medial collateral ligament of the elbow joint: anatomy and kinematics', *Journal of shoulder and elbow surgery* **7**(4), 345–351.
- Fluit, R., Andersen, M. S., Kolk, S., Verdonschot, N. and Koopman, H. F. (2014), 'Prediction of ground reaction forces and moments during various activities of daily living', *Journal of biomechanics* **47**(10), 2321–2329.
- Forman, D. A., Forman, G. N., Robathan, J. and Holmes, M. W. (2019), 'The influence of simultaneous handgrip and wrist force on forearm muscle activity', *Journal of Electromyography and Kinesiology* **45**, 53–60.
- Frangiamore, S. J., Bigart, K., Nagle, T., Colbrunn, R., Millis, A. and Schickendantz, M. S. (2018), 'Biomechanical analysis of elbow medial ulnar collateral ligament tear location and its effect on rotational stability', *Journal of shoulder and elbow surgery* **27**(11), 2068–2076.
- Franko, O. I., Winters, T. M., Tirrell, T. F., Hentzen, E. R. and Lieber, R. L. (2011), 'Moment arms of the human digital flexors', *Journal of biomechanics* **44**(10), 1987–1990.
- Gagnon, D., Arjmand, N., Plamondon, A., Shirazi-Adl, A. and Larivière, C. (2011), 'An improved multi-joint emg-assisted optimization approach to estimate joint and muscle forces in a musculoskeletal model of the lumbar spine', *Journal of biomechanics* **44**(8), 1521–1529.
- Gallagher, A., Ní Annaidh, A., Bruyère, K. et al. (2012), Dynamic tensile properties of human skin, in 'IRCOBI Conference 2012, 12-14 September 2012, Dublin (Ireland)', International Research Council on the Biomechanics of Injury.
- Gallagher, S. and Heberger, J. R. (2013), 'Examining the interaction of force and repetition on musculoskeletal disorder risk: a systematic literature review', *Human factors* **55**(1), 108–124.
- Gallagher, S. and Marras, W. S. (2012), 'Tolerance of the lumbar spine to shear: a review and recommended exposure limits', *Clinical Biomechanics* **27**(10), 973–978.

- Garner, B. A. and Pandy, M. G. (2001), ‘Musculoskeletal model of the upper limb based on the visible human male dataset’, *Computer methods in biomechanics and biomedical engineering* **4**(2), 93–126.
- Giannini, S., Buda, R., Di Caprio, F., Agati, P., Bigi, A., De Pasquale, V. and Ruggeri, A. (2008), ‘Effects of freezing on the biomechanical and structural properties of human posterior tibial tendons’, *International orthopaedics* **32**(2), 145–151.
- Gonzalez, R. V., Hutchins, E., Barr, R. E. and Abraham, L. D. (1996), ‘Development and evaluation of a musculoskeletal model of the elbow joint complex’, *Journal of biomechanical engineering* **118**(1), 32–40.
- Gustafsson, E., Johnson, P. W. and Hagberg, M. (2010), ‘Thumb postures and physical loads during mobile phone use—a comparison of young adults with and without musculoskeletal symptoms’, *Journal of Electromyography and Kinesiology* **20**(1), 127–135.
- Hausman, M. R. and Lang, P. (2014), ‘Examination of the elbow: current concepts’, *The Journal of hand surgery* **39**(12), 2534–2541.
- Havelková, L., Zítka, T., Fiala, P., Rybarova, M., Tupý, R., Kalis, V. and Ismail, K. (2020), ‘Data for: Hand muscles attachments: A geometrical model (version pre pub sc v1.1) [data set]’, *Zenodo: [accessed 2020 Nov 20] <http://doi.org/10.5281/zenodo.3954024>* .
- Helton, J. C. and Davis, F. J. (2003), ‘Latin hypercube sampling and the propagation of uncertainty in analyses of complex systems’, *Reliability Engineering and System Safety* **81**(1), 23–69.
- Herzog, W. (1992), ‘Sensitivity of muscle force estimations to changes in muscle input parameters using nonlinear optimization approaches’.
- Hicks, J. L., Uchida, T. K., Seth, A., Rajagopal, A. and Delp, S. L. (2015), ‘Is my model good enough? best practices for verification and validation of musculoskeletal models and simulations of movement’, *Journal of biomechanical engineering* **137**(2).

- Hill, A. V. (1938), 'The heat of shortening and the dynamic constants of muscle', *Proceedings of the Royal Society of London. Series B-Biological Sciences* **126**(843), 136–195.
- Hirt, B. (2016), *Hand and wrist anatomy and biomechanics*, Thieme.
- Hochschild, J. (2015), *Functional anatomy for physical therapists*, Thieme.
- Hollister, A., Giurintano, D. J., Buford, W. L., Myers, L. M. and Novick, A. (1995), 'The axes of rotation of the thumb interphalangeal and metacarpophalangeal joints', *Clinical Orthopaedics and Related Research*® **320**, 188–193.
- Holzbour, K. R., Murray, W. M. and Delp, S. L. (2005), 'A model of the upper extremity for simulating musculoskeletal surgery and analyzing neuromuscular control', *Annals of biomedical engineering* **33**(6), 829–840.
- Houngbedji, G. M., Abathan, M. S., Alagnide, E. and Kpadonou, T. G. (2017), 'Prevalence of low back pain in midwives and nurses', *Annals of Physical and Rehabilitation Medicine* **60**, e20–e21.
- Hwang, J., Shields, M., Berglund, L., Hooke, A., Fitzsimmons, J. and O'Driscoll, S. (2018), 'The role of the posterior bundle of the medial collateral ligament in posteromedial rotatory instability of the elbow', *Bone Joint J* **100**(8), 1060–1065.
- Israely, S., Leisman, G. and Carmeli, E. (2018), 'Neuromuscular synergies in motor control in normal and poststroke individuals', *Reviews in the Neurosciences* **29**(6), 593–612.
- Jacobson, M. D., Raab, R., Fazeli, B. M., Abrams, R. A., Botte, M. J. and Lieber, R. L. (1992), 'Architectural design of the human intrinsic hand muscles', *Journal of Hand Surgery* **17**(5), 804–809.
- Jansova, M., Kalis, V., Rusavy, Z., Räsänen, S., Lobovsky, L. and Laine, K. (2017), 'Fetal head size and effect of manual perineal protection', *PloS one* **12**(12), e0189842.

- Jansova, M., Kalis, V., Rusavy, Z., Zemcik, R., Lobovsky, L. and Laine, K. (2014), ‘Modeling manual perineal protection during vaginal delivery’, *International urogynecology journal* **25**(1), 65–71.
- Jian-Qiao Peng, M., Chen, C.-T., Ma, L., Ju, X. and Khambay, B. (2021), ‘Dynamic effect of three locking plates fixated to humeral fracture based on multi-body musculoskeletal model’, *The International Journal of Medical Robotics and Computer Assisted Surgery* **17**(6), e2323.
- Jungtäubl, D., Spicka, J., Aurbach, M., Süß, F., Melzner, M. and Dendorfer, S. (2018), Emg-based validation of musculoskeletal models considering crosstalk, in ‘2018 International Conference BIOMDL0RE’, IEEE, pp. 1–4.
- Kalis, V., Rusavy, Z., Havelkova, L., Zitka, T., Tolar, D. and Ismail, K. M. (2020), ‘Metrics of perineal support (mops) study’, *BMC Pregnancy and Childbirth* **20**(1), 1–6.
- Karahan, A., Kav, S., Abbasoglu, A. and Dogan, N. (2009), ‘Low back pain: prevalence and associated risk factors among hospital staff’, *Journal of advanced nursing* **65**(3), 516–524.
- Karbach, L. E. and Elfar, J. (2017), ‘Elbow instability: anatomy, biomechanics, diagnostic maneuvers, and testing’, *The Journal of hand surgery* **42**(2), 118–126.
- Kasprisin, J. and Grabiner, M. (1998), ‘Emg variability during maximum voluntary isometric and anisometric contractions is reduced using spatial averaging’, *Journal of Electromyography and Kinesiology* **8**(1), 45–50.
- Kehr, P. and Graftiaux, A. G. (2017), ‘B. Hirt, H. Seyhan, M. Wagner, R. Zumhasch: Hand and wrist anatomy and biomechanics: a comprehensive guide’, *European Journal of Orthopaedic Surgery and Traumatology* **27**(7), 1029–1029.
- Kendall, F. P., McCreary, E. K., Provance, P. G., Rodgers, M., Romani, W. A. et al. (1993), *Muscles, testing and function: with posture and pain*, Vol. 103, Williams and Wilkins Baltimore, MD.

- Kerkhof, F., Brugman, E., D'Agostino, P., Dourthe, B., van Lenthe, G., Stockmans, F., Jonkers, I. and Vereecke, E. (2016), 'Quantifying thumb opposition kinematics using dynamic computed tomography', *Journal of biomechanics* **49**(9), 1994–1999.
- Kerkhof, F. D., Van Leeuwen, T. and Vereecke, E. E. (2018), 'The digital human forearm and hand', *Journal of Anatomy* **233**(5), 557–566.
- Killick, R., Fearnhead, P. and Eckley, I. A. (2012), 'Optimal detection of change-points with a linear computational cost', *Journal of the American Statistical Association* **107**(500), 1590–1598.
- King, J. C. (2013), 'Strategies to reduce maternal mortality in developed countries', *Current Opinion in Obstetrics and Gynecology* **25**(2), 117–123.
- Kleprlikova, H., Kalis, V., Lucovnik, M., Rusavy, Z., Blaganje, M., Thakar, R. and Ismail, K. M. (2020), 'Manual perineal protection: The know-how and the know-why', *Acta obstetrica et gynecologica Scandinavica* **99**(4), 445–450.
- Kobayashi, M., Berger, R. A., Nagy, L., Linscheid, R. L., Uchiyama, S., Ritt, M. and An, K.-N. (1997), 'Normal kinematics of carpal bones: a three-dimensional analysis of carpal bone motion relative to the radius', *Journal of biomechanics* **30**(8), 787–793.
- Kong, Y.-K., Hallbeck, M. S. and Jung, M.-C. (2010), 'Crosstalk effect on surface electromyogram of the forearm flexors during a static grip task', *Journal of Electromyography and Kinesiology* **20**(6), 1223–1229.
- Konrad, P. (2005), 'The abc of emg', *A practical introduction to kinesiological electromyography* **1**(2005), 30–5.
- Kwan, M., Andersen, M. S., Cheng, C.-L., Tang, W.-T. and Rasmussen, J. (2011), 'Investigation of high-speed badminton racket kinematics by motion capture', *Sports Engineering* **13**(2), 57–63.
- LaCross, A., Groff, M. and Smaldone, A. (2015), 'Obstetric anal sphincter injury and anal incontinence following vaginal birth: a systematic review and meta-analysis', *Journal of midwifery and women's health* **60**(1), 37–47.

- Laine, K., Pirhonen, T., Rolland, R. and Pirhonen, J. (2008), ‘Decreasing the incidence of anal sphincter tears during delivery’, *Obstetrics and Gynecology* **111**(5), 1053–1057.
- Laine, K., Rotvold, W. and Staff, A. C. (2013), ‘Are obstetric anal sphincter ruptures preventable?—large and consistent rupture rate variations between the nordic countries and between delivery units in norway’, *Acta obstetricia et gynecologica Scandinavica* **92**(1), 94–100.
- Landsmeer, J. (1961), ‘Studies in the anatomy of articulation. i. the equilibrium of the intercalated bone.’, *Acta Morphologica Neerlandico-Scandinavica* **3**, 287.
- Lee, J. H., Asakawa, D. S., Dennerlein, J. T. and Jindrich, D. L. (2015a), ‘Extrinsic and intrinsic index finger muscle attachments in an opensim upper-extremity model’, *Annals of biomedical engineering* **43**(4), 937–948.
- Lee, J. H., Asakawa, D. S., Dennerlein, J. T. and Jindrich, D. L. (2015b), ‘Finger muscle attachments for an opensim upper-extremity model’, *PloS one* **10**(4).
- Lee, J. H., Shim, H., Lee, H. S., Lee, Y. H. and Yoon, Y. R. (2007), Detection of onset and offset time of muscle activity in surface emgs using the kalman smoother, *in* ‘World Congress on Medical Physics and Biomedical Engineering 2006’, Springer, pp. 1103–1106.
- Lee, P. J., Lee, E. L. and Hayes, W. C. (2013), ‘The ratio of thoracic to lumbar compression force is posture dependent’, *Ergonomics* **56**(5), 832–841.
- Lee, S. W. and Kamper, D. G. (2009), ‘Modeling of multiarticular muscles: Importance of inclusion of tendon–pulley interactions in the finger’, *IEEE Transactions on Biomedical Engineering* **56**(9), 2253–2262.
- Lemay, M. A. and Crago, P. E. (1996), ‘A dynamic model for simulating movements of the elbow, forearm, and wrist’, *Journal of biomechanics* **29**(10), 1319–1330.
- Lieber, R. L., Fazeli, B. M. and Botte, M. J. (1990), ‘Architecture of selected wrist flexor and extensor muscles’, *The Journal of hand surgery* **15**(2), 244–250.

- Lieber, R. L., Jacobson, M. D., Fazeli, B. M., Abrams, R. A. and Botte, M. J. (1992), ‘Architecture of selected muscles of the arm and forearm: anatomy and implications for tendon transfer’, *The Journal of hand surgery* **17**(5), 787–798.
- Lippert, L. (2006), ‘R. library’, *Clinical Kinesiology and Anatomy*, FA Davis, Philadelphia .
- Litin, S. C. and Nanda, S. (2018), Mayo clinic family health book, Mayo Clinic.
- Loren, G., Shoemaker, S., Burkholder, T., Jacobson, M., Friden, J. and Lieber, R. L. (1996), ‘Human wrist motors: biomechanical design and application to tendon transfers’, *Journal of biomechanics* **29**(3), 331–342.
- Lund, M. E., de Zee, M., Andersen, M. S. and Rasmussen, J. (2012), ‘On validation of multibody musculoskeletal models’, *Proceedings of the Institution of Mechanical Engineers, Part H: Journal of Engineering in Medicine* **226**(2), 82–94.
- Lund, M., Torholm, S., Dzialo, C. and Jensen, B. (2019), ‘The anybody managed model repository’, *AMMR, Zenodo* .
- MacIntosh, A. R. and Keir, P. J. (2017), ‘An open-source model and solution method to predict co-contraction in the finger’, *Computer methods in Biomechanics and Biomedical engineering* **20**(13), 1373–1381.
- Marra, M. A., Vanheule, V., Fluit, R., Koopman, B. H., Rasmussen, J., Verdonschot, N. and Andersen, M. S. (2015), ‘A subject-specific musculoskeletal modeling framework to predict in vivo mechanics of total knee arthroplasty’, *Journal of biomechanical engineering* **137**(2).
- Ma’touq, J., Hu, T. and Haddadin, S. (2019), ‘A validated combined musculotendon path and muscle-joint kinematics model for the human hand’, *Computer methods in biomechanics and biomedical engineering* **22**(7), 727–739.
- Maury, A., Nussbaum, Chaffin, Don, B., Rechten and Catherine, J. (1995), ‘Muscle lines-of-action affect predicted forces in optimization-based spine muscle modeling’, *Journal of Biomechanics* **28**(4), 401–409.

- Mehrvarz, S., Towliat, S. M., Mohebbi, H. A., Heydari, S., Farahani, M. and Rasouli, H. R. (2015), ‘Obstructed defecation syndrome after delivery trauma’, *Trauma monthly* **20**(4).
- Melzner, M., Engelhardt, L., Simon, U. and Dendorfer, S. (2022), ‘Electromyography-based validation of a musculoskeletal hand model’, *Journal of Biomechanical Engineering* **144**(2), 021005.
- Melzner, M., Ismail, K. M., Rušavý, Z., Kališ, V., Süß, F. and Dendorfer, S. (2021), ‘Musculoskeletal lower back load of accoucheurs during childbirth—a pilot and feasibility study’, *European Journal of Obstetrics and Gynecology and Reproductive Biology* **264**, 306–313.
- Melzner, M., Süß, F. and Dendorfer, S. (2022), ‘The impact of anatomical uncertainties on the predictions of a musculoskeletal hand model – a sensitivity study’, *Computer methods in biomechanics and biomedical engineering* **25**(2), 156–164.
- Mirakhorlo, M., Van Beek, N., Wesseling, M., Maas, H., Veeger, H. and Jonkers, I. (2018), ‘A musculoskeletal model of the hand and wrist: model definition and evaluation’, *Computer methods in biomechanics and biomedical engineering* **21**(9), 548–557.
- Mirakhorlo, M., Visser, J. M., Goislard de Monsabert, B., Van der Helm, F., Maas, H. and Veeger, H. (2016), ‘Anatomical parameters for musculoskeletal modeling of the hand and wrist’, *International Biomechanics* **3**(1), 40–49.
- Morrey, B. F. (2009), *The Elbow and Its Disorders*, Elsevier Health Sciences.
- Morrey, B. F. and An, K. (1985), ‘Functional anatomy of the ligaments of the elbow’, *Clinical orthopaedics and related research* (201), 84–90.
- Morrey, B. F. and An, K.-N. (1983), ‘Articular and ligamentous contributions to the stability of the elbow joint’, *The American journal of sports medicine* **11**(5), 315–319.
- Morrey, B. F. and An, K.-N. (2005), ‘Stability of the elbow: osseous constraints’, *Journal of shoulder and elbow surgery* **14**(1), S174–S178.

- Murray, W. M., Buchanan, T. S. and Delp, S. L. (2000), 'The isometric functional capacity of muscles that cross the elbow', *Journal of biomechanics* **33**(8), 943–952.
- Murray, W. M., Delp, S. L. and Buchanan, T. S. (1995), 'Variation of muscle moment arms with elbow and forearm position', *Journal of biomechanics* **28**(5), 513–525.
- Myers, C. A., Laz, P. J., Shelburne, K. B. and Davidson, B. S. (2015), 'A probabilistic approach to quantify the impact of uncertainty propagation in musculoskeletal simulations', *Annals of biomedical engineering* **43**(5), 1098–1111.
- Nakashima, M., Hasegawa, T., Kamiya, S. and Takagi, H. (2013), 'Musculoskeletal simulation of the breaststroke', *Journal of Biomechanical Science and Engineering* **8**(2), 152–163.
- Okuyucu, K., Gyi, D., Hignett, S. and Doshani, A. (2019), 'Midwives are getting hurt: Uk survey of the prevalence and risk factors for developing musculoskeletal symptoms', *Midwifery* **79**, 102546.
- Oppenheim, W. L., Clader, T. J., Smith, C. and Bayer, M. (1984), 'Supracondylar humeral osteotomy for traumatic childhood cubitus varus deformity.', *Clinical orthopaedics and related research* (188), 34–39.
- Plagenhoef, S., Evans, F. G. and Abdelnour, T. (1983), 'Anatomical data for analyzing human motion', *Research quarterly for exercise and sport* **54**(2), 169–178.
- Prilutsky, B. I. and Zatsiorsky, V. M. (2002), 'Optimization-based models of muscle coordination', *Exercise and sport sciences reviews* **30**(1), 32.
- Putzer, M., Auer, S., Malpica, W., Suess, F. and Dendorfer, S. (2016), 'A numerical study to determine the effect of ligament stiffness on kinematics of the lumbar spine during flexion', *BMC musculoskeletal disorders* **17**(1), 95.
- Rahman, M., Sharifi Renani, M., Cil, A. and Stylianou, A. P. (2018), 'Musculoskeletal model development of the elbow joint with an experimental evaluation', *Bioengineering* **5**(2), 31.

- Raikova, R. T. and Prilutsky, B. I. (2001), ‘Sensitivity of predicted muscle forces to parameters of the optimization-based human leg model revealed by analytical and numerical analyses’, *Journal of biomechanics* **34**(10), 1243–1255.
- Rainoldi, A., Nazzaro, M., Merletti, R., Farina, D., Caruso, I. and Gaudenti, S. (2000), ‘Geometrical factors in surface emg of the vastus medialis and lateralis muscles’, *Journal of Electromyography and Kinesiology* **10**(5), 327–336.
- Rebba, R. and Mahadevan, S. (2008), ‘Computational methods for model reliability assessment’, *Reliability Engineering and System Safety* **93**(8), 1197–1207.
- Regan, W. D., Korinek, S. L., Morrey, B. F. and An, K.-N. (1991), ‘Biomechanical study of ligaments around the elbow joint.’, *Clinical orthopaedics and related research* (271), 170–179.
- Reinbolt, J. A., Schutte, J. F., Fregly, B. J., Koh, B. I., Haftka, R. T., George, A. D. and Mitchell, K. H. (2005), ‘Determination of patient-specific multi-joint kinematic models through two-level optimization’, *Journal of biomechanics* **38**(3), 621–626.
- Robertson, D. G. E., Caldwell, G. E., Hamill, J., Kamen, G. and Whittlesey, S. (2013), *Research methods in biomechanics*, Human kinetics.
- Safran, M. R. and Baillargeon, D. (2005), ‘Soft-tissue stabilizers of the elbow’, *Journal of shoulder and elbow surgery* **14**(1), S179–S185.
- Safran, M. R., McGarry, M. H., Shin, S., Han, S. and Lee, T. Q. (2005), ‘Effects of elbow flexion and forearm rotation on valgus laxity of the elbow’, *JBJS* **87**(9), 2065–2074.
- Scheys, L., Loeckx, D., Spaepen, A., Suetens, P. and Jonkers, I. (2009), ‘Atlas-based non-rigid image registration to automatically define line-of-action muscle models: a validation study’, *Journal of biomechanics* **42**(5), 565–572.
- Scheys, L., Van Campenhout, A., Spaepen, A., Suetens, P. and Jonkers, I. (2008), ‘Personalized mr-based musculoskeletal models compared to rescaled generic models in the presence of increased femoral anteversion: effect on hip moment arm lengths’, *Gait and posture* **28**(3), 358–365.

- Schmidt, H.-M. and Lanz, U. (2011), *Surgical anatomy of the hand*, Thieme.
- Schönegg, D., Müller, G. T., Blumer, M., Essig, H. and Wagner, M. E. (2022), ‘Two-versus three-screw osteosynthesis of the mandibular condylar head: A finite element analysis’, *Journal of the Mechanical Behavior of Biomedical Materials* p. 105077.
- Schuind, F., Cooney, W., Linscheid, R., An, K. and Chao, E. (1995), ‘Force and pressure transmission through the normal wrist. a theoretical two-dimensional study in the posteroanterior plane’, *Journal of biomechanics* **28**(5), 587–601.
- Schünke, M., Schulte, E., Schumacher, U., Ross, L. M. and Lamperti, E. D. (2014), *Thieme atlas of anatomy: general anatomy and musculoskeletal system*, Thieme Medical Publishers, Incorporated.
- Seiber, K., Gupta, R., McGarry, M. H., Safran, M. R. and Lee, T. Q. (2009), ‘The role of the elbow musculature, forearm rotation, and elbow flexion in elbow stability: an in vitro study’, *Journal of shoulder and elbow surgery* **18**(2), 260–268.
- Seth, A., Hicks, J. L., Uchida, T. K., Habib, A., Dembia, C. L., Dunne, J. J., Ong, C. F., DeMers, M. S., Rajagopal, A., Millard, M. et al. (2018), ‘Opensim: Simulating musculoskeletal dynamics and neuromuscular control to study human and animal movement’, *PLoS computational biology* **14**(7).
- Seth, A. and Pandy, M. G. (2007), ‘A neuromusculoskeletal tracking method for estimating individual muscle forces in human movement’, *Journal of biomechanics* **40**(2), 356–366.
- Singh, J., Elvey, M. H., Hamoodi, Z. and Watts, A. C. (2020), ‘Current perspectives on elbow dislocation and instability’, *Annals of Joint* .
- Skipper Andersen, M., De Zee, M., Damsgaard, M., Nolte, D. and Rasmussen, J. (2017), ‘Introduction to force-dependent kinematics: theory and application to mandible modeling’, *Journal of biomechanical engineering* **139**(9).
- Smith, T. J., Henning, R. A., Wade, M. G. and Fisher, T. (2014), *Variability in human performance*, CRC Press.

- Smutz, W. P., Kongsayreepong, A., Hughes, R. E., Niebur, G., Cooney, W. P. and An, K.-N. (1998), ‘Mechanical advantage of the thumb muscles’, *Journal of biomechanics* **31**(6), 565–570.
- Solnik, S., Rider, P., Steinweg, K., DeVita, P. and Hortobágyi, T. (2010), ‘Teager–kaiser energy operator signal conditioning improves emg onset detection’, *European journal of applied physiology* **110**(3), 489–498.
- Taddei, F., Martelli, S., Valente, G., Leardini, A., Benedetti, M. G., Manfrini, M. and Viceconti, M. (2012), ‘Femoral loads during gait in a patient with massive skeletal reconstruction’, *Clinical Biomechanics* **27**(3), 273–280.
- Tanaka, S., An, K.-N. and Morrey, B. F. (1998), ‘Kinematics and laxity of ulno-humeral joint under valgus-varus stress’, *Journal of Musculoskeletal Research* **2**(01), 45–54.
- Tenan, M. S., Tweedell, A. J. and Haynes, C. A. (2017), ‘Analysis of statistical and standard algorithms for detecting muscle onset with surface electromyography’, *PloS one* **12**(5).
- Tillmann, B. N. (2016), *Atlas der Anatomie des Menschen*, Springer-Verlag.
- Valente, G., Pitto, L., Testi, D., Seth, A., Delp, S. L., Stagni, R., Viceconti, M. and Taddei, F. (2014), ‘Are subject-specific musculoskeletal models robust to the uncertainties in parameter identification?’, *PLoS One* **9**(11), e112625.
- Valero-Cuevas, F. J., Johanson, M. E. and Towles, J. D. (2003), ‘Towards a realistic biomechanical model of the thumb: the choice of kinematic description may be more critical than the solution method or the variability/uncertainty of musculoskeletal parameters’, *Journal of biomechanics* **36**(7), 1019–1030.
- van der Helm, F., Chadwick, E. and Veeger, H. (2001), A large-scale musculoskeletal model of the shoulder and elbow: The delft shoulder (and elbow) model, in ‘Proceedings of the XVIIIth Conference of the International Society of Biomechanics, Zurich’, pp. 8–13.
- van Riet, R. P. (2017), ‘Assessment and decision making in the unstable elbow: management of simple dislocations’, *Shoulder and elbow* **9**(2), 136–143.

- Van Roy, P., Baeyens, J.-P., Fauvart, D., Lanssiers, R. and Clarijs, J. (2005), 'Arthro-kinematics of the elbow: study of the carrying angle', *Ergonomics* **48**(11-14), 1645–1656.
- Van Zwieten, K. J., Schmidt, K. P., Bex, G. J., Lippens, P. L. and Duyvendak, W. (2015), 'An analytical expression for the dip–pip flexion interdependence in human fingers'.
- Vannozzi, G., Conforto, S. and D'Alessio, T. (2010), 'Automatic detection of surface emg activation timing using a wavelet transform based method', *Journal of Electromyography and Kinesiology* **20**(4), 767–772.
- Waldt, S. and Woertler, K. (2014), 'Measurements and classifications in musculoskeletal radiology', *J. Magn. Reson. Imaging* **40**, 248–249.
- Weber, T., Al-Munajjed, A. A., Verkerke, G. J., Dendorfer, S. and Renkawitz, T. (2014), 'Influence of minimally invasive total hip replacement on hip reaction forces and their orientations', *Journal of orthopaedic research* **32**(12), 1680–1687.
- Wibawa, A., Verdonschot, N., Burgerhof, J., Purnama, I., Andersen, M., Halbertsma, J., Diercks, R. and Verkerke, G. (2013), A validation study on muscle activity prediction of a lower limb musculoskeletal model using emg during normal walking, in '2013 3rd International Conference on Instrumentation, Communications, Information Technology and Biomedical Engineering (ICICI-BME)', IEEE, pp. 260–264.
- Winter, D. A. (2009), *Biomechanics and motor control of human movement*, John Wiley and Sons.
- Wu, G., Van der Helm, F. C., Veeger, H. D., Makhsous, M., Van Roy, P., Anglin, C., Nagels, J., Karduna, A. R., McQuade, K., Wang, X. et al. (2005), 'Isb recommendation on definitions of joint coordinate systems of various joints for the reporting of human joint motion—part ii: shoulder, elbow, wrist and hand', *Journal of biomechanics* **38**(5), 981–992.

- Wu, J. Z., An, K.-N., Cutlip, R. G., Andrew, M. E. and Dong, R. G. (2009), 'Modeling of the muscle/tendon excursions and moment arms in the thumb using the commercial software anybody', *Journal of biomechanics* **42**(3), 383–388.
- Wu, J. Z., An, K.-N., Cutlip, R. G., Krajnak, K., Welcome, D. and Dong, R. G. (2008), 'Analysis of musculoskeletal loading in an index finger during tapping', *Journal of biomechanics* **41**(3), 668–676.
- Wu, J. Z., Sinsel, E. W., Shroyer, J. F., Warren, C. M., Welcome, D. E., Zhao, K. D., An, K.-N. and Buczek, F. L. (2014), 'Analysis of the musculoskeletal loading of the thumb during pipetting—a pilot study', *Journal of biomechanics* **47**(2), 392–399.
- Yeomans, E. R. (2010), 'Operative vaginal delivery', *Obstetrics and Gynecology* **115**(3), 645–653.
- Żuk, M. and Pezowicz, C. (2016), The influence of uncertainty in body segment mass on calculated joint moments and muscle forces, *in* 'Conference of Information Technologies in Biomedicine', Springer, pp. 349–359.

Declaration of authorship

I, Maximilian Melzner, born on 17.10.1990 in Munich confirm, that I have produced the present work *Development and validation of a new musculoskeletal hand and elbow model and its application in the medical field* without the improper assistance of third parties and without the use of aids other than those indicated.

The data and concepts taken directly or indirectly from other sources are marked with indication of the source. In particular I did not receive the assistance of intermediary or advisory services (promotional advisers or other persons).

The thesis has not yet been submitted to another examination office in the same or a similar form, neither in Germany nor abroad.

Regensburg, 9th of June 2022



Maximilian Melzner

Publications

The content presented in this thesis has already been published at international conferences as well as in peer reviewed journals. The following is an overview of the conferences and journals where parts have already been published.

Peer-reviewed Journals

A new musculoskeletal AnyBody™ detailed hand model

Authors: Lucas Engelhardt¹ and Maximilian Melzner¹, Linda Havelkova, Pavel Fiala, Patrik Christen, Sebastian Dendorfer, Ulrich Simon

Year: 2021

Journal: Computer Methods in Biomechanics and Biomedical Engineering

Electromyography based validation of a musculoskeletal hand model

Authors: Maximilian Melzner¹ and Lucas Engelhardt¹, Ulrich Simon, Sebastian Dendorfer

Year: 2021

Journal: Journal of Biomechanical Engineering

¹shared first authors

The impact of anatomical uncertainties on the predictions of a musculoskeletal hand model – a sensitivity study

Authors: Maximilian Melzner, Franz Süß, Sebastian Dendorfer

Year: 2021

Journal: Computer Methods in Biomechanics and Biomedical Engineering

Musculoskeletal lower back load of accoucheurs during childbirth - A pilot and feasibility study

Authors: Maximilian Melzner, Khaled M Ismail, Zdeněk Rušavý, Vladimír Kališ, Franz Süß, Sebastian Dendorfer

Year: 2021

Journal: European Journal of Obstetrics and Gynecology and Reproductive Biology

International Conferences

A new musculoskeletal AnyBody™ detailed hand model

Authors: Lucas Engelhardt¹ and Maximilian Melzner¹, Linda Havelkova, Pavel Fiala, Patrik Christen, Sebastian Dendorfer, Ulrich Simon

Format: Podium presentation

Conference: 25th Congress of the European Society of Biomechanics, July 2019, Vienna, Austria

A new musculoskeletal AnyBody detailed hand model validated by electromyography

Authors: Maximilian Melzner¹ and Lucas Engelhardt¹, Linda Havelkova, Ulrich Simon, Sebastian Dendorfer

Format: Podium presentation

Conference: 16th International Symposium on Computer Methods in Biomechanics and Biomedical Engineering, August 2019, New York, United States of America

¹shared first authors

Änderung der Gelenkreaktionskraft bei Schädigung des medialen Bandapparates im Ellenbogen

Authors: Maximilian Melzner, Christian Pfeifer, Volker Alt, Fran Süß, Sebastian Dendorfer

Format: Poster presentation

Conference: Deutscher Kongress für Orthopädie und Unfallchirurgie, Oktober 2020, Online

Sensitivity evaluation of a musculoskeletal hand model using Latin hypercube sampling

Authors: Maximilian Melzner, Lucas Engelhardt, Franz Süß, Sebastian Dendorfer

Format: Poster presentation

Conference: European Society for Movement Analysis in Adults and Children, September 2020, Online

Musculoskeletal lower back load of accoucheurs during delivery

Authors: Maximilian Melzner, Khaled M. Ismail, Zdeněk Rušavý, Vladimír Kališ, Franz Süß, Sebastian Dendorfer

Format: Podium presentation

Conference: 26th Congress of the European Society of Biomechanics, July 2021, Milan, Italy

Musculoskeletal analysis of elbow stability for common injury patterns

Authors: Maximilian Melzner, Christian Pfeifer, Franz Süß, Sebastian Dendorfer

Format: Poster presentation

Conference: 27th Congress of the European Society of Biomechanics, June 2022, Porto, Portugal

Acknowledgments

First of all, I would like to thank my supervisor Sebastian Dendorfer, who took the risk of hiring someone external into his laboratory team - I hope he did not regret it. In any case, I can say that in my numerous stations in my academic and professional career, I have never been in a team where I felt as comfortable and at home as I do in the laboratory for biomechanics under Sebastian's leadership. Through his style of leadership and wide-ranging expertise, he manages to create a perfect atmosphere for the personal development during the doctoral period.

If I have to thank someone, it is definitely the person who fished my application out of the garbage bin back then and without whom I would thus never have ended up here - Franz Süß. His constantly critical spirit has always encouraged me to question my own way of thinking and thus open up new perspectives.

Furthermore, I would like to thank my mentors Christian Pfeifer, who always supported me in medical issues. I have always experienced the joint research as productive and characterised by mutual trust.

I would also like to express my special thanks to my mentor Elmar Lang, in whose working group I was already able to write my bachelor's thesis. He always helped me with any minor and major issues during my doctoral phase without fuss or quibble.

People with whom one deals on a daily basis and thus are not only colleagues, but also become good friends, are most important of course. Therefore, I would like to thank Simon Auer, Lukas Reinker, Michael Kögler, Clemens Birkenmaier, Florian Erzinger, Melina Tauwald and Bernd Gamisch for the years spent together. Special thanks go to Simon Groß and especially Maximilian Aurbach, who supported me in all stages during my doctoral phase, especially in the early days.

In general, I would like to thank the Regensburg Centre of Biomedical Engineering - specifically Alexander Leis - who provided the organisational framework for my work and supported me in every administrative matter.

As described in my work, parts of it were created in cooperation with the University of Ulm. The trips to Ulm and the collaboration with my colleague and friend Lucas Engelhardt and his doctoral supervisor Ulrich Simon were always a joyful, uncomplicated and enriching experience - many thanks for that.

In my work, in addition to the medical expertise I have gained, it has always been a great pleasure to promote cultural exchange. Through numerous visits to Pilsen, I was able to get to know and appreciate Czech culture. I have always enjoyed working with our project partners from Pilsen. Therefore, I would like to thank Jan Vychytil on behalf of everyone for the friendly and productive cooperation.

I am also deeply grateful to the financial and non-material support from the College 'Health' of the Bavarian Science Forum (BayWISS) and the Friedrich-Ebert-Foundation, without which my research work would never have been possible to the extent it has been.

Finally, I would like to profoundly thank my family - my father Johann, my mother Ursula and my two brothers Eli and Hansi, as well as his wife Asante - and of course Sandra and all the friends who have unfortunately not been listed so far for their support during all this time.